ON THE VIBRATIONS OF A ROTATING SHAFT

TOSHIO YAMAMOTO

Department of Mechanical Engineering

(Received May 31, 1957)

CONTENTS

Page

Nomenclature 21
Introduction 24
Chapter I. Experimental Apparatus and Methods of Experiments 24
Chapter II. Non-Linear and Non-Symmetrical Spring Characteristics of the Shaft Supported by Single-Row Radial Ball Bearings 25
1. Preliminaries 25
2. Angular clearance of single-row radial ball bearing 25
3. Non-linearity of spring characteristics 26
4. Results of experiments 30
5. Differential equations of motions of disc when single-row radial ball bearings are used 32
Chapter III. On the Critical Speed of a Shaft of Sub-Harmonic Oscillation and on Sub-Harmonic Oscillation of Rectilinear Vibrations 33
1. Introduction 33
2. Results of experiments 34
3. Jump phenomena 37
4. Sub-harmonic oscillation when shaft does not rotate ($\omega = 0$) 38
5. Sub-harmonic oscillation in multiple degrees of freedom system 40
6. Conclusions 42
Chapter IV. On Critical Speeds of "Summed and Differential Harmonic Oscillations" 43
1. Introduction 43
2. Behavior of vibrations in resonant rotating speed 43
3. Relations between magnitudes of critical rotating speeds and modes of vibrations 48
4. Influence of ball bearing 50
5. Conclusions 52
Chapter V. On Sub-Harmonic Oscillations and on "Summed and Differential Harmonic Oscillations" in Non-Linear Systems Having Multiple Degrees of Freedom 53
1. Introduction 53
2. Transformation into normal coordiates 53
3. Occurrence of sub-harmonic oscillations 58
4. Stability of sub-harmonic oscillations 62
5. In the case in which p_2, p_3 etc. are integral multiples of p_1 64

6. Occurrence of "summed and differential harmonic oscillations"... 67
7. Multiple degrees of freedom system without gyroscopic terms... 70
Chapter VI. On the Critical Speed of Synchronous Backward Precession ... 71
1. Introduction ... 71
2. Effects of fit of ball bearing (the case where self-aligning double-row ball bearing is used) ... 71
3. Where single-row radial ball bearings are used ... 75
4. Effect of guard ring ... 76
5. Forced vibrations of synchronous backward precession ... 77
6. Conclusions ... 78
Chapter VII. On Critical Speed of a Shaft at Lower Rotating Speeds... 79
1. Introduction ... 79
2. Results of experiments ... 79
3. Cause of occurrence of the critical speed of $[+2\omega]$ and $[-2\omega]$... 81
4. Conclusions ... 86
Chapter VIII. On Critical Speeds Induced by Ball Bearings Appearing at Lower Rotating Speeds ... 86
1. Introduction ... 86
2. The cause of occurrence of the critical speeds ... 87
3. The location of the critical speeds ... 90
4. Conclusions ... 92
Chapter IX. Vibrations of Rotating Shaft Generated by Passing through Critical Speed ... 92
1. Introduction ... 92
2. Experimental apparatus ... 93
3. Diagrams of retardation ... 93
4. Motion of disc ... 93
5. Measurment of natural frequency ... 99
6. Determination of direction and magnitude of eccentricity of disc ... 100
7. Summary ... 105
Chapter X. On Stability Critieria for Forced Vibrations in Non-Linear Systems ... 105
1. Introduction ... 105
2. Stability criteria ... 105
3. General expression of stability criteria ... 108
4. Physical meaning of stability criteria ... 110
5. Examples ... 112
Acknowledgement ... 114
Notes and References ... 114

Nomenclature

The following nomenclature is used in this paper:

A' = external force in normal coordinates
$A_i = A_i'/\omega_1^2$
A_i' = amplitude of forced vibration in normal coordinates
B' = external force in normal coordinates
$B_i = B_i'/\omega_1^2$
B_i' = amplitude of forced vibration in normal coordinates
$C_i = C_i'/\omega_1$
C_i' = damping coefficient in normal coordinates
D = diameter of inner ring of ball bearing
E_1, E_2 = energy
F = disturbing force; spring force
F_1, F_2, F_x, F_y, F_{0x}, F_{0y} = components of external force
G = gravitational center of disc
I = moment of inertia of the disc about diameter of the disc
I_p = polar moment of inertia of the disc
I_1 = dimensionless quantity of I_p $(= I_p/I)$
N_1, N_2, N_n = number of revolutions of shaft
P_x, P_y = components of external force
R = statical deflection
S = disc center
W = force; weight
X_1, X_2, X_3, X_4, X_i = normal coordinates
$X_i' = dX_i/dt_1$
$a : b$ = ratio representing the position of the disc on the shaft
a, a_i' = amplitudes of forced vibration
a_i = amplitude of free vibration
b, b_i' = amplitudes of forced vibration
b_i = amplitude of free vibration
c = amplitude of forced vibration; damping coefficient
c_1, c_2, c_3, c_4, c_x, c_y, c_{0x}, c_{0y} = damping coefficients
d = diameter of steel ball in ball bearing
e = eccentricity of disc
e_0 = small deviation of shaft end from bearing center line caused by steel balls in ball bearing
e_1 = displacement of disc center S caused by e_0
$\bar{e}_0$ = vector of statical deflection of shaft
f = amplitude of free vibration; non-linear term
f_1, f_2, f_3, f_4, f_x, f_0, f_{0x} = non-linear terms
g = gravitational acceleration
i = integer $(= 1, 2, 3, 4)$
j = integer $(= 1, 2, 3, 4)$
k = integer $(= 1, 2, 3, 4)$; spring constant
l = length of the shaft
m = mass of the disc
n = integer

p = natural frequency; major critical speed
$p_1, p_2, p_3, p_4, p_i, p_j$ = natural frequencies of the vibratory system
p_1 = lower major critical speed
p_2 = higher major critical speed
$p_{1/2}$ = resonant speed of sub-harmonic oscillation of order 1/2
$p_{1/3}$ = resonant speed of sub-harmonic oscillation of order 1/3
p_0 = natual frequency of the shaft system when $\omega = 0$
q = circular frequency of external force
r = deflection of the shaft
s = radial clearance
t = time
t_1 = $\omega t/\nu$
u = ω/p
(x, y, z) = coordinates of the shaft center S
x = displacement
x_1, x_2, x_3, x_4 = dimensionless quantities of x, y θ_x and θ_y, respectively
y = displacement
z = number of steel balls in a ball bearing
Θ = angle between x axis and major or minor axis of elliptical locus of disc center S
Φ = $\tan^{-1} y/x$
Φ_i = Φ_i'/ω_1^2
Φ_i' = non-linear terms in normal coordinates
α = spring constant of the shaft; phase angle
α_i = ω_i/ω
α_i = phase angle
α_{ij} = elements of determinant D
β = phase angle between eccentricity e and deviational angle τ; phase angle between statical deflection $\bar{e}_0$ and eccentricity e; angular acceleration of shaft ($= d\omega/dt$)
γ = spring constant of the shaft; dimensionless quantity of angular acceleration of the shaft ($= \beta/p^2$)
ε = small quantity; phase angle between eccentricity e and deviational angle τ
η = small deviation from a steady state
θ = inclination angle of the disc; rotating angle of the disc
θ_x, θ_y = components of θ in x and y directions, respectively
κ = integer ($= p_2/p_1$)
λ_i = p_i/ω; ratio of amplitude of forced vibration to that of free vibration
μ = coefficient of friction
ξ = small deviation from a steady state
τ = small deviational angle between the plane of the disc and the plane which is orthogonal to the tangent of the deflection curve of shaft at the disc center S
τ_1 = inclination angle of disc caused by e_0
τ_{0x}, τ_{0y} = inclination angles caused by e_{0x} and e_{0y}, respectively
ν = integer; phase angles
ω = angular velocity of the rotating disc
ω_1 = critical speed of forward precession of sub-harmonic oscillation of order

1/2; critical speed of "summed and differential harmonic oscillations"; ω/ν; rotating speed of precessional motion of steel balls in ball bearing

ω_2, ω_3 = critical speed of backward precession of sub-harmonic oscillation of order 1/3; critical speed of "summed and differential harmonic oscillations"

ω_5 = critical speed of "summed and differential harmonic oscillations"

ω_0 = circular frequency of disturbing force

ω_c = major critical speed

ω_{b1}, ω_{b2} = higher and lower critical speeds of synchronous backward precession, respectively

ω_{cA}, ω_{cB} = major critical speeds in OA and OB directions, respectively.

Introduction

In 1954 the author presented a paper, published by the Faculty of Engineering, Nagoya University, "On the Critical Speeds of a Shaft"[1] in which he describes the whirl of shaft supported by self-aligning double-row ball bearings and explains the causes of various kinds of vibrations based of his studies. The present paper is a continuation of that report wherein is principally discussed the whirling and vibrations of a shaft supported by single-row radial ball bearings. In addition, vibrations appearing in the retarded shaft are studied in the present paper.

When single-row radial ball bearings are used, non-linear spring characteristics appear in the shaft, inducing many kinds of critical speeds,[2] *i.e.*, the critical speed of sub-harmonic oscillation; the critical speed of "summed and differential harmonic oscillations"; the secondary critical speed and others. Furthermore, use of single-row radial ball bearings results in directional non-uniformity of stiffness of shaft, and thus the critical speeds of synchronous backward precession can appear.

For the vibratory system of the retarded shaft, external force represented by $F\sin(\omega t+1/2\beta t^2)$ is exerted on the rotating body, and a very complicated and peculiar whirling motion takes place in the neighborhood of the major critical speed.

In this paper, the author describes various kinds of vibrations appearing in the system with non-linear spring characteristics and in the system with the external force having gradually increasing periods.

Chapter I. Experimental Apparatus and Methods of Experiments

The greater part of our experiments are performed on the vertical shaft mounting one disc and experimental apparatus is shown in Fig. 1 where V is a V-pulley. In order to eliminate the disturbance from the belt and from the driving motor, the spring coupling S is inserted between the V-pulley and the shaft. The guard ring G is arranged to check the increase of shaft deflections for greater safety. The whirling motion is obtained by projections of motion of disc with relation to rectangular coordinates OA (x-direction) and OB (y-direction), that is, the motions of the disc edge at points A and B (Fig. 1) are recorded on oscillographic paper by the optical method. A small piece of paper P is attached to one point on the disc edge; the light is intercepted by this paper at each revolution of the shaft and thus the angular speed of rotation of the shaft is recorded.

The disc and the shaft dimensions used in experiments are shown in the following tables.

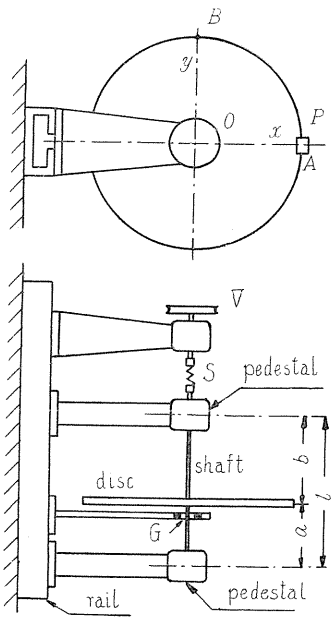

FIG. 1. Experimental apparatus.

Dimensions of Disc

Diameter in mm	Thickness in mm	Weight W in kg	Moment of inertia about a diameter I in kg cm sec.^{2}
482.8	5.22	7.804	1.114

Dimensions of Shaft

Shaft No.	$a : b$ (see Fig. 1)	Shaft length l in mm	Dia. of shaft in mm	Remarks
1	3 : 7	508.3	11.89	$a < b$
2	1 : 3	507.8	11.74	$a < b$
3	1 : 4	506.3	11.72	$a < b$
4	1 : 1	505.9	11.15	$a = b$
5	3 : 1	506.7	11.54	$a > b$

Chapter II. Non-Linear and Non-Symmetrical Spring Characteristics of the Shaft Supported by Single-Row Radial Ball Bearings[3)]

1. Preliminaries

By observing the motions of the shaft supported by single-row radial ball bearings, we find that the behavior of the whirling motion is quite different from that of the shaft when supported by self-aligning double-row ball bearings. For example, the critical speeds of sub-harmonic oscillation appear only in the shaft suported by single-row radial ball bearings. By experiments it has been cleared up that such difference of the whirling motions of shafts occurs because of the difference in the spring characteristics. In other words, when we use self-aligning double-row ball bearings, the spring characteristics are always linear; on the other hand, a shaft supported by single-row radial ball bearings has non-linear and non-symmetrical spring characteristics provided that the bearing center lines of upper and lower bearing pedestals are not in alignment.

2. Angular clearance of single-row radial ball bearing

When we fix the outer ring of radial ball bearing to bearing pedestal, the inner ring of the self-aligning double-row ball bearing turns freely around the axis perpendicular to the center line of bearing, and the inner ring of the single-row radial ball bearing does not seem to turn. But on closer observation, we find that even the latter can move slightly within a very small angle, *viz.*, the single-row radial ball bearing also has the self-alignment but within a very small angle.

To observe this behavior, we perform the following experiment for single-row radial ball bearing of 10 mm dia. (#6200) which is used in our experimental apparatus. As shown in Fig. 2, force W is exerted upon the horizontal shaft supported by single-row radial ball bearing, the outer ring of which is fixed to the pedestal and thus the moment about the center point O of the bearing exerts on the shaft. The inclination angle of shaft is measured by the dial gauge, as shown in Fig. 2. According to such procedure, we can obtain moment—inclination angle curves, as illustrated in Fig. 3. Observing these curves, we can see that there is an "angular clearance" in which the magnitude of inclination angle suddenly

changes. The angular clearance is about 1.5° in the curves of the left-hand figure of Fig. 3 and about 0.35° in the right-hand figure. As the result of measuring numerous ball bearings, it is found that the magnitudes of anglar clearance are within 0.2°~2.0°, and chiefly within 0.3°~0.5°. In Fig. 3, the curves shift to right-hand side because of the pressure needed for measurement of dial gauge.

In Fig. 4, let O be the center of single-row radial ball bearing and $\angle AOB$ a small angular clearance of ball bearing, and CC a center line of the shaft. Inclination of shaft requires no moment so long as the center line CC is located within the angle $\angle AOB$. As we can easily see in Fig. 3, if we wish to incline the shaft beyond $\angle AOB$, a moment must be applied to the shaft. Consequently, when the inclination angle of the elastic curve of the shaft at both ends of the shaft are smaller than angular clearance, the shaft is supported freely, even if we use single-row radial ball bearings, and the shaft does not become a fixed shaft until the inclination angles increase beyond the angular clearance.

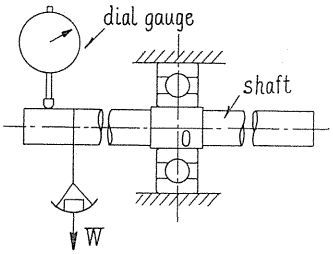

FIG. 2. Measurement of angular clearance.

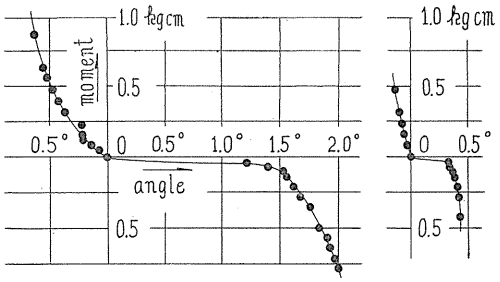

FIG. 3. Moment—inclination angle curves.

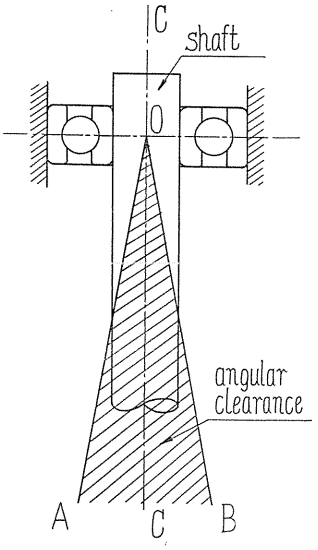

FIG. 4

3. Non-linearity of spring characteristics[3]

If bearing center lines of both upper and lower bearing pedestals are in alignment, the equilibrium position of shaft is located at the middle of an angular clearance as shown in Fig. 5, and spring constants of the shaft are those found in a shaft freely supported when deflection of shaft is smaller than a certain magnitude. Obviously this magnitude of deflection is the one which appears in shaft when the inclination angle of elastic curve of shaft at shaft ends are equal to one-half the angular clearance of ball bearing.

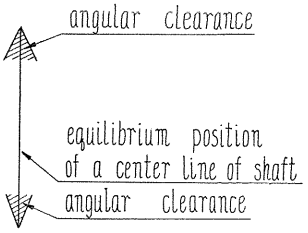

FIG. 5. Angular clearance.

Because it is impossible for the principal axis of the disc to coincide exactly with the center line of shaft, a small angle τ as well as inevitable eccentricity e may exist as a result of the deviation from an ideal mounting of disc. Additionally, since the disc is not mounted on the shaft at the middle, *i.e.*, $a \neq b$ (see Fig. 1), gyroscopic moment appears when the shaft rotates and deflects. Therefore not only force but also moment is exerted on the disc during rotation of shaft because of the existance of a small deviational angle τ and a gyroscopic moment.

Although the deflection and inclination angle of the disc are determined by both magnitudes of force and moment exerted on the disc, if we assume that only force is exerted, the angular clearance is equal to 1.0°, the length of the shaft l (see Fig. 1) is 500 mm (in our experimental apparatus $l \fallingdotseq 500$ mm) and bearing center lines of both pedestals are in alignment, then the shaft is supported freely when the deflection is smaller than 0.75~1.5 mm, and the shaft becomes fixed when the deflection builds up more than 0.75~1.5 mm. This critical magnitude of deflection of shaft is determined by the ratio $a : b$, and 1.45 mm, 1.05 mm, 0.95 mm and 0.75 mm correspond to $a : b = 1 : 1$, $3 : 7$, $1 : 3$ and $1 : 4$ respectively. These critical magnitudes are considered to be fairly large deflections for our experimental apparatus and if the deflection of shaft increases more than these critical values, there is a risk of breaking the apparatus and therefore the guard ring G (see Fig. 1) is equipped to check the increase of deflections. Consequently in as much as we treat vibrations with amplitudes smaller than these critical deflections, spring constants of the shaft are those found in a shaft freely supported even if we use single-row radial ball bearings, provided that bearing center lines of both upper and lower pedestals are in alignment, *viz.*, the equilibrium position of the shaft is located at the middle of the angular clearance, as shown in Fig. 5.

However it is impossible for both bearing pedestals to be in exact alignment, and the equilibrium position of the shaft is not located at the middle of the angular clearance, as shown in Fig. 6. Accordingly, the shaft has various kinds of non-linear, non-symmetrical spring characteristics as will be explained later. In Fig. 7, we classify various conditions at the shaft ends. Denotion ① means that the equilibrium position of the shaft is at the middle of angular clearance and the condition of freely supported shaft is held during motion of the shaft; ② shows that the equlibrium position is located outside angular clearance and the shaft is always fixed; ③ indicates that the equlibrium position is located just at the boundary of angular clearance so that when the shaft deflects to one side, in Fig. 7 to the right-hand side, the shaft is supported freely and on the other hand when the shaft deflects to the other side, in Fig. 7 to the left-hand side, the shaft becomes fixed. Consequently in the case of ③, non-linear, non-symmetrical spring characteristics appear in the shaft. In the case of ④, the resting position of the shaft is located in the angular clearance but not at the middle of angular clearance; thus when the shaft displaces to one side, in Fig. 7 to the left-hand side, the shaft is freely supported for a comparatively small deflection and the shaft becomes fixed when the deflection reaches a certain magnitude, *viz.*, when the inclination

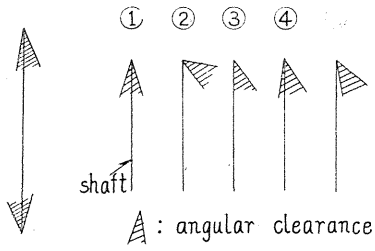

FIG. 6

FIG. 7

angle of the elastic curve at the shaft end reaches the boundary of the angular clearance, so that the condition of supporting of shaft changes at a certain value of deflection, and the shaft is fixed for a deflection larger than this critical value. On the other hand, if the shaft deflects to the other side, in Fig. 7 to the right-hand side, the shaft is always fixed; then in the case of ④ the non-linear, non-symmetrical characteristics also appear. In the case of ⑤, the equilibrium position is located outside the angular clearance, close to the boundary. Therefore when the shaft deflects to one side, in Fig. 7 to the right-hand side, it is fixed within a somewhat smaller deflection but the deflection increases beyond a certain value where the center line of shaft reaches a boundary of angular clearance, and the condition of supporting changes and the shaft becomes freely supported. But if the shaft displaces to the other side, in Fig. 7 to the left-hand side, it is always fixed during motion. Consequently the non-linear, non-symmetrical characteristics also take place.

Furthermore, we may consider the case in which the center line of the shaft is located outside angular clearance when the deflection does not take place, and while the deflection is increasing, the center line enters within angular clearance and goes over the boundary line of angular clearance on the other side, increasing the deflection, and then again it is located outside angular clearance. But since deflection of shaft is considerably large in the above case, we should not take it into consideration for the reason already given. Therefore we can consider that all cases are only ①～⑤ as above stated.

In Fig. 8, we assume that straight line I represents the spring characteristic when the shaft is fixed at both ends of shaft; line II is the case in which the shaft is supported freely at the upper pedestal and is fixed at the lower pedestal; line III is a vice versa, and IV is the case when the shaft is supported freely at both pedestals. Thus, according to various combinations of the five cases represented in Fig. 7, many types of non-linear spring characteristics appear, as shown in Fig. 9. In Fig. 9, for example, the notation ⑤+① means a combination in which the situation at upper pedestal is ⑤ and that in lower pedestal is ①, other notations representing similar meanings. In so far as we consider the five situations at shaft ends, above mentioned, all cases of combinations are shown in Fig. 9. In Fig. 9, we may group all conditions into three classes, 1～11, 12～19 and 20～25, according to qualitative analogy of spring characteristics. The center lines of the shaft at both upper and lower ends reach the boundary line of angular clearance simultaneously in the cases of 7, 9 and 11. In cases 15 and 16; 17 and 18; 24 and 25, Nos. 15, 17 and 24 represent cases in which the center line at upper shaft end reaches the boundary line earlier than at lower shaft end, and Nos. 16, 18 and 25 are vice versa. Although spring characteristic curves shown in Fig. 9 have distinct breaking points at which stiffness of shaft changes suddenly, the stiffness may vary somewhat slowly in actual characteristic curves, as shown in Fig. 12. In assembling experimental apparatus, it was practically impossible for the bearing center lines of both pedestals to be in exact alignment. Furthermore, even if we could assemble the apparatus in alignment, the situation would become the same as that not in alignment when the outer ring

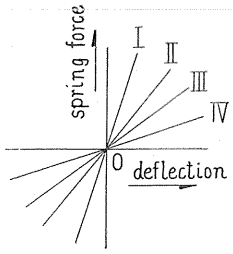

FIG. 8

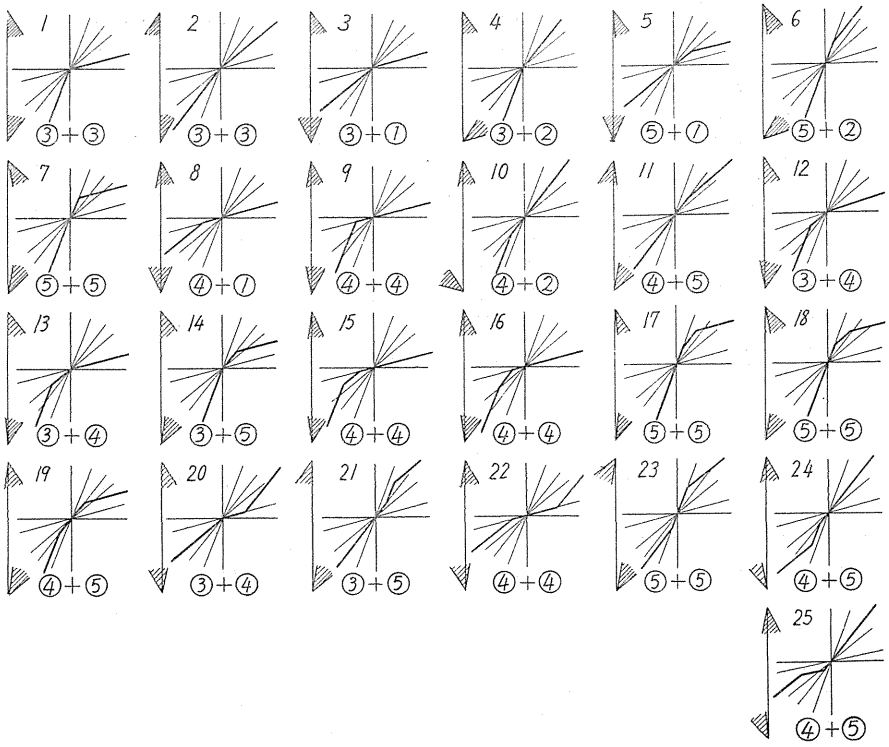

FIG. 9. Various types of non-linear spring characteristics.

of ball bearing is not correctly inserted into the bearing pedestal, or the groove in outer ring is incorrectly machined. Consequently it is inevitable that non-linear, non-symmetrical spring characteristics appear in stiffness of shaft, as shown in Fig. 9. Fig. 12 illustrates non-linear spring characteristics obtained by experiment.

We should next take into consideration the fact that the shaft is never equally stiff in all directions, *viz.*, the shaft has a directional non-uniformity of stiffness. If the non-linearity appears in spring characteristics and, moreover, if this non-linear spring characteristic itself is equal in all directions, the magnitude of stiffness of the shaft does not change and is always held constant during the circular whirl of shaft with a constant deflection of shaft. Consequently such a circular motion is substantially different from the rectilinear non-linear vibration in which the spring stiffness continuously varies according to the changing magnitude of deflection. Thus such circular motion cannot be regarded as essentialy the same as that in non-linear system, and high-harmonic oscillation or sub-harmonic oscillation does not take place in such a system. In so for as whirling motion is concerned, occurrence of sub-harmonic oscillation and of other non-linear vibrations needs the directional non-uniformity of non-linear spring characteristics.

Observing the construction of single-row radial ball bearings, we can conclude that this directional non-uniformity can take place. In Fig. 10, if the tangent of elastic curve of shaft at the shaft end reaches boundary line of angular clearance of ball bearing and the shaft becomes a fixed shaft, then the inner ring of ball bearing moves slightly on the center point O and the center line of the inner ring

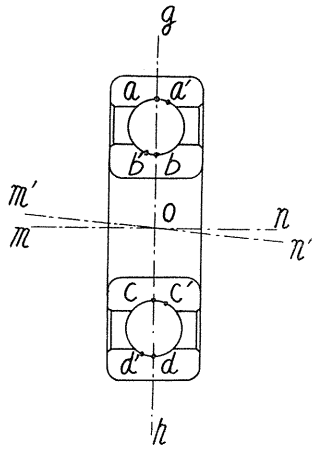

FIG. 10

moves from mn to $m'n'$. Thus the contact points a, b, c and d where balls contact the inner and outer ring of bearing move to a', b', c' and d' respectively, as shown in Fig. 10. Assuming that in this situation the inner ring turns around the axis gh perpendicular to axis mn, the resisting moment against rotation about axis gh takes place because of the forces existing at points a', b', c' and d' which are induced by inner ring twisting. But as moment arms aa', bb', cc' and dd' are very small, we may consider this resisting moment to be negligibly small. Therefore magnitude of rotation of inner ring $\angle non'$ does not exert any influence upon rotating motion of inner ring around axis gh. Consequently, for example, magnitude of deflection of shaft or inclination angle of disc in x-direction has no effect on the spring characteristic of shaft in y-direction. Then, for instance, if there is out of alignment between the center lines of both pedestals in x-direction (OA direction in Fig. 1), the non-linearity of spring characteristics of shaft takes place only in this direction and the stiffness of shaft is approximately linear in y-direction (OB direction) perpendicular to x-direction. Accordingly, non-linear, non-symmetrical spring characteristics with directional non-uniformity result from construction of single-row radial ball bearings.

4. Results of experiments

To prove that non-linearity appears in stiffness of shaft when single-row radial ball bearings are used, we perform the following experiment. As shown in Fig. 11, force W is exerted upon the edge of disc, and thus the moment about the disc center S exerts on disc. The inclination angle θ of disc is measured by a dial gauge and we can obtain moment-inclination angle θ curves, as illustrated in Fig. 12.

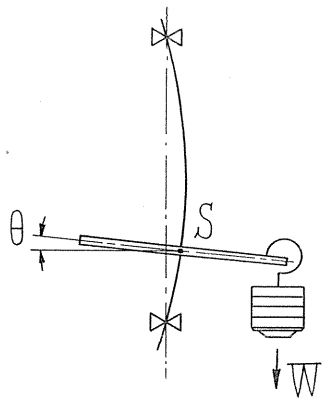

FIG. 11

Fig. 12 (a) shows results when a single-row radial ball bearing with angular clearance 0.6° is used in the upper bearing pedestal, and when ball bearing with angular clearance 1.5° is inserted into the lower pedestal. Ball bearings having angular clearances 0.2° and 0.5° are used in the upper and lower pedestals respectively in experiments shown in Fig. 12 (b). In Fig. 12, mark ○ indicates measuring point for single-row radial ball bearing and, for comparison, mark ● with straight lines is used for spring characteristics when self-aligning double-row ball bearings are used. AA in Fig. 12 shows spring characteristics in OA direction (x-direction) and BB in OB direction (y-direction) when single-row radial ball bearings are used; CC indicates spring characteristic when self-aligning double-row ball bearings are used. Characteristic curve CC shows that when self-aligning

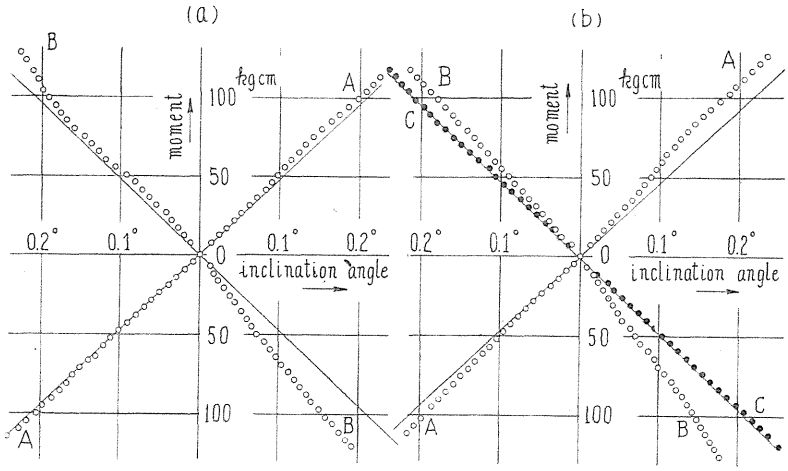

FIG. 12. Moment—inclination angle curves (shaft No. 1, $a : b = 3 : 7$)

double-row ball bearings are used the spring characteristics become perfectly linear and, moreover, the stiffness of shaft is smaller than when single-row radial ball bearings are used. In experiments shown in Fig. 12, the disc diameter is 482.8 mm, thickness 5.22 mm, weight 7.804 kg, moment of inertia I about disc diameter 1.114 kg cm sec.^{2}, and the shaft diameter is 11.89 ϕ, length 508.3 mm, $a : b = 3 : 7$. Observing characteristic curves AA and BB in Fig. 12, we can see that they are non-linear and non-symmetrical and differ from each other, that is, there is directional non-uniformity of stiffness of shaft. Although there is a difference between x- and y-directions, the natural frequency p which is a function of rotating speed of shaft ω is the same in all directions when $\omega \neq 0$ since the gyroscopic moment appears in this system and the motions in x- and y-directions are coupled together.[1] But when $\omega = 0$, the motions in these directions are independent of each other; thus the natural frequency p_0 when $\omega = 0$ in x-direction is not equal to that in y-direction provided that spring characteristics in x- and y-directions are different from each other. The values of p_0 obtained by experiment are as follows:

1) For Fig. 12 (a). Angular Clearance Upper: 0.6°, Lower: 1.5°

	p_0 in r.p.m.		
OA direction (curve AA)	1,035	1,036	1,038
OB direction (curve BB)	1,052	1,053	1,056

2) For Fig. 12 (b). Angular Clearance Upper: 0.2°, Lower: 0.5°

	p_0 in r.p.m.		
OA direction (curve AA)	1,136	1,138	1,147
OB direction (curve BB)	1,190	1,191	1,192

3) For Self-Aligning Double-Row Ball Bearing

	p_0 in r.p.m.		
OA direction	1,029	1,029	1,030
OB direction	1,024	1,025	1,026

When a self-aligning double-row ball bearing is used, p_0 in *OA* direction is 0.4% larger than in *OB* direction as shown in 3). On the contrary, for 1) and 2) (single-row radial ball bearing), p_0 in *OA* direction is less than in *OB* direction by 1.7% for the former and 4.6% for the latter. The fact that p_0 in *OB* direction is larger in 1) and 2) is verified by observation of characteristic curves *AA* and *BB* in Fig. 12. Because the upper and the lower pedestals are not made in one body but are manufactured separately, lack of alignment of center lines in assembling of bearing pedestals is apt to appear in *OB* direction and not in *OA*. Thus non-linearity appears remarkably only in *OB* direction and stiffness of shaft is larger there; therefore p_0 in *OB* is larger than in *OA*. On the other hand, since the shaft is always freely supported and the spring characteristic is linear when self-aligning double-row ball bearings are used, the spring constant of shaft itself is equal in all directions. The bearing pedestals have some little elasticity and the flexibility of pedestals in *OB* direction is more marked than in *OA* direction. Taking this into consideration, rigidity of shaft in *OB* is less than in *OA* when the stiffness of shaft is considered together with that of pedestals. Consequently, in 3), p_0 in *OA* is somewhat larger than in *OB*, as shown in the above table.

By experiments shown in Fig. 12, or by considering the values of p_0, we prove that non-linearity with directional non-uniformity takes place in practical experimental apparatus when single-row radial ball bearings are used.

Incidentally, when $a \neq b$ the shaft has four spring characteristics: the relation between force-deflection, between force-inclination angle θ, between moment-deflection, and between moment-inclination angle.[1] Of these characteristics, the moment-inclination angle curve can be experimentally obtained most exactly, therefore in the present section we consider this curve as shown in Fig. 12.

5. Differential equations of motions of disc when single-row radial ball bearings are used

When the spring characteristics are linear,[1] the differential equations of motion of disc are

$$\left.\begin{aligned} &m\ddot{x} + \alpha x + \gamma\theta_x = me\omega^2 \cos \omega t, \\ &m\ddot{y} + \alpha y + \gamma\theta_y = me\omega^2 \sin \omega t, \\ &I\ddot{\theta}_x + I_p\omega\dot{\theta}_y + \gamma x + \delta\theta_x = (I_p - I)\tau\omega^2 \cos(\omega t + \beta), \\ &I\ddot{\theta}_y - I_p\omega\dot{\theta}_x + \gamma y + \delta\theta_y = (I_p - I)\tau\omega^2 \sin(\omega t + \beta). \end{aligned}\right\} \tag{2.1}$$

When there is no alignment between center lines of bearing pedestals in x-direction, and furthermore, there are small damping forces in the system, the equations can be rewritten

$$\left.\begin{aligned} &m\ddot{x}+c_x\dot{x}+\alpha x+\gamma\theta_x+f_x(x,\ \theta_x)=me\omega^2\cos\omega t,\\ &m\ddot{y}+c_y\dot{y}+\alpha y+\gamma\theta_y=me\omega^2\sin\omega t,\\ &I\ddot{\theta}_x+I_p\omega\dot{\theta}_y+c_{\theta x}\dot{\theta}_x+\gamma x+\delta\theta_x+f_{\theta x}(x,\ \theta_x)=(I_p-I)\tau\omega^2\cos(\omega t+\beta),\\ &I\ddot{\theta}_y-I_p\omega\dot{\theta}_x+c_{\theta y}\dot{\theta}_y+\gamma y+\delta\theta_y=(I_p-I)\tau\omega^2\sin(\omega t-\beta). \end{aligned}\right\} \quad (2.2)$$

In (2.1) and (2.2), x and y are deflections of disc center S in x and y directions respectively; θ_x and θ_y are components of inclination angles of disc θ in x and y directions; α, γ and δ are spring constants of shaft; m is mass of disc; I_p is polar moment of inertia; I moment of inertia about diameter of disc; e eccentricity of disc; τ small deviational angle between the plane of disc and the plane which is orthogonal to the tangent of the deflection curve of shaft at the disc center S; β the angle between directions e and τ; ω the rotating speed of shaft; c_x, c_y, $c_{\theta x}$ and $c_{\theta y}$ coefficients of damping, and f_x and $f_{\theta x}$ are non-linear terms of x and θ_x. When the disc is mounted correctly on the shaft and the principal axis of moment of inertia at the disc center S coincides with the center line of shaft, deviational angle τ has obviously vanished. As remarked in section 4, when there is no alignment of center lines of bearing pedestals in x-direction, non-linearity of stiffness appears only in x-direction and stiffness of shaft in y-direction is linear; therefore non-linear terms appear only in equations of x and θ_x. Furthermore, magnitudes of x and θ_x do not have any influence upon spring characteristics in y-direction, and y and θ_y are independent of characteristics in x-direction; hence non-linear terms f_x and $f_{\theta x}$ are not functions of y and θ_y but only of x and θ_x.

In general f_x and $f_{\theta x}$ can be represented as follows:

$$f_x=A_0+\sum_{n=1}^{\infty}A_nx^n+\sum_{n=1}^{\infty}B_n\theta_x^n+\sum_{\substack{j=1\\k=1}}^{\infty}C_{jk}x^j\theta_x^k. \qquad (j\neq k) \quad (2.3)$$

Eq. of $f_{\theta x}$ is similar to (2.3). In (2.3), A_0 is a constant term and n is not only an odd number but also an even number because of non-linear and non-symmetrical spring characteristics.

Chapter III. On the Critical Speed of a Shaft of Sub-Harmonic Oscillation and on Sub-Harmonic Oscillation of Rectilinear Vibrations[3]

1. Introduction

When we rotate a shaft supported by single-row radial ball bearings, a whirling motion in which the whirling angular speed is just one-half of the rotating speed of shaft ω appears at higher speed than the major critical speed ω_c. This whirling motion is that of forward precession and the deflection curve of shaft makes just one revolution during the time the shaft makes two revolutions. Amplitude of this motion builds up remarkably at some rotating speed higher than ω_c, and the phenomenon of critical speed takes place. In the region about this critical speed, only amplitudes of vibrations with frequency $1/2\,\omega$ increase to form the peak of this critical speed; amplitudes with frequency ω are unchanged and very small. When self-aligning double-row ball bearing are used, these vibrations do not occur.[1] This fact suggests that the cause of occurrence of these vibrations is the non-

linearity of spring characteristics of shaft.

2. Results of experiments

In Fig. 13 we give experimental results of the critical speed of sub-harmonic oscillations of order 1/2 obtained by using single-row radial ball bearings with angular crearance. In Fig. 13, the marks ◫ and ◑ represent amplitudes of harmonic oscillation with frequency ω; ○ and ● represent amplitudes of sub-harmonic oscillation of order 1/2 with frequency $1/2\,\omega$; ◫ and ○ are vibrations in x-direction, ◑ and ● those in y-direction. Shaft No. 1 used in experiment shown in Fig. 12 is also used in experiment shown in Fig. 13. In Fig. 13 (a) ball bearings with angular clearance 0.3° are used in both upper and lower pedestals. In Figs. 13 (b_1) and (b_2) ball bearings with 0.2° and 1.5° angular clearances are used, and in Figs. 13 (c_1), (c_2) and (c_3) the upper and the lower ball bearings have angular clearances 0.6° and 1.5° respectively. In Figs. 13 (b_1) and (b_2); (c_1), (c_2) and (c_3), the only difference is in the assembly condition of bearing pedestals; all other conditions remain the same. On close observation, we find that there is a considerable difference in magnitudes of peaks of critical speeds and in locations of critical speeds between Figs. 13 (b_1) and (b_2); (c_1), (c_2) and (c_3), and that this difference is because of a difference in assembly condition of the pedestals. According to results of experiments, the considerable out of alignment between the center lines of both pedestals does not always furnish large peaks of amplitudes of sub-harmonic oscillation, and it is difficult to anticipate the magnitude of amplitudes by the degree of angular clearance and the assembly condition of pedestals. In as much as single-row radial ball bearings are used, critical speeds of whirling motion of sub-harmonic oscillations almost always take place, the exceptions being very few.

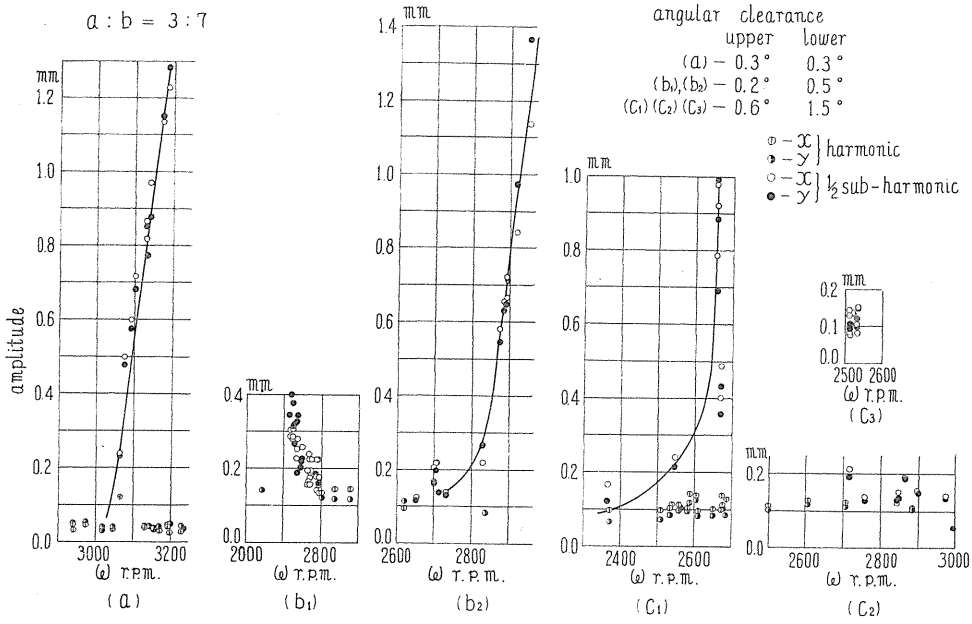

FIG. 13. Response curves of sub-harmonic oscillation of order 1/2 (whirl of forward precession) (shaft No.1).

Experimental results of occurrence of sub-harmonic oscillation in horizontal shaft No. 4 are shown in Fig. 14. In this experiment disc is mounted in middle of shaft ($a=b$ in Fig. 1), the angular clearances are 0.2° and 0.5°, and disc is the same as in Figs. 12 and 13. In Fig. 15, critical speed appearing in vertical shaft No. 5 ($a:b=3:1$, $a>b$) is shown where disc is the same as in Figs. 12, 13 and 14, and angular clearances are 0.3° in both ball bearings. In experiment shown in Fig. 16, shaft No. 3 ($a:b=1:4$) is used, and angular clearances in both upper and lower ball bearings are 0.3°.

Curves of natural frequency p to rotating speed ω in experiment shown in Fig. 13 (a), are given in Fig. 17. Although the system is non-linear, and stiffness of shaft varies somewhat according to magnitudes of deflection, $p-\omega$ curves in Fig. 17 are given by the values of p_0, ω_c, m and I all of which are obtained by experiment or actual measurement. Here p_0 is the natural frequency when $\omega=0$, and ω_c is the major critical speed. Evidently the four $p-\omega$ curves in Fig. 17 are qualitatively the same as those in the linear system where self-aligning double-row ball bearings are used,[1] and we can see that four natural frequencies p_1, p_2, p_3 and p_4 exist in a certain revolution ω. In Fig. 17, curves I and II give free vibrations having the mode of forward precession in which the direction of whirling is the same as that of rotation of the shaft; curves III and IV represent free vibrations having the mode of backward precession, in reverse direction to ω. In Fig. 17 point A, at which the straight line $\omega=p$ and curve II intersect, shows the major critical speed ω_c and point B, where line $\omega=2p$ and curve II cross, gives the critical speed ω_1 of sub-harmonic oscillation of order 1/2 at which the peak of whirling of forward precession takes place. We obtain from Fig. 17, $\omega_c=1{,}490$ r.p.m. and $\omega_1=3{,}170$ r.p.m.

In numerous experiments the peaks of sub-harmonic oscillation of order 1/2 with the mode of backward precession did not appear. For instance, if such vibrations were obtained in experiment shown in Fig. 13 (a), these peaks would appear in the neighborhood of ω_2 and ω_3 given in Fig. 17 by cross points C and D where line $\omega=-2p$ intersects curves III and IV. But in actual experiments no vibration occurs in the neighborhood of ω_2 and ω_3.

Reproduction of the oscillographic paper of whirling of sub-harmonic oscillation with the mode of forward precession is given in Fig. 18 where vertical white lines are rotating marks recorded at each revolution by a small piece of paper P (see Fig. 1), and fine white horizontal lines are furnished by a scale of 1.0 mm put on the slit for measuring the amplitudes of vibration. In Fig. 18-I amplitudes are the largest; in Fig. 18-III the smallest. Optical magnification in x-direction is smaller than that in y-direction. Observing vibratory waves in Fig. 18, we can see that the deflection curve of shaft turns just one revolution during each two revolutions of shaft. Determination of the whirling motion which is forward and backward precession is carried out by comparing phases of vibratory waves in x and y directions. The locus of disc center S in xy-plane obtained from vibratory waves on the oscillographic paper is shown in Fig. 19 where the interval from one double circular mark ◎ to the next indicates one revolution of shaft, and the curve is the locus on which the disc center S moves during the time interval of two revolutions of shaft. The direction of rotation of shaft is anti-clockwise in the figure. In whirling motion of sub-harmonic oscillation of order 1/2, the motion of disc center S is represented by

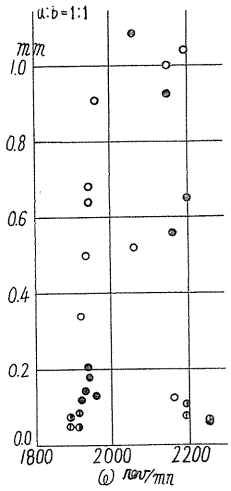

FIG. 14. Resonance diagram of sub-harmonic oscillation (shaft No. 4, $a : b = 1 : 1$).

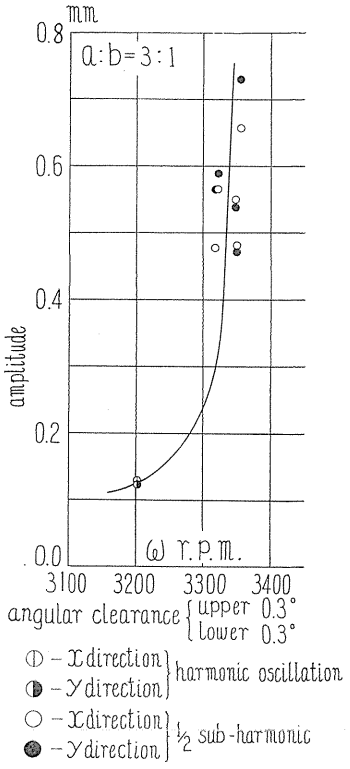

FIG. 15. Peak of sub-harmonic oscillation of order 1/2 (shaft No. 5, $a : b = 3 : 1$).

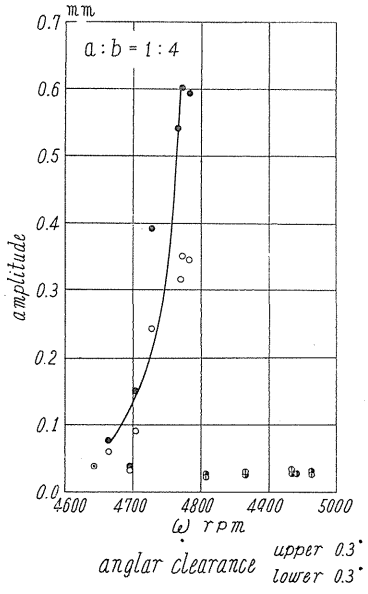

FIG. 16. Response curve of sub-harmonic oscillation of order 1/2 (shaft No. 3).

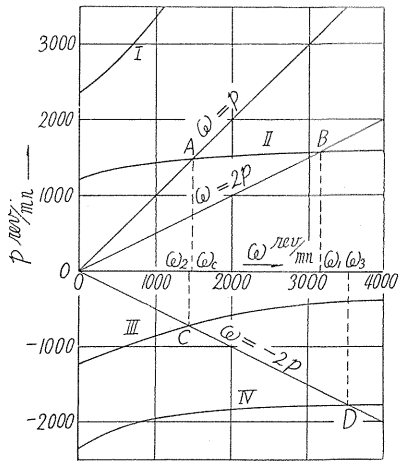

FIG. 17. $p - \omega$ diagram (shaft No. 1, $a : b = 3 : 7$).

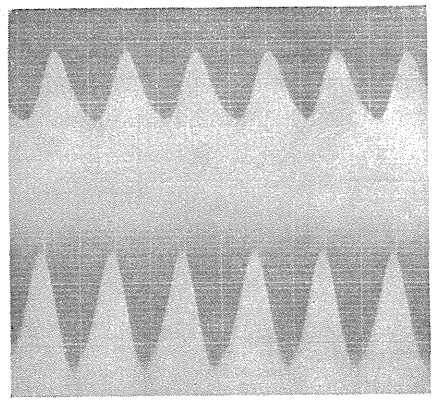

FIG. 18-I

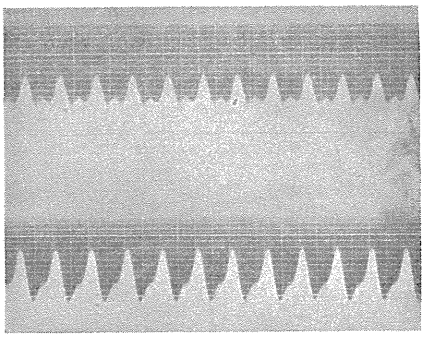

FIG. 18-II

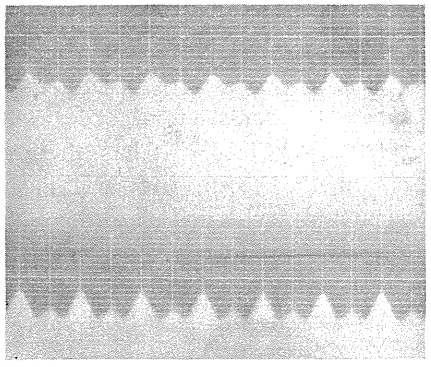

FIG. 18-III

FIG. 18. Oscillographic paper of sub-harmonic oscillation of order 1/2 (forward precession).

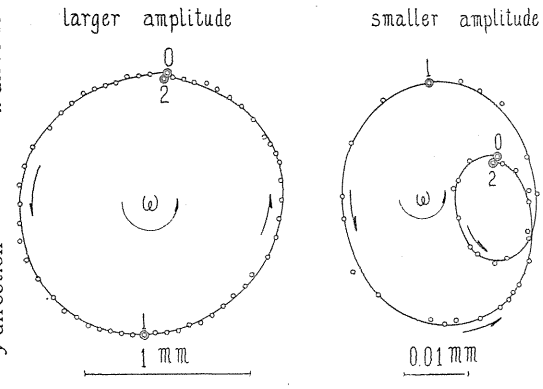

FIG. 19. Path of whirl in sub-harmonic oscillation of order 1/2.

$$\left.\begin{aligned} x &= A\cos\omega t + B\cos\frac{1}{2}\omega t, \\ y &= A\sin\omega t + B\sin\frac{1}{2}\omega t, \end{aligned}\right\} \qquad (3.1)$$

where A is amplitude of forced vibration induced by eccentricity e and deviational angle τ, B is that of sub-harmonic oscillation and takes positive value because of forward precession. Consequently, locus given by (3.1) is an epitrochoid as shown in the right-hand side of Fig. 19. But when amplitude B builds up remarkably large, *i.e.*, $A \ll B$, locus becomes almost circular as shown in the left-hand side of Fig. 19. In Fig. 19, the direction of whirling motion is anti-clockwise as well as ω, because of forward precession.

3. Jump phenomena

It is well known that jump phenomena appear in sub-harmonic oscillation of rectilinear vibration in the non-linear system with one degree of freedom. Even in whirling motion of sub-harmonic oscillation in non-linear system with multiple degrees of freedom and gyroscopic terms, jump phenomena take place in the response curve obtained by experiments.

When the scale of abscissa in Fig. 13 (a) is enlarged, response curve shown in Fig. 20 is given. As the rotating speed of shaft ω increases, amplitude of

harmonic oscillation moves along AB and reaches B where whirling motion of sub-harmonic oscillation takes place. When ω successively increases, amplitude of sub-harmonic oscillation gradually enlarges and passes through B, G and C; then jumps from C to D, where sub-harmonic oscillation has already vanished, to reach E. When ω is retarded, amplitude of harmonic oscillation moves along E, D and F, and the jump phenomenon takes place at $\overrightarrow{FG}$. Thereafter amplitude of sub-harmonic oscillation changes along GB. Rotating speeds at points C and F, where jump phenomena occur, are 3,180 r.p.m. and 3,124 r.p.m. respectively. Fig. 20 clearly shows that response curves of whirling motion of sub-harmonic oscillation as well as those of rectilinear vibration, have well known figures peculiar to non-linear systems.

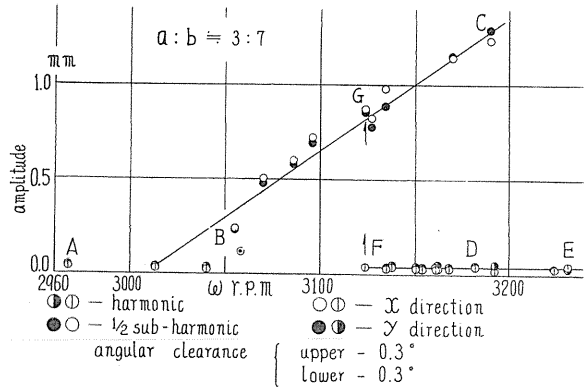

FIG. 20. Jump phenomena in response curves of sub-harmonic oscillation of order 1/2 (shaft No. 1, $a : b = 3 : 7$).

In our experiments, whirling motion of sub-harmonic oscillation of order 1/3 and so on does not appear; only that of order 1/2 is obtained. It has already been reported that in rectilinear vibrations of non-linear system with back-lash and non-symmetrical spring characteristics, sub-harmonic oscillation of order 1/2 most frequently takes place; occurrence of order 1/3 is rather exceptional.[4] Results of our experiments are in good agreement with this.

4. Sub-harmonic oscillation when shaft does not rotate ($\omega = 0$)

Although there are various kinds of vibration induced by exciting forces furnished by rotating ball bearings with machining errors, we can conclude experimentally that the sub-harmonic oscillation of order 1/2 appearing in the rotating shaft is not caused by such a rotating ball bearing, but simply by non-linear, non-symmetrical spring characteristics of shaft. For the purpose of proving this point, the following experiments are carried out. Another purpose is to verify experimentally that the shaft has non-linear stiffness when single-row radial ball bearings are used and, further, that sub-harmonic oscillation of rectilinear vibration can

take place also in multiple degrees of freedom system without gyroscopic terms.

When a flexible pedestal, as indicated by pedestal I in Fig. 38 (a), is used for the upper pedestal, and rotating body with eccentricity is set up on top of this pedestal, the pedestal deflects slightly in OB-direction (see Fig. 1) by the centrifugal force due to eccentricity and does not deform in OA-direction where stiffness of pedestal is considerable. Consequently a periodic external force with frequency ω_0 exerts on disc in OB-direction and the forced vibration in this direction takes place. Here ω_0 is the angular velocity of the rotating body set up on pedestal, and stiffness of the upper flexible pedestal is about 1.15×10^3 kg/cm at the top of pedestal. When the shaft does not rotate ($\omega=0$) and external force of frequncy ω_0 is applied only in OB-direction, then the system becomes two degrees of freedom system and the differential equations are

$$\left.\begin{aligned} m\ddot{x}+\alpha x+\gamma\theta &= F_1\omega_0^2\cos\omega_0 t,\\ I\ddot{\theta}+\gamma x+\delta\theta &= F_2\omega_0^2\cos\omega_0 t,\end{aligned}\right\} \tag{3.2}$$

$$\left.\begin{aligned} m\ddot{x}+\alpha x+\gamma\theta+f_x(x,\ \theta) &= F_1\omega_0^2\cos\omega_0 t,\\ I\ddot{\theta}+\gamma x+\delta\theta=f_\theta(x,\ \theta) &= F_2\omega_0^2\cos\omega_0 t,\end{aligned}\right\} \tag{3.3}$$

where x is defection in OB-direction, θ inclination angle of disc, f_x and f_θ non-linear terms. Linear system is governed by (3.2), and (3.3) represents motions in non-linear system. Clearly (3.2) and (3.3) are differential equations of two degrees of freedom system without gyroscopic terms.

Response curves when $\omega=0$ are shown in Fig. 21, where p_1 ($=1{,}025$ r.p.m.) is the lower major critical speed, and p_2 ($=1{,}940$ r.p.m.) the higher major critical speed. In neighborhood of $\omega_0=2p_1=2{,}050$ r.p.m., the peak of sub-harmonic oscillation of order 1/2 of rectilinear vibration occurs. In this experiment, shaft No. 1 ($a:b=3:7$) is used and

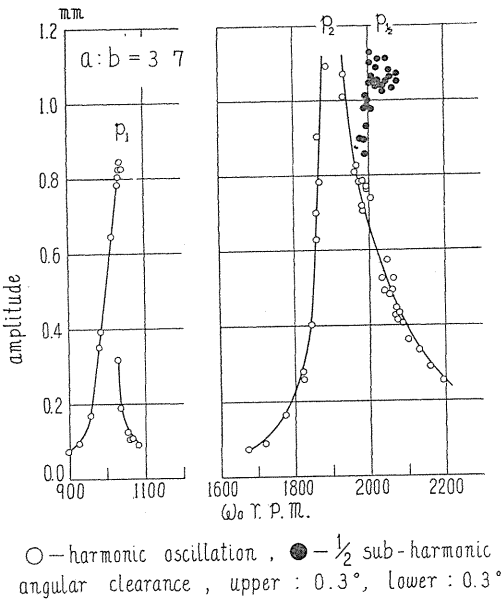

FIG. 21. Response curve of rectilinear vibration (ω_0: frequency of external force, shaft No. 1).

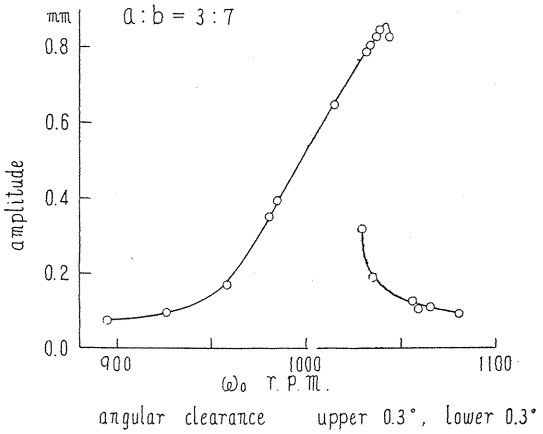

FIG. 22. Typical response curve of non-linear system.

angular clearance in both upper and lower ball bearings are 0.3. In Fig. 21, vibrations with amplitudes larger than 1.0 mm contact guard ring G (Fig. 1). Enlarging the scale of abscissa of the left-hand figure in Fig. 21, we obtain Fig. 22 which shows a typical response curve of non-linear system with hard spring. When eccentricity of rotating body set on pedestal is small, that is when F_1 and F_2 in (3.2) and (3.3) are small, the response curve becomes that as shown in Fig. 23.

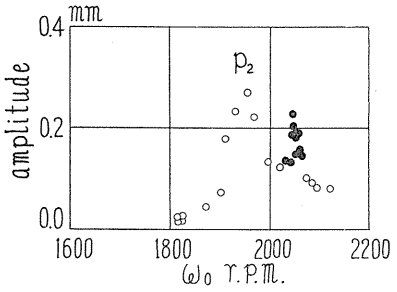

FIG. 23

By experimental results given in Figs. 21, 22 and 23, we can conclude that non-linearity appears in stiffness of shaft when single-row radial ball bearings are used, and that sub-harmonic oscillation of order 1/2 of rectilinear can occur even in multiple degrees of freedom systems without gyroscopic terms.

5. Sub-harmonic oscillation in multiple degrees of freedom system

To verify the occurrence of sub-harmonic oscillation in the multiple degrees of freedom system with non-linear spring characteristics and without gyroscopic terms, the following experimental apparatus is used. As shown in Fig. 24, a vertical shaft of 2.0 ϕ mounting two masses D_1 and D_2 is supported by a ball bearing at B_1 and at B_2. By varying clearances C_1 and C_2 between one end of the shaft and the ajusting screws S_1 and S_2, we can obtain various spring characteristics of shaft. Frame F, on which the shaft is set up, is mounted on a vibratory table T which is supported on a flat surface by steel balls and is oscillated by crank and connecting-rod mechanism; thus external force can exert on mass D_1 and mass D_2 and forced vibration appears. Amplitude of oscillation of oscillatory table is about 0.2 mm and span of shaft is about 260 mm. In experiment, amplitudes of mass D_2 and frequency ω_0 of external force are recorded on oscillographic paper by optical method. In this vibratory system, let x_1 and x_2 be displacements of D_1 and D_2; let θ_1 and θ_2 be inclination angles of D_1 and D_2; let m_1 and m_2 be masses of D_1 and D_2, and let I_1 and I_2 be moments of inertia of D_1 and D_2. Differential equations of motions then are

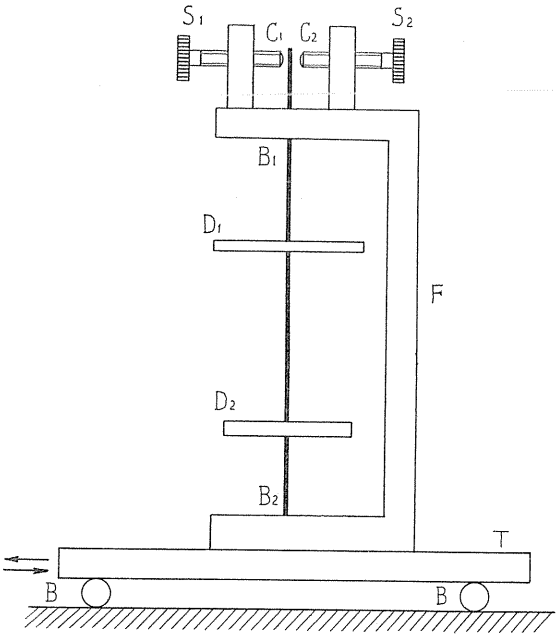

FIG. 24. Experimental apparatus.

$$\left.\begin{aligned} &m_1\ddot{x}_1+\alpha_{11}x_1+\alpha_{12}x_2+\alpha_{13}\theta_1+\alpha_{14}\theta_2=F_1\cos\omega_0 t,\\ &m_2\ddot{x}_2+\alpha_{21}x_1+\alpha_{22}x_2+\alpha_{23}\theta_1+\alpha_{24}\theta_2=F_2\cos\omega_0 t,\\ &I_1\ddot{\theta}_1+\alpha_{31}x_1+\alpha_{32}x_2+\alpha_{33}\theta_1+\alpha_{34}\theta_2=F_3\cos\omega_0 t,\\ &I_2\ddot{\theta}_2+\alpha_{41}x_1+\alpha_{42}x_2+\alpha_{43}\theta_1+\alpha_{44}\theta_2=F_4\cos\omega_0 t, \end{aligned}\right\} \tag{3.4}$$

where α_{ij} is spring constant of shaft. Consequently this system is four degrees of freedom system without gyroscopic terms. When non-linearity appears in spring characteristics, differential equations become

$$\left.\begin{aligned} &m_1\ddot{x}_1+\alpha_{11}x_1+\alpha_{12}x_2+\alpha_{13}\theta_1+\alpha_{14}\theta_2+f_1(x_1,\ x_2,\ \theta_1,\ \theta_2)=F_1\cos\omega_0 t,\\ &m_2\ddot{x}_2+\alpha_{21}x_1+\alpha_{22}x_2+\alpha_{23}\theta_1+\alpha_{24}\theta_2+f_2(x_1,\ x_2,\ \theta_1,\ \theta_2)=F_2\cos\omega_0 t,\\ &I_1\ddot{\theta}_1+\alpha_{31}x_1+\alpha_{32}x_2+\alpha_{33}\theta_1+\alpha_{34}\theta_2+f_3(x_1,\ x_2,\ \theta_1,\ \theta_2)=F_3\cos\omega_0 t,\\ &I_2\ddot{\theta}_2+\alpha_{41}x_1+\alpha_{42}x_2+\alpha_{43}\theta_1+\alpha_{44}\theta_2+f_4(x_1,\ x_2,\ \theta_1,\ \theta_2)=F_4\cos\omega_0 t, \end{aligned}\right\} \tag{3.5}$$

where $f_{1,2,3,4}$ are non-linear terms.

Two samples of experimental results are given in Figs. 25 and 26. Harmonic oscillation is represented by, ○, sub-harmonic oscillation of order 1/2 by ◑, sub-harmonic oscillation of order 1/3 by ●, and ω_0 is frequency of external force. In Figs. 25 and 26, p_1 and p_2 are peaks of harmonic oscillation, and $p_{1/2}$ and $p_{1/3}$ peaks of sub-harmonic oscillation of orders 1/2 and 1/3 respectively. It is readily seen that jump phenomena can take place at p_1, p_2, $p_{1/2}$ and $p_{1/3}$. Fig. 25 shows the response curve of non-linear system with hard spring, and Fig. 26 with soft spring. For the case in Fig. 26, by actual measurement of the deflection x_2 of D_2 when only a force is exerted on D_2, we obtain the relation

$$F=10.32x_2-0.091x_2^2-0.0039x_2^3, \tag{3.6}$$

in which F is spring force and is expressed in grams and x_2 in mm. Since the coefficient of x_2^3 takes negative value, the system shown in Fig. 26 is that with soft spring, and thus response curve necessarily becomes that shown in Fig. 26.

In Figs. 27 and 28, vibratory waves of sub-harmonic oscillation of orders 1/2 and 1/3 obtained by experiments are shown. In Fig. 27 vertical short segment of line shows one period of external force. Obviously, the vibrations shown in Figs. 25, 26, 27 and 28 are not whirling motions but are all rectilinear vibrations.

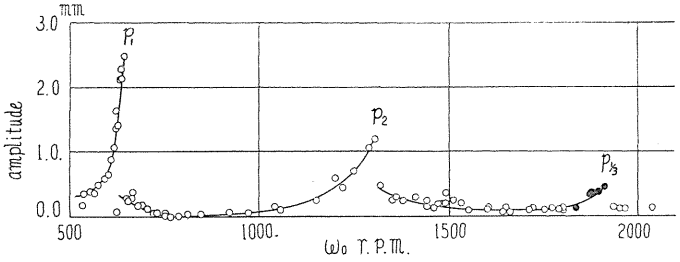

○ : harmonic oscillation
● : sub-harmonic oscillation of order 1/3

FIG. 25. Response curve.

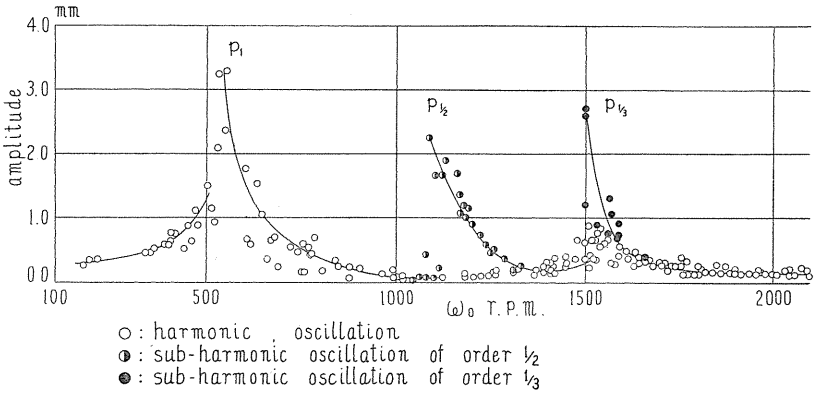

FIG. 26. Response curve.

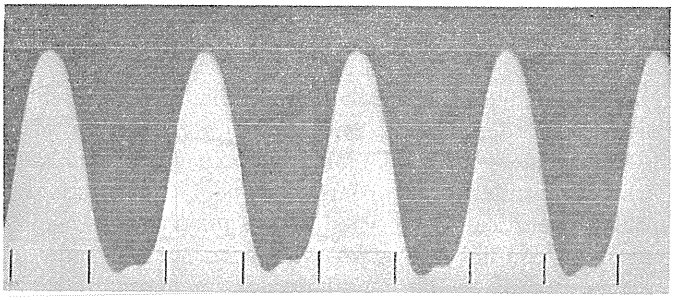

FIG. 27. Vibratory waves of sub-harmonic oscillation of order 1/2.

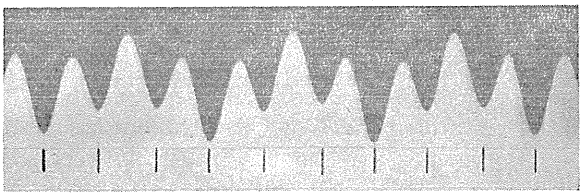

FIG. 28. Vibratory waves of sub-harmonic oscillation of order 1/3.

6. Conclusions

Obtained results by experiments stated in the present chapter may be summarized as follows:

1) When single-row radial ball bearings are used, non-linearity appears in stiffness of shaft, and whirling motion of sub-harmonic oscillation of order 1/2 builds up remarkably.

2) Such whirling motion is of forward precession and the peak of backward precession does not occur.

3) Whirling motion of sub-harmonic oscillation of order 1/3 or other orders does not appear.

4) Sub-harmonic oscillation order 1/2 can still take place in shaft when $\omega = 0$

and gyroscopic terms vanish.

5) Sub-harmonic oscillations can occur even in multiple degrees of freedom system without gyroscopic term as well as in one degree of freedom system.

6) In four degrees of freedom system, rectilinear sub-harmonic oscillation of order 1/3 as well as that of order 1/2 takes place in cases of both hard and soft springs.

For the shaft supported by journal bearings, and for the horizontal shaft supported by pedestals in alignment, sub-harmonic oscillation may take place through the same mechanism described in the present chapter. For the latter, occurrence of sub-harmonic oscillation is caused by the statical deflection of shaft through weight of rotor.

Chapter IV. On Critical Speeds of "Summed and Differential Harmonic Oscillations"[5]

1. Introduction

When a shaft is supported by single-row radial ball bearings, the stiffness of the shaft has non-symmetrical and non-linear spring characteristics, as explained in Chapter II. In experiments using such a shaft mounting one disc, several critical speeds of peculiar modes of vibration occur with the whirling motion of sub-harmonic oscillation of order 1/2. These critical speeds consist of two vibrations having the same frequencies of p_i and p_j as the natural frequencies of this system. Furthermore, it is remarkable that the absolute value of sum of or difference in two frequencies p_i and p_j is equal to the rotating speed of the shaft ω which is also the frequency of periodic external force induced by eccentricity e and small deviational angle τ, *i.e.*, $|p_i + p_j| = \omega$, and we may properly give the name of "summed and differential harmonic oscillations" to these vibrations. Although sub-harmonic oscillations can take place in one degree or multiple degrees of freedom system, these vibrations appear only in multiple degrees of freedom system with non-linear spring characteristics.

It is most interesting and worth while to point out here that in such critical speeds both of these two amplitudes of vibrations with frequencies p_i and p_j build up and form one peak of critical speed. This behavior is in distinct contrast to that of any other vibration. For instance, in forced, in sub-harmonic, and in self-excited vibrations, only one vibration builds up in resonance condition and forms the peak of amplitude of critical speed.

There are several kinds of these critical speeds with peculiar modes of vibrations which we call "summed and differential harmonic oscillations," and these vibrations as are also those described in Chapter III are whirling motions and not rectilinear vibrations. They are not induced by errors in ball bearing machining, as we shall see later.

2. Behavior of vibrations in resonant rotating speed

In this paper the following expressions are used to represent modes of vibration. Notation $[+ m\omega]$ is the motion having frequency of m times that of angular velocity ω where the positive sign $+$ represents a whirling motion of forward precession. On the other hand, negative sign $-$ means a backward precession, hence notation $[- n\omega]$ represents a whirling motion of backward precession with whirling speed

$n\omega$. For example, in accordance with this notation, the whirling motion of forward precession of sub-harmonic oscillation of order 1/2 discussed in the previous chapter is expressed by the notation $[+1/2 \cdot \omega]$.

Results of experiment in which we use shaft No. 3 ($a : b = 1 : 4$) supported by upper and lower single-row radial ball bearings, both with angular clearance of 0.3°, are shown in Fig. 29 where seven peaks of amplitudes appear. Peak II at $\omega_{1/2}$ = 4,780 r.p.m. of $[+1/2 \cdot \omega]$ is the critical speed of sub-harmonic oscillation of order 1/2 caused by non-linear, non-symmetrical spring characteristics, and Peak IV represented by $[-\omega]$ at $\omega_{b_1} = 2{,}788$ r.p.m. is the critical speed of synchronous backward precession, the occurrence of which shall be explained later, and Peak VI of $[+\omega]$ at $\omega_c = 2{,}200$ r.p.m. is the major critical speed. The remaining Peaks I, III, V and VII occurring at ω_1, ω_2, ω_3 and ω_5 respectively are those of vibrations discussed here. For example, expression $[p_2]+[p_4]$ or $[p_2]+[p_4] \fallingdotseq [7/15 \cdot \omega] + [-8/15 \cdot \omega]$ in Peak I means that Peak I consists of whirls of forward precession with frequency $p_2 = 7/15 \cdot \omega$ and of backward precession having frequency $p_4 = -8/15 \cdot \omega$.

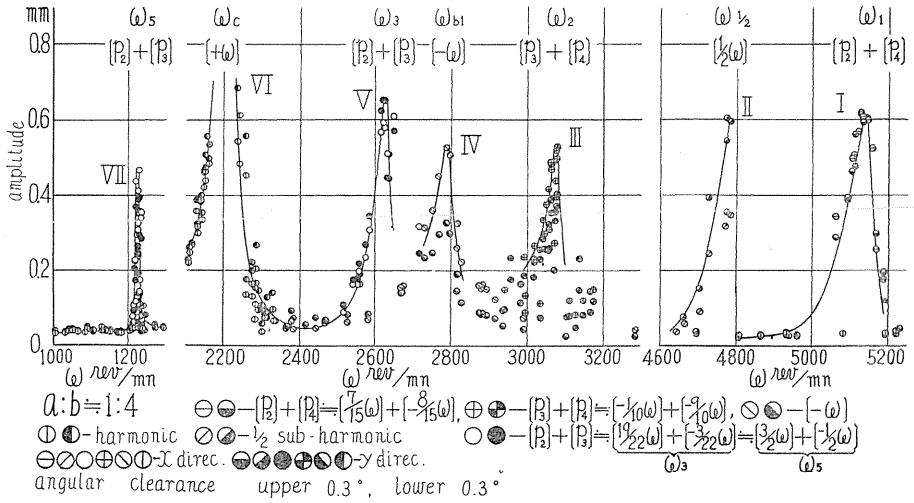

FIG. 29. Response curves of "summed and differential harmonic oscillations" (shaft No. 3).

Vibratory waves at Peaks I, III, V and VII of Fig. 29 are seen in Fig. 30. By comparing vibratory waves with rotating marks, we can easily see that vibrations in Peak I consist of vibrations of $[7/15 \cdot \omega]$ and $[-8/15 \cdot \omega]$; in Peak III of $[-1/10 \cdot \omega]$ and $[-9/10 \cdot \omega]$; in Peak V of $[19/22 \cdot \omega]$ and $[-3/22 \cdot \omega]$, and in Peak VII of $[3/2 \cdot \omega]$ and $[-1/2 \cdot \omega]$. By analizing the vibratory waves, we have the results as given in Table 4.1.

Even if we use the shaft in which ratio $a : b$ is different from 1 : 4 (shaft No. 3), these vibrations also occur. In Fig. 31, for shaft No. 1 ($a : b = 3 : 7$) we give results of experiments in which the same disc and the same ball bearings are used as in Figs. 29 and 30. In Fig. 31, Peak II at $\omega_{1/2} = 3{,}180$ r.p.m. is vibration of $[+1/2 \cdot \omega]$; Peak V at $\omega_{b1} = 1{,}845$ r.p.m. is that of $[-\omega]$; Peaks I, III and IV at ω_1, ω_2 and

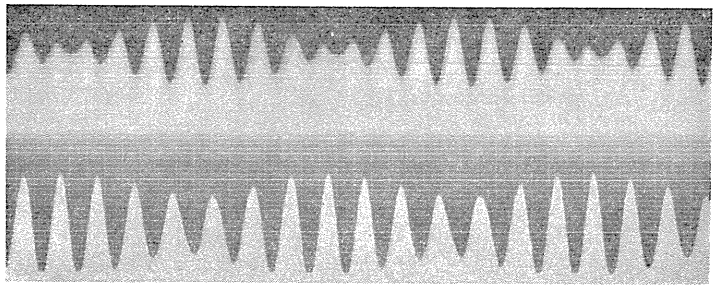

Peak I. $\left[\frac{7}{15}\omega\right]+\left[-\frac{8}{15}\omega\right]$

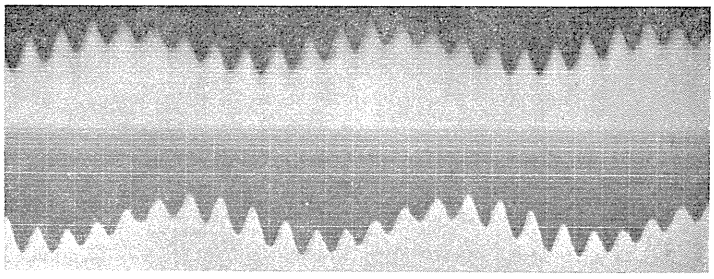

Peak III. $\left[-\frac{1}{10}\omega\right]+\left[-\frac{9}{10}\omega\right]$

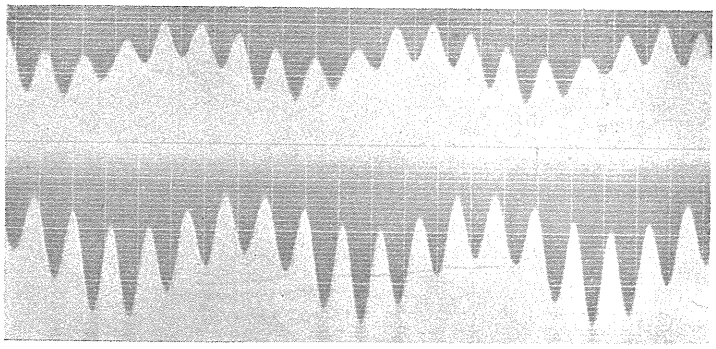

Peak V. $\left[\frac{19}{22}\omega\right]+\left[-\frac{3}{22}\omega\right]$

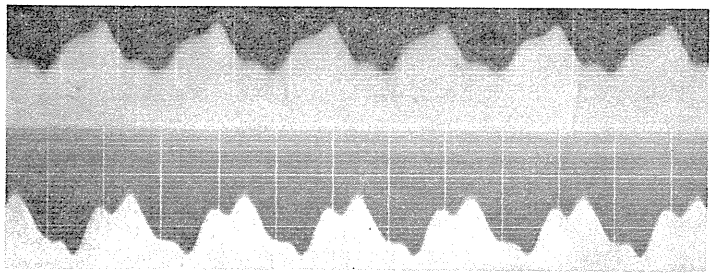

Peak VII. $\left[\frac{3}{2}\omega\right]+\left[-\frac{2}{1}\right]$

FIG. 30. Vibratory waves of "summed and differential harmonic oscillations" (shaft No. 3) (cf. Fig. 29).

TABLE 4.1. (Shaft No. 3, $a : b = 1 : 4$) (cf. Figs. 29 and 30)

Peak No.	Critical speed in r.p.m.	Modes of vibrations	Max. amplitude in mm
Peak I	$\omega_1 = 5{,}135$	$\left[\frac{7}{15}\omega\right]+\left[-\frac{8}{15}\omega\right]$	0.615
Peak III	$\omega_2 = 3{,}075$	$\left[-\frac{1}{10}\omega\right]+\left[-\frac{9}{10}\omega\right]$	0.528
Peak V	$\omega_3 = 2{,}625$	$\left[\frac{19}{22}\omega\right]+\left[-\frac{3}{22}\omega\right]$	0.652
Peak VII	$\omega_5 = 1{,}226$	$\left[\frac{3}{2}\omega\right]+\left[-\frac{1}{2}\omega\right]$	0.467

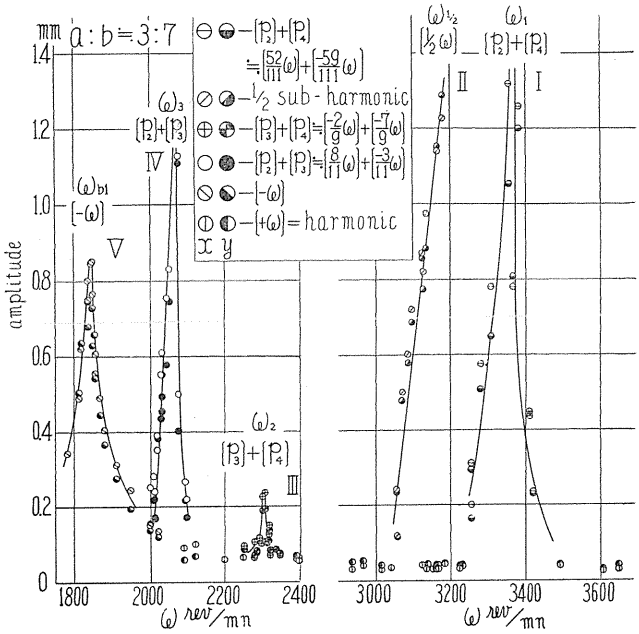

FIG. 31. Response curves (shaft No. 1).

TABLE 4.2. (Shaft No. 1, $a : b = 3 : 7$) (cf. Figs. 31 and 32)

Peak No.	Critical speed in r.p.m.	Modes of vibrations	Max. amplitude in mm
Peak I	$\omega_1 = 3{,}370$	$\left[\frac{52}{111}\omega\right]+\left[-\frac{59}{111}\omega\right]$	Remarkably large
Peak III	$\omega_2 = 2{,}307$	$\left[-\frac{2}{9}\omega\right]+\left[-\frac{7}{9}\omega\right]$	0.235
Peak IV	$\omega_3 = 2{,}075$	$\left[\frac{8}{11}\omega\right]+\left[-\frac{3}{11}\omega\right]$	1.130

ω_3 respectively are the critical speeds of "summed and differential harmonic oscillations" as well as the vibrations as given in Table 4.1. Vibratory waves in Peaks I and IV in Fig. 31 are shown in Fig. 32, and by analizing the vibratory waves, we have the results as given in Table 4.2. Amplitudes of Peak I are so large that the shaft contacts guard ring G (see Fig. 1).

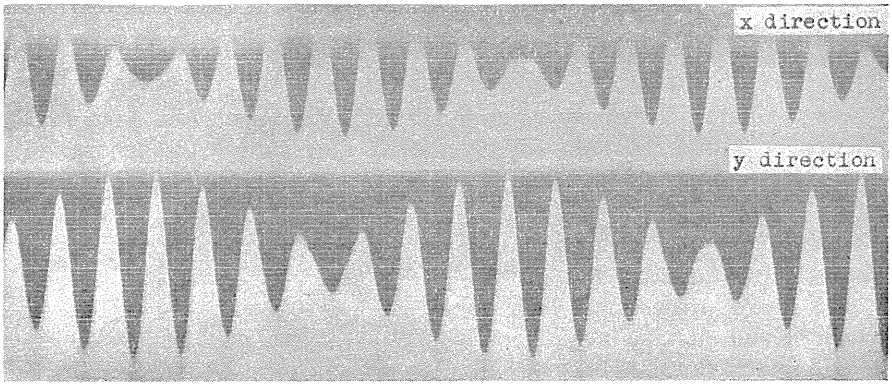

Peak I. $\left[\frac{52}{111}\omega\right]+\left[-\frac{59}{111}\omega\right]$

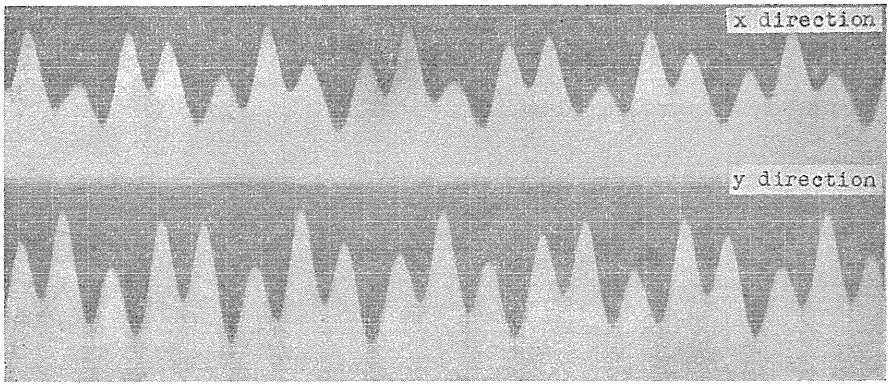

Peak IV. $\left[\frac{8}{11}\omega\right]+\left[-\frac{3}{11}\omega\right]$

FIG. 32. Vibratory waves (shaft No. 1) ($a : b = 3 : 7$, cf. Fig. 31).

Observing the vibratory waves shown in Figs. 30 or 32, it is easy to see that these peaks are formed by building up two vibrations as remarked in section 1.

We find in Tables 4.1 and 4.2 that in all critical speeds the absolute values of the sum of, or the difference in, two vibrations simultaneously building up is equal to the frequency of external force ω; for instance, for Peak I, Table 4.1, $7/15 \cdot \omega + |-8/15 \cdot \omega| = \omega$, and for Peak III, Table 4.2, $|-2/9 \cdot \omega| + |-7/9 \cdot \omega| = \omega$. Consequently putting modes of two vibrations as $[m_1\omega]$ and $[m_2\omega]$, the relation

$$|m_1\omega \pm m_2\omega| = \omega, \quad \text{or} \quad |m_1 \pm m_2| = 1 \tag{4.1}$$

can always held for all these vibrations. This is the distinctive nature of these vibrations which no other vibration has.

3. Relations between magnitudes of critical rotating speeds and modes of vibrations

When the shaft has linear spring characteristics, the frequency equation of the system can be obtained from (2.1) as follows:

$$\{(\alpha - mp^2)(\delta + I_p\omega p - Ip^2) - \gamma^2\}\{(\alpha - mp^2)(\delta - I_p\omega p - Ip^2) - \gamma^2\} = 0, \qquad (4.2)$$

where p is the natural frequency of this system. As we can see from (4.2), p is the function of ω, and for a certain vaues of ω, four natural frequencies p_1, p_2, p_3 and p_4 are obtained as roots of (4.2). Among p_1, p_2, p_3 and p_4, two natural frequencies p_1 and p_2 are positive and free vibrations of p_1 and p_2 are those of forward precession. The other two p_3 and p_4 take negative values and free vibrations corresponding to them become whirling motions of backward precession.[11] For example, in Fig. 17, curves p_1, p_2, p_3 and p_4 represented as functions ω are curves I, II, III and IV respectively. Although the system is non-linear and stiffness varies accordingly as deflections vary, by the same procedure as that used to obtain Fig. 17, $p-\omega$ curves shown in Figs. 33 and 34 can be given. Fig. 33 is the $p-\omega$ curves for experiments shown in Figs. 29 and 30. In Fig. 33, curves $p_2-\omega$, $p_3-\omega$ and $p_4-\omega$ when single-row radial ball bearings are used, are shown by full lines, but here $p_1-\omega$ curve is omitted because it is not necessary for later discussion. For the shaft supported by self-aligning double-row ball bearings, $p-\omega$ curves obtained by experiment are given by chain lines, for comparison. Since the shaft is freely supported and has linear spring characteristics when self-aligning double-row ball bearings are used, the stiffness of shaft supported by single-row radial ball bearings becomes larger than that for self-aligning double-row ball bearings, as well as becoming non-linear; thus the absolute values of natural frequencies p_1, p_2, p_3 and p_4 for single-row radial ball bearing are larger than those for self-aligning double-row ball bearings, as shown in Fig. 33.

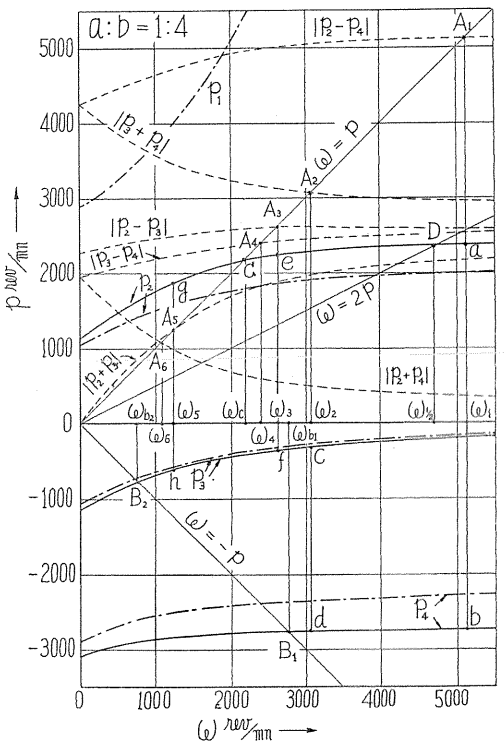

FIG. 33. $p-\omega$ diagram (shaft No. 3, $a:b=1:4$, cf. Figs. 29, 30).

Where critical speeds of "summed and differential harmonic oscillations" occur,

whatever modes these vibrations may have, they must by determined by using $p-\omega$ diagram. Writing curve $|p_i \pm p_j|(i, j=1, 2, 3, 4$ and $i \neq j)$ against ω, and obtaining intersecting point where curve $|p_i \pm p_j|$ and straight line $\omega = p$ cross, we are given critical speed from abscissa of this intersection point. Because at rotating speed ω as determined by this intersecting point, we have

$$|p_i \pm p_j| = \omega, \tag{4.3}$$

and putting

$$p_i = m_1 \omega, \qquad p_j = m_2 \omega, \tag{4.4}$$

the relation (4.1) is held. Although there are twelve $|p_i \pm p_j| - \omega$ curves in all, only six curves $|p_2+p_3|$, $|p_2-p_3|$, $|p_2+p_4|$, $|p_2-p_4|$, $|p_3+p_4|$ and $|p_3-p_4|$ as expressed by dotted lines, are indicated in Fig. 33 since none of the six $|p_1 \pm p_j| - \omega$ curves intersect a straight line $\omega = p$.

In Fig. 33, for example, a point A_1 is the intersecting point of curve $|p_2-p_4|-\omega$ with line $\omega = p$, and the abscissa of point A_1 takes the value of $\omega_1 = 5{,}130$ r.p.m. The values of $p_2 = 2{,}380$ r.p.m. $= 6.96/15 \cdot \omega$ and $p_4 = -2{,}750$ r.p.m. $= -8.04/15 \cdot \omega$ are given from ordinates of points a and b respectively where a vertical line $\omega_1 = 5{,}130$ r.p.m. intersects curves $p_2 - \omega$ and $p_4 - \omega$. Thus we can determine that at rotating speed ω_1 $(= 5{,}130$ r.p.m.), two vibrations with frequencies 2,380 r.p.m. $(\fallingdotseq 7/15 \cdot \omega)$ and $-2{,}750$ r.p.m. $(\fallingdotseq -8/15 \cdot \omega)$ build up and form the ctitical speed of Peak I shown in Fig. 29. These results obtained from $p-\omega$ curves of Fig. 33 clearly coincide with the results given in Table 4.1. We can also see by the above procedure, for instance, that vibrations with frequencies p_2 and p_4 shown in $p_2-\omega$ and $p_4-\omega$ curves in Fig. 33, build up and form the critical speed of Peak I in Fig. 29. Consequently Peak I is given by $[p_2]+[p_4]$ as shown in Fig. 29.

Similarly, in Fig. 33, a point A_2 is the intersecting point of curve $|p_3+p_4|-\omega$ with line $\omega = p$, and the abscissa of point A_2 determines the critical speed ω_2 $(=3{,}065$ r.p.m.) of Peak III in Fig. 29; ordinates of points c and d give $p_3 = -305$ r.p.m. $\fallingdotseq -1/10 \cdot \omega$ and $p_4 = -2{,}760$ r.p.m. $\fallingdotseq -9/10 \cdot \omega$ respectively, which agree with experimental results. Furthermore, in Fig. 33, intersecting points A_3 and A_5 on curves $|p_2-p_3|-\omega$ and $|p_2+p_3|-\omega$ give critical speeds ω_3 and ω_5 of Peaks V and VII respecticely, and modes of vibrations are determined by points e, f and points g, h.

From the above we can conclude that these critical speeds appear at the rotating speeds of shaft where the absolute value of sum of, or difference in, any two natural frequencies becomes equal to the rotatin speed ω, and the peaks of critical speeds are formed by building up of two vibrations with the same frequencies as these two natural frequencies.

Although in Fig. 33 there are two more intersecting points A_4 $(\omega_4 = 2{,}400$ r.p.m.) and A_6 $(\omega_6 = 1{,}080$ r.p.m.) where curves $|p_3-p_4|-\omega$ and $|p_2+p_4|-\omega$ cross line $\omega = p$, the critical speeds corresponding to A_4 and A_6 do not appear in experiment. If they appeared, it would be in the neighborhood of $\omega_4 = 2{,}400$ r.p.m. and $\omega_6 = 1{,}080$ r.p.m., but they do not. Incidentally, intersecting points C and D determine respectively the major critical speed ω_c and the critical speed $\omega_{1/2}$ of sub-harmonic oscillation of order 1/2. Points B_1 and B_2 give two critical speeds ω_{b_1} and ω_{b_2} of synchronous backward precession.

Fig. 34 is the $p-\omega$ diagram for experiment shown in Fig. 31 where shaft No. 1 $(a : b = 3 : 7)$ is used. Although Fig. 34 is similar to Fig. 33, there is a difference

in the following point: In Fig. 34, a straight line $\omega = p$ cannot intersect $|p_1 \pm p_j| - \omega$ curves and $|p_2 + p_3| - \omega$ curves. It can intersect only five other curves at A_1, A_2, A_3, A_4 and A_5 in all. In Fig. 34, too, the peaks do not appear at ω_4 and ω_5 given by points A_4 and A_5, *viz.*, by curves $|p_3 - p_4|$ and $|p_2 + p_4|$; only three critical speeds ω_1, ω_2 and ω_3 can be obtained by our experiments. Peaks I, III and IV in Fig. 31 are critical speeds ω_1, ω_2 and ω_3 respectively.

For all response curves shown in the present chapter, several kinds of marks are used to represent amplitudes in order to distinguish modes of vibrations. One certain mark is plotted for the critical speed induced by the same $|p_i \pm p_j| - \omega$ curve.

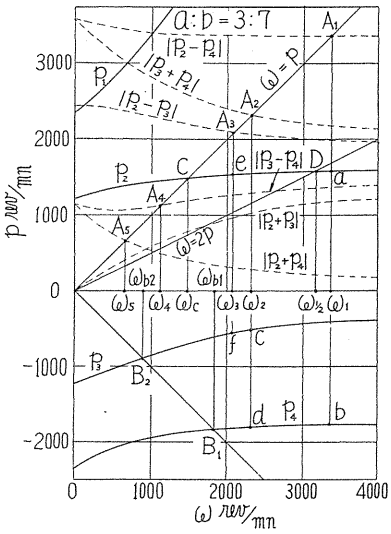

FIG. 34. $p - \omega$ diagram (shaft No. 1, $a : b = 3 : 7$, cf. Figs. 31, 32).

4. Influence of ball bearing

Since the angular clearance of single-row radial ball bearing does not take the same magnitude for the same kind of ball bearing, being peculiar to each ball bearing, spring characteristics vary when ball bearings are exchanged. Furthermore, because the degree of out of alignment between center lines of pedestals may differ each time the apparatus is assembled, stiffness of shaft varies and the magnitudes of critical speeds change in each reassembling of apparatus, even if we use the same shaft and disc. Since the modes of these vibrations in critical speeds are prescribed by (4.1), changes in location of critical speeds result in changes in modes of vibrations. This nature, too, distinguishes these vibrations from other kinds.

For instance, in the critical speed of shaft No. 5 ($a : b = 3 : 1$) obtained from $|p_2 - p_3| - \omega$ curves, an exchange of ball bearings brings on changes in the critical speed and in the modes of vibrations, as shown in Fig. 35. In the left-hand figure of Fig. 35, (i) critical speed ω is 2,290 r.p.m. and (ii) amplitude is large enough to contact guard ring and (iii) modes of vibrations are $p_2 = 43/55 \cdot \omega = 0.782\ \omega$ and $p_3 = -12/55 \cdot \omega = -0.218\ \omega$. On the other hand, in the right-hand figure, (i) $\omega = 2{,}030$ r.p.m., (ii) max. amplitude = 0.813 mm, (iii) $p_2 = 23/30 \cdot \omega = 0.767\ \omega$ and $p_3 = -7/30 \cdot \omega = -0.233\ \omega$.

For the critical speed of shaft No. 1 ($a : b = 3 : 7$) given by $|p_2 - p_3| - \omega$ curve, variations induced by reassembling of pedestal or by exchange of ball bearings are shown in Table 4.3.

Here we see that the relation (4.1) is held in all cases in spite of variations of critical speeds and modes of vibrations.

Comparison of all kinds of critical speeds given in Figs. 31 and 36 is made in Table 4.4. In Figs. 31 and 36 the same disc and shaft are used in both experiments, but in these figures the single-row radial ball bearings are different, and further, rigid pedestal II shown in Fig. 38 (a) is used in Fig. 31 and flexible pedestal I in Fig. 36. Consequently, stiffness of system in the latter becomes smaller than that in the former and critical speeds shown in Fig. 36 take place at a somewhat lower

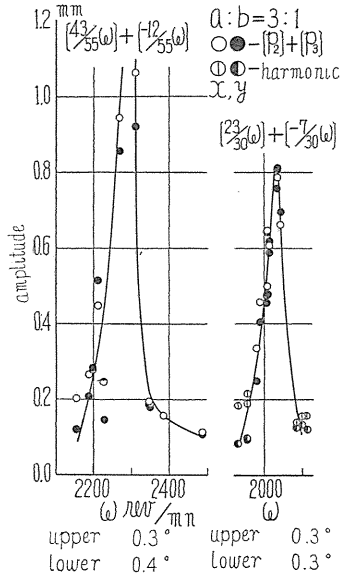

FIG. 35. Variation in the critical speed (shaft No. 5).

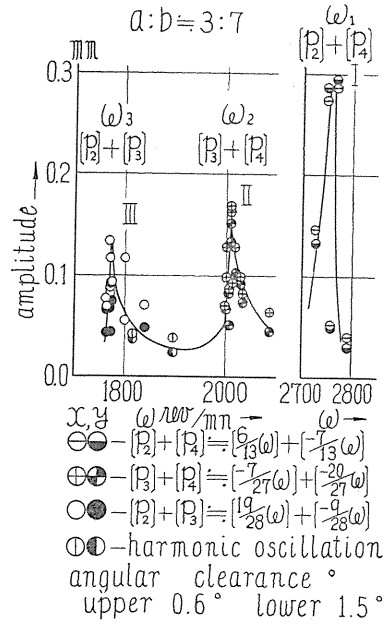

FIG. 36. Resonanse curve (shaft No. 1).

TABLE 4.3. Variations in Critical Speed Given by $|p_2 - p_3| - \omega$ Curve (Shaft No. 1, $a : b = 3 : 7$)

	Critical speed in r.p.m.	Max. amplitude in mm	Modes of vibrations		Angular clearance		Remarks
			p_2	p_3	Upper	Lower	
(1)	1,948	0.646	$\frac{23}{33}\omega = 0.697\ \omega$	$-\frac{10}{33}\omega = -0.303\ \omega$	0.2°	0.5°	
(2)	2,018	Remarkably large	$\frac{31}{44}\omega = 0.705\ \omega$	$-\frac{13}{44}\omega = -0.295\ \omega$	0.2°	0.5°	
(3)	1,761	Remarkably large	$\frac{23}{31}\omega = 0.742\ \omega$	$-\frac{8}{31}\omega = -0.258\ \omega$	0.6°	1.5°	
(4)	2,075	1.130	$\frac{8}{11}\omega = 0.727\ \omega$	$-\frac{3}{11}\omega = -0.273\ \omega$	0.3°	0.3°	Peak IV in Fig. 31
(5)	1,770	0.134	$\frac{19}{28}\omega = 0.679\ \omega$	$-\frac{9}{28}\omega = -0.321\ \omega$	0.6°	1.5°	Peak III in Fig. 36

TABLE 4.4. Comparison of Figs. 31 and 36 (Shaft No. 1, $a : b = 3 : 7$)

Kinds of critical speeds	Fig. No.	Critical speed in r.p.m.	Modes of vibrations	Max. amplitude in mm
$\lvert p_2 - p_4 \rvert$	31	3,370	$\left[\frac{52}{111}\omega\right] = [0.469\ \omega] + \left[-\frac{59}{111}\omega\right] = [-0.531\ \omega]$	Remarkably large
	36	2,760	$\left[\frac{6}{13}\omega\right] = [0.462\ \omega] + \left[-\frac{7}{13}\omega\right] = [-0.538\ \omega]$	0.295
$\lvert p_3 + p_4 \rvert$	31	2,307	$\left[-\frac{2}{9}\omega\right] = [-0.222\ \omega] + \left[-\frac{7}{9}\omega\right] = [-0.778\ \omega]$	0.235
	36	2,005	$\left[-\frac{7}{27}\omega\right] = [-0.259\ \omega] + \left[-\frac{20}{27}\omega\right] = [-0.741\ \omega]$	0.168
$\lvert p_2 - p_4 \rvert$	31	2,075	$\left[\frac{8}{11}\omega\right] = [0.727\ \omega] + \left[-\frac{3}{11}\omega\right] = [-0.723\ \omega]$	1.130
	36	1,770	$\left[\frac{19}{28}\omega\right] = [0.679\ \omega] + \left[-\frac{9}{28}\omega\right] = [-0.321\ \omega]$	0.134

rotating speed ω with change of modes of vibrations. Comparison between both is made in Table 4.4.

Here the question arises whether or not these critical speeds occur through external force due to errors in ball bearing machining. Disturbing forces induced by rotating ball bearings with errors have their own frequencies determined only by dimensions of such ball bearings.[20)21)] Accordingly frequencies of vibrations caused by these forces can also be determined only by dimensions of ball bearing, independent of dimensions of shaft or disc. Nevertheless, although the same ball bearings are used in both experiments of Figs. 29 and 31, as well as in right-hand figure of Fig. 35, every mode of vibrations differs from the others and all frequencies can be described only by dimensions of shaft and disc and by spring characteristics of the shaft. In lines (1) and (2) of Table 4.3, despite use of the same ball bearings, modes of vibrations are not same, and this is true also of lines (3) and (5). Accordingly, these critical speeds are not caused by external forces such as might be induced by ball bearings.

5. Conclusions

From experiments described above we can conclude the following.

1) When single-row radial ball bearings are used, several critical speeds appear and increasing amplitudes of two vibrations result.

2) These critical speeds do not take place when self-aligning double-row ball bearings are used and when stiffness of shaft is linear.

3) Frequencies of two vibrations which build up at critical speeds coincide with natural frequencies of p_i and p_j, and the relation $|p_i \pm p_j| = \omega$ is held at critical speed.

4) These critical speeds occur in multiple degrees of freedom system with several natural frequencies, and appear at rotating speed of ω which satisfies the relation $|p_i \pm p_j| = \omega$.

5) Even when the same disc and shaft are used, there are changes in locations of critical speeds, magnitudes of amplitudes and modes of vibrations, accordingly as there are variations in conditions of assembling of pedestals and as there is an exchange of ball bearings.

6) These critical speeds do not always occur at rotating speeds ω satisfying $|p_i \pm p_j| = \omega$; some appear and some do not.

7) These critical speeds are not induced by ball bearings with machining errors.

The appearance or non-appearance of these critical speeds is shown in Table 4.5 where they are arranged according to rotating speed, *viz.*, the critical speeds are given in columns from left to right. Here the mark ○ means appearance, × non-appearance, and ×× means that curve $|p_i \pm p_j|$ does not intersect line $\omega = p$ and therefore the critical speed does not, of course, appear.

TABLE 4.5. Appearance of Critical Speeds

Shaft No.	$a : b$	$\lvert p_2-p_4 \rvert$	$\lvert p_3+p_4 \rvert$	$\lvert p_2-p_3 \rvert$	$\lvert p_3-p_4 \rvert$	$\lvert p_2+p_3 \rvert$	$\lvert p_2+p_4 \rvert$
3	1 : 4	○	○	○	×	○	×
1	3 : 7	○	○	○	×	××	×
5	3 : 1	○	○	○	×	××	×

Critical speeds from $|p_2-p_4|$, $|p_3+p_4|$ and $|p_2-p_3|$ always appear; peaks of $|p_3-p_4|$ and $|p_2+p_4|$ never appear. Amplitudes of peaks of $|p_2-p_4|$ and $|p_2-p_3|$ are usually large; those of $|p_3+p_4|$ are somewhat smaller, and the peak of $|p_3+p_4|$ of shaft No. 5 is the smallest.

Occurrence of these vibrations is discussed along purely mathematical lines in the next chapter.

Chapter V. On Sub-Harmonic Oscillations and on "Summed and Differential Harmonic Oscillations" in Non-Linear Systems Having Multiple Degrees of Freedom[6]

1. Introduction

In Chapters III and IV, we have found experimentally that sub-harmonic oscillations and "summed and differential harmonic oscillations" take place in the shaft system with non-linear spring characteristics and multiple degrees of freedom. In the present chapter we will state mathematically and analytically the possibility of occurrence of these vibrations.

In those systems with multiple degrees of freedom, as in systems with one degree of freedom, there is the possibility of an occurrence of sub-harmonic oscillations provided the system has non-linear spring characteristics. There is the further possibility of the appearance of vibrations of "summed and differential harmonic oscillations" in multiple degrees of freedom systems which are entirely impossible in systems having only one degree of freedom. Adopting normal coodinates, the occurrence of these vibrations can be anticipated, as discussed in the present chapter. There are generally two kinds of dynamic systems, one with and one without gyroscopic terms; both considered in this chapter. In the first, the transformation into normal coordinates cannot be performed by simple linear transformation, and we discuss a vibratory system consisting of rotating shaft mounting one disc, as an example of the system with gyroscopic terms.

As we see in Chapter IV, the vibrations of "summed and differential harmonic oscillations" consist of two vibrations both having the same frequencies (p_i and p_j) as the natural frequencies of the system. The absolute value of the sum of, or difference in, the two frequencies p_i and p_j is equal to the frequency of the disturbing force ω, *i.e.*, $|p_i \pm p_j| = \omega$. In a system having linear spring characteristics or a system with one degree of freedom, these types of vibrations do not occur; they appear only in systems with multiple degrees of freedom and non-linearity.

2. Transformation into normal coordinates

The differential equations of a rotating shaft system consisting of a light shaft and a rotating disc, as shown in Fig. 37, are

$$\left.\begin{aligned} &m\ddot{x}+\alpha x+\gamma\theta_x = me\omega^2\cos\omega t,\\ &m\ddot{y}+\alpha y+\gamma\theta_y = me\omega^2\sin\omega t,\\ &I\ddot{\theta}_x+I_p\omega\dot{\theta}_y+\delta\theta_x+\gamma x = (I_p-I)\tau\omega^2\cos(\omega t+\beta),\\ &I\ddot{\theta}_y-I_p\omega\dot{\theta}_x+\delta\theta_y+\gamma y = (I_p-I)\tau\omega^2\sin(\omega t+\beta), \end{aligned}\right\} \qquad (5.1)$$

which coincide with (2.1).

Here we consider the rectangular coordinate system o-xyz shown in Fig. 37 in which the z-axis coincides with the bearing center line and o is the position of the shaft center when no whirl exists.

Since the terms $I_p\omega\dot{\theta}_y$ and $-I_p\omega\dot{\theta}_x$ in the 3rd and 4th equations of (5.1) are gyroscopic terms, this system is a vibratory system with gyroscopic terms, and the motions in x and y directions are coupled together. For convenience, we introduce the dimensionless quantities as follows:

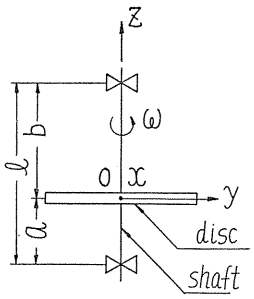

FIG. 37

$$\left.\begin{aligned} &\frac{x}{e}=x_1,\quad \frac{y}{e}=x_2,\quad \theta_x\sqrt{\frac{I}{m}}\Big/e=x_3,\quad \theta_y\sqrt{\frac{I}{m}}\Big/e=x_4,\quad \frac{I_p}{I}=I_1,\\ &\frac{\gamma}{\alpha}\sqrt{\frac{m}{I}}=\gamma',\quad \frac{\delta m}{\alpha I}=\delta',\quad \omega\sqrt{\frac{m}{\alpha}}=\omega',\quad t\sqrt{\frac{\alpha}{m}}=t',\quad \frac{\tau}{e}\sqrt{\frac{I}{m}}=\tau', \end{aligned}\right\} \tag{5.2}$$

in which t is time. Substituting (5.2) into (5.1) and omitting primes on the dimensionless quantities, we have

$$\left.\begin{aligned} &\ddot{x}_1+x_1+\gamma x_3=\omega^2\cos\omega t,\\ &\ddot{x}_2+x_2+\gamma x_4=\omega^2\sin\omega t,\\ &\ddot{x}_3+I_1\omega\dot{x}_4+\gamma x_1+\delta x_3=(I_1-1)\tau\omega^2\cos(\omega t+\beta),\\ &\ddot{x}_4-I_1\omega\dot{x}_3+\gamma x_2+\delta x_4=(I_1-1)\tau\omega^2\sin(\omega t+\beta). \end{aligned}\right\} \tag{5.3}$$

Since the vibratory system shown in Fig. 37 is that with 4 degrees of freedom when $\omega\neq 0$ and $a\neq b$ (see Fig. 37), the solutions of free vibrations are

$$\left.\begin{aligned} &x_1=\sum_{i=1}^{4}a_i\cos(p_it+\alpha_i), \qquad x_2=\sum_{i=1}^{4}a_i\sin(p_it+\alpha_i),\\ &x_3=\sum_{i=1}^{4}b_i\cos(p_it+\alpha_i), \qquad x_4=\sum_{i=1}^{4}b_i\sin(p_it+\alpha_i), \end{aligned}\right\} \tag{5.4}$$

and the relation

$$\frac{a_i}{bi}=-\frac{\gamma}{1-p_i^2}, \tag{5.5}$$

between amplitudes of free vibrations is held.

In (5.4), $p_i=p_1, p_2, p_3, p_4$ are the natural frequencies of this system and the roots of the frequency equation

$$(1-p^2)(\delta+I_1p\omega-p^2)-\gamma^2=(p-p_1)(p-p_2)(p-p_3)(p-p_4)=0, \tag{5.6}$$

easily obtained from (5.4). Observing (5.4), we find that the phase angle of free vibrations of $x_1(x)$ is the same as that of $x_3(\theta_x)$, and also that the phase angle of $x_2(y)$ is the same as that of $x_4(\theta_y)$. We also see that there is a 90° difference of phase angle between vibrations x_1 and x_3, and x_2 and x_4.

If p_i is positive, vibrations of x_1 and x_3 are 90° faster than those of x_2 and x_4 and the shaft whirls in the same direction as it rotates, so that the whirling motion becomes one of forward precession. On the other hand, when p_i is negative, vibrations of x_1 and x_3 are behind by 90° and the shaft whirls in the opposite direction; thus the motion is backward precession. This behavior is a distinctive feature of the systems having gyroscopic terms as distinguished from the general systems without gyroscopic terms where the free vibrations of all coordinates have the same phase angle. Obviously this nature is influenced by the terms $I_1\omega\dot{x}_4$ and $-I_1\omega\dot{x}_3$ in (5.3). Among p_1, p_2, p_3 and p_4, two natural frequencies take positive values and the other two are negative, and p_i is the functions of ω.

Now we intend to transform coordinates x_1, x_2, x_3 and x_4 into normal coordinates. Although it is usually impossible to perform transformation into normal coordinates by adopting simple linear transformation of coordinates without using a rather complicated canonical transformation,[7] in the present case (5.3), we can perform this transformation somewhat easily as we now show.

Considering the relations of (5.5) and $-\frac{1}{p_i}\frac{d}{dt}(\cos p_i t) = \sin p_i t$, it is understood that transformation into normal coordinates can be carried out by putting

$$\left.\begin{aligned} x_1 &= X_1 + X_2 + X_3 + X_4, \\ x_2 &= -\left(\frac{\dot{X}_1}{p_1} + \frac{\dot{X}_2}{p_2} + \frac{\dot{X}_3}{p_3} + \frac{\dot{X}_4}{p_4}\right), \\ x_3 &= \frac{-1}{r}\{(1-p_1^2)X_1 + (1-p_2^2)X_2 + (1-p_3^2)X_3 + (1-p_4^2)X_4\}, \\ x_4 &= \frac{1}{r}\left(\frac{1-p_1^2}{p_1}\dot{X}_1 + \frac{1-p_2^2}{p_2}\dot{X}_2 + \frac{1-p_3^2}{p_3}\dot{X}_3 + \frac{1-p_4^2}{p_4}\dot{X}_4\right). \end{aligned}\right\} \tag{5.7}$$

Inserting (5.7) into (5.3) and considering the relation (5.6), we can rewrite (5.3) as follows:

$$\left.\begin{aligned} &(\ddot{X}_1 + p_1^2 X_1) + (\ddot{X}_2 + p_2^2 X_2) + (\ddot{X}_3 + p_3^2 X_3) + (\ddot{X}_4 + p_4^2 X_4) = \omega^2 \cos\omega t, \\ &\frac{1}{p_1}(\ddot{X}_1 + p_1^2 X_1) + \frac{1}{p_2}(\ddot{X}_2 + p_2^2 X_2) + \frac{1}{p_3}(\ddot{X}_3 + p_3^2 X_3) + \frac{1}{p_4}(\ddot{X}_4 + p_4^2 X_4) = \omega \cos\omega t, \\ &\frac{(1-p_1^2)(I_1\omega - p_1)}{rp_1}(\ddot{X}_1 + p_1^2 X_1) + \frac{(1-p_2^2)(I_1\omega - p_2)}{rp_2}(\ddot{X}_2 + p_2^2 X_2) \\ &\quad + \frac{(1-p_3^2)(I_1\omega - p_3)}{rp_3}(\ddot{X}_3 + p_3^2 X_3) + \frac{(1-p_4^2)(I_1\omega - p_4)}{rp_4}(\ddot{X}_4 + p_4^2 X_4) \\ &\quad = (I_1 - 1)\tau\omega^2 \cos(\omega t + \beta), \\ &-\frac{(1-p_1^2)}{rp_1}(\ddot{X}_1 + p_1^2 X_1) - \frac{(1-p_2^2)}{rp_2}(\ddot{X}_2 + p_2^2 X_2) - \frac{(1-p_3^2)}{rp_3}(\ddot{X}_3 + p_3^2 X_3) \\ &\quad - \frac{(1-p_4^2)}{rp_4}(\ddot{X}_4 + p_4^2 X_4) = (I_1 - 1)\tau\omega \cos(\omega t + \beta). \end{aligned}\right\} \tag{5.8}$$

Let the determinant consisting of coefficients in (5.8) be $D = |\alpha_{ij}|$, then

$$D=|\alpha_{ij}|=\begin{vmatrix} 1 & 1 & 1 & 1 \\ \dfrac{1}{p_1} & \dfrac{1}{p_2} & \dfrac{1}{p_3} & \dfrac{1}{p_4} \\ \dfrac{(1-p_1^2)(p_1-I_1\omega)}{\gamma p_1} & \dfrac{(1-p_2^2)(p_2-I_1\omega)}{\gamma p_2} & \dfrac{(1-p_3^2)(p_3-I_1\omega)}{\gamma p_3} & \dfrac{(1-p_4^2)(p_4-I_1\omega)}{\gamma p_4} \\ \dfrac{1-p_1^2}{\gamma p_1} & \dfrac{1-p_2^2}{\gamma p_2} & \dfrac{1-p_3^2}{\gamma p_3} & \dfrac{1-p_4^2}{\gamma p_4} \end{vmatrix}$$

$$=\frac{1}{p_1p_2p_3p_4\gamma^2}\begin{vmatrix} 1 & 1 & 1 & 1 \\ p_1 & p_2 & p_3 & p_4 \\ p_1^2 & p_2^2 & p_3^2 & p_4^2 \\ p_1^3 & p_2^3 & p_3^3 & p_4^2 \end{vmatrix}=\frac{(p_1-p_2)(p_1-p_3)(p_1-p_4)(p_2-p_3)(p_2-p_4)(p_3-p_4)}{\gamma^2(\delta-\gamma^2)} \tag{5.9}$$

Since $p_1 \neq p_2 \neq p_3 \neq p_4$ is always held provided that $\omega \neq 0$, D is not equal to zero. Let the determinants in which elements α_{1i}, α_{2i}, α_{3i} and α_{4i} in D are replaced by ω^2, ω, 0 and 0, and, in turn, by 0, 0, $(1-I_1)\tau\omega^2$ and $(1-I_1)\tau\omega$ be A_i'' and B_i'' respectively, and denoting

$$\frac{A_i''}{D}=A_i', \qquad \frac{B_i''}{D}=B_i',$$

then we obtain

$$\ddot{X}_i+p_i^2X_i=A_i'\cos\omega t+B_i'\cos(\omega t+\beta), \qquad (i=1,\ 2,\ 3,\ 4) \tag{5.10}$$

in which A_i' and B_i' are known. As (5.10) contains only X_i and its derivative $\ddot{X}_i$, X_i is the normal coordinate without doubt and thus the transformation into normal coordinates has been carried out, as shown in (5.10).

Although we have used in transformation from (5.3) into (5.10) not only linear transformation but also that having differential calculation, as shown in (5.7), we can prove that the solution of differential equations obtained directly from (5.3) coincides with that obtained from (5.10). For instance, we make a comparison between two solutions, one from (5.3) and one from (5.10) where the external force $F_1\cos qt$ with a circular frequency q exists in the right-hand side of the first equation of (5.3). Let the amplitude of the forced vibration of x_i be a_i', then a_i' is obtained from the simultaneous linear equation

$$\begin{bmatrix} 1-q^2 & 0 & \gamma & 0 \\ 0 & 1-q^2 & 0 & \gamma \\ \gamma & 0 & \delta-q^2 & I_1\omega q \\ 0 & \gamma & I_1\omega q & \delta-q^2 \end{bmatrix}\begin{bmatrix} a_1' \\ a_2' \\ a_3' \\ a_4' \end{bmatrix}=[\beta_{ij}][\alpha_i']=\begin{bmatrix} F_1 \\ 0 \\ 0 \\ 0 \end{bmatrix} \tag{5.11}$$

which is taken from (5.3). Expression [ ] means matrix and [ ] [ ] means product of matrix. On the other hand, the amplitude b_i' of vibration in X_i is the solution of the equation obtained from (5.8) as follows:

$$\begin{bmatrix} p_1^2-q^2 & p_2^2-q^2 \\ \dfrac{p_1^2-q^2}{p_1} & \dfrac{p_2^2-q^2}{p_2} \\ \dfrac{(p_1^2-q^2)(1-p_1^2)(p_1-I_1\omega)}{\gamma p_1} & \dfrac{(p_2^2-q^2)(1-p_2^2)(p_2-I_1\omega)}{\gamma p_2} \\ \dfrac{(p_1^2-q^2)(1-p_1^2)}{\gamma p_1} & \dfrac{(p_2^2-q^2)(1-p_2^2)}{\gamma p_2} \end{bmatrix}$$

$$\begin{bmatrix} p_3^2-q^2 & p_4^2-q^2 \\ \dfrac{p_3^2-q^2}{p_3} & \dfrac{p_4^2-q^2}{p_4} \\ \dfrac{(p_3^2-q^2)(1-p_3^2)(p_3-I_1\omega)}{\gamma p_3} & \dfrac{(p_4^2-q^2)(1-p_4^2)(p_4-I_1\omega)}{\gamma p_4} \\ \dfrac{(p_3^2-q^2)(1-p_3^2)}{\gamma p_3} & \dfrac{(p_4^2-q^2)(1-p_4^2)}{\gamma p_4} \end{bmatrix} \begin{bmatrix} b_1' \\ b_2' \\ b_3' \\ b_4' \end{bmatrix}$$

$$= [\gamma_{ij}][b_i'] = \begin{bmatrix} F_1 \\ 0 \\ 0 \\ 0 \end{bmatrix}, \tag{5.12}$$

while at the same time as is easily seen from (5.7), we have

$$\begin{bmatrix} a_1' \\ a_2' \\ a_3' \\ a_4' \end{bmatrix} = \begin{bmatrix} 1 & 1 & 1 & 1 \\ \dfrac{q}{p_1} & \dfrac{q}{p_2} & \dfrac{q}{p_3} & \dfrac{q}{p_4} \\ \dfrac{1-p_1^2}{\gamma} & \dfrac{1-p_2^2}{\gamma} & \dfrac{1-p_3^2}{\gamma} & \dfrac{1-p_4^2}{\gamma} \\ \dfrac{q(1-p_1^2)}{\gamma p_1} & \dfrac{q(1-p_2^2)}{\gamma p_2} & \dfrac{q(1-p_3^2)}{\gamma p_3} & \dfrac{q(1-p_4^2)}{\gamma p_4} \end{bmatrix} \begin{bmatrix} b_1' \\ b_2' \\ b_3' \\ b_4' \end{bmatrix} = [\delta_{ij}][b_i']. \tag{5.13}$$

Inserting (5.13) into (5.11), we have

$$[\beta_{ij}][\delta_{ij}][b_i'] = \begin{bmatrix} F_1 \\ 0 \\ 0 \\ 0 \end{bmatrix}. \tag{5.14}$$

Since we can verify

$$[\beta_{ij}][\delta_{ij}] = \begin{bmatrix} -\gamma_{1i} \\ q\gamma_{2i} \\ -\gamma_{3i} \\ -q\gamma_{4i} \end{bmatrix}, \qquad (i=1,\ 2,\ 3,\ 4),$$

by calculation, (5.12) coincides with (5.14) and thus it can be proved that the solutions of (5.3) and (5.10) agree.

Hereafter on the basis of (5.10) which is represented by only normal coordinates X_i, we will treat with sub-harmonic oscillations and "summed and differential harmonic oscillations" in non-linear systems with multiple degrees of freedom.

3. Occurrence of sub-harmonic oscillations

A shaft supported by self-aligning double-row ball bearings has linear spring characteristics, but since single-row radial ball bearings have small "angular clearance," a shaft supported by them has non-linear and non-symmetical spring characteristics provided that the bearing center lines of both pedestals are not in alignment. Furthermore, the non-linearity of spring characteristics of shaft takes place only on the plane in which there is out of alignment between center lines of both pedestals, and the stiffness of shaft is approximately linear in the direction perpendicular to this plane. Consequantly the shaft is never equally stiff in all directions and the directional non-uniformity of non-linear spring characteristics appears in shaft. Supposing that non-linearity takes place in x-direction and does not appear in y-direction, then by modifying (5.3) and (2.2) the equations of motion can be written

$$\left.\begin{aligned}
&\ddot{x}_1+\varepsilon c_1\dot{x}_1+x_1+\gamma x_3+\varepsilon f_1(x_1,\ x_3)=\omega^2\cos\omega t,\\
&\ddot{x}_2+\varepsilon c_2\dot{x}_2+x_2+\gamma x_4=\omega^2\sin\omega t,\\
&\ddot{x}_3+I_1\omega\dot{x}_4+\varepsilon c_3\dot{x}_3+\gamma x_1+\delta x_3+\varepsilon f_3(x_1,\ x_3)=(I_1-1)\tau\omega^2\cos(\omega t+\beta),\\
&\ddot{x}_4-I_1\omega\dot{x}_3+\varepsilon c_4\dot{x}_4+\gamma x_2+\delta x_4=(I_1-1)\tau\omega^2\sin(\omega t+\beta),
\end{aligned}\right\}\qquad(5.15)$$

in which f_1 and f_3 are non-linear terms of x_1 and x_3, $\varepsilon c_i\dot{x}_i$ is damping term and ε is small quantity compared with unity. For the reason of directional non-uniformity just mentioned, there are no non-linear terms in the equations with respect to $x_2(y)$ and $x_4(\theta_y)$. Let the determinants in which elements α_{1i}, α_{2i}, α_{3i} and α_{4i} in D are replaced by $-c_1\dot{x}_1$, c_2x_2, $c_3\dot{x}_3$ and $-c_4x_4$ and, in turn, by $-f_1$, 0, f_3 and 0 be C_i'' and Φ_i'' respectively, and denoting

$$\frac{C_i''}{D}=C_i',\qquad \frac{\Phi_i''}{D}=\Phi_i',\qquad (D\neq 0)$$

then (5.15) can be transformed into

$$\begin{aligned}
\ddot{X}_i+p_i^2X_i=\varepsilon C_i'(\dot{X}_1,\ \dot{X}_2,\ \dot{X}_3,\ \dot{X}_4)+\varepsilon\Phi_i'(X_1,\ X_2,\ X_3,\ X_4)\\
+A_i'\cos\omega t+B_i'\cos(\omega t+\beta),
\end{aligned}\qquad(5.16)$$

where C_i' is linear equation of $\dot{X}_i$, and Φ_i' non-linear term of X_i.

Now using a procedure similar to that of the perturbation method in systems having one degree of freedom,[8] we will treat with (5.16) which is the non-linear differential equation of multiple degrees of freedom system. For simplification of treatment, we introduce new variables as follows:

$$\omega = \nu\omega_1, \quad t_1 = \omega_1 t = \frac{\omega t}{\nu}, \quad \frac{p_i}{\omega} = \lambda_i, \quad \frac{C_i'}{\omega_1} = C_i(X_1', X_2', X_3', X_4'),$$

$$\frac{dX_i}{dt_1} = X_i', \quad \frac{d^2X_i}{dt^2} = X_i'', \quad \frac{\Phi_i'}{\omega_1^2} = \Phi_i(X_1, X_2, X_3, X_4), \quad \frac{A_i'}{\omega_1^2} = A_i, \quad \frac{B_i'}{\omega_1^2} = B_i,$$

in which ν is positive integer. Inserting these variables into (5.16), we have

$$X_i'' + \lambda_i^2 X_i = \varepsilon C_i(X_j') + \varepsilon\Phi_i(X_j) + A_i \cos \nu t_1 + \beta_i \cos(\nu t_1 + \beta). \qquad (5.17)$$
$$(j = 1, 2, 3, 4)$$

From now on, as concerns the present section and sections 4 and 5, we designate that the prime on the quantity means differentiation with respect to t_1.

Now we will consider sub-harmonic oscillations based on $\lambda_1(p_1)$. Rewriting (5.17), we get

$$\left.\begin{aligned} X_1'' + X_1 &= \{(1-\lambda_1^2)X_1 + \varepsilon C_1(X_j') + \varepsilon\Phi_1(X_j)\} + A_1 \cos \nu t_1 + B_1 \cos(\nu t_1 + \beta), \\ X_k'' + \lambda_k^2 X_k &= \varepsilon C_k(X_j') + \varepsilon\Phi_k(X_j) + A_k \cos \nu t_1 + B_k \cos(\nu t_1 + \beta). \end{aligned}\right\} \qquad (5.18)$$
$$(k = 2, 3, 4)$$

We assume that $(1-\lambda_1^2)$ is as small as the order of ε, thus $\lambda_1^2 \fallingdotseq 1$, $p_1 \fallingdotseq \omega/\nu$. Accordingly, in this dynamic system we now study the motion which takes place in rotating speed ω and here ω is almost equal to the integral demultiples of natural frequency p_1. Since ε has small value, the solutions of (5.18) may be developed in a power series with respect to a small parameter ε as follows:

$$X_i = X_{i0} + \varepsilon X_{i1} + \varepsilon^2 X_{i2} + \varepsilon^3 X_{i3} + \cdots, \qquad (5.19)$$

in which $X_{in}(n = 0, 1, 2, 3, \ldots)$ are functions of time t_1 and do not contain ε. As C_i is a linear equation of X_i', substituting (5.19) into $C_i(X_j')$, we have

$$C_i(X_1', X_2', X_3', X_4') = C_i(X_{j0}') + \varepsilon C_i(X_{j1}') + \varepsilon^2 C_i(X_{j2}') + \cdots. \qquad (5.20)$$

Since Φ_i is a non-linear term, then

$$\Phi_i(X_1, X_2, X_3, X_4) = \Phi_i(X_{10}, X_{20}, X_{30}, X_{40}) + \varepsilon G_{i1} + \varepsilon^2 G_{i2} + \cdots, \qquad (5.21)$$

where

$$\left.\begin{aligned} G_{i1} &= \sum_{j=1}^{4} X_{j1}\left(\frac{\partial\Phi_i}{\partial X_j}\right)_{\varepsilon=0} = G_{i1}(X_{10}, X_{20}, X_{30}, X_{40}, X_{11}, X_{21}, X_{31}, X_{41}), \\ G_{i2} &= \sum_{j=1}^{4} X_{j2}\left(\frac{\partial\Phi_i}{\partial X_j}\right)_{\varepsilon=0} + \frac{1}{2}\sum_{j=1}^{4} X_{j1}^2\left(\frac{\partial^2\Phi_i}{\partial X_j^2}\right)_{\varepsilon=0} + \sum_{\substack{j=1 \\ k=1}}^{4}{}_{(j\neq k)} X_{j1}X_{k1}\left(\frac{\partial^2\Phi_i}{\partial X_j \partial X_k}\right)_{\varepsilon=0} \\ &= \sum_{j=1}^{4} X_{j2}\left(\frac{\partial\Phi_i}{\partial X_j}\right)_{\varepsilon=0} + Z_{i2}(X_{j0}, X_{j1}), \\ &\cdots\cdots\cdots\cdots\cdots\cdots\cdots\cdots\cdots\cdots\cdots\cdots\cdots\cdots\cdots\cdots \\ G_{in} &= \sum_{j=1}^{4} X_{jn}\left(\frac{\partial\Phi_i}{\partial X_j}\right)_{\varepsilon=0} + Z_{in}(X_{j0}, X_{j1}, \ldots, X_{j,n-1}), \end{aligned}\right\} \qquad (5.22)$$

Inserting (5.19), (5.20) and (5.21) into (5.18), and comparing the terms having the same power of ε, we have

$$\left.\begin{aligned} &X_{10}''+X_{10}=A_1\cos\nu t_1+B_1\cos(\nu t_1+\beta),\\ &X_{k0}''+\lambda_k^2X_{k0}=A_k\cos\nu t_1+B_k\cos(\nu t_1+\beta),\end{aligned}\right\} \tag{5.23}$$

$$\left.\begin{aligned} &X_{11}'+X_{11}=\frac{1}{\varepsilon}(1-\lambda_1^2)X_{10}+C_1(X_{j0}')+\Phi_1(X_{j0})=H_1(X_{j0},\ X_{j0}'),\\ &X_{k1}''+\lambda_k^2X_{k1}=C_k(X_{j0}')+\Phi_k(X_{j0})=H_k(X_{j0},\ X_{j0}'),\end{aligned}\right\} \tag{5.24}$$

$$\left.\begin{aligned} &X_{1n}''+X_{1n}=\frac{1}{\varepsilon}(1-\lambda_1^2)X_{1,n-1}+C_1(X_{1,n-1}',\ X_{2,n-1}',\ X_{3,n-1}',\ X_{4,n-1}')\\ &\quad+G_{1,n-1}=J_{1,n-1},\\ &X_{kn}''+\lambda_k^2X_{kn}=C_k(X_{1,n-1}',\ X_{2,n-1}',\ X_{3,n-1}',\ X_{4,n-1}')+G_{k,n-1}=J_{k,n-1}.\end{aligned}\right\} \tag{5.25}$$

$$(k=2,\ 3,\ 4\ ;\ n=2,\ 3,\ 4,\ \ldots\ ;\ j=1,\ 2,\ 3,\ 4)$$

Now we intend to obtain the solutions of 1st approximation from (5.23). In the present step, we must assume that only the free vibrations of X_1 occur. We must further assume that p_2, p_3 and p_4 are not equal to integral multiples of p_1, that is, λ_2, λ_3 and λ_4 are not integers. Consequently the solutions of the 1st approximation can be represented by the following forms:

$$\left.\begin{aligned} &X_{10}=P_0\cos t_1+Q_0\sin t_1+\frac{A_1}{1-\nu^2}\cos\nu t_1+\frac{B_1}{1-\nu^2}\cos(\nu t_1+\beta),\\ &X_{k0}=\frac{A_k}{\lambda_k^2-\nu^2}\cos\nu t_1+\frac{B_k}{\lambda_k^2-\nu^2}\cos(\nu t_1+\beta).\end{aligned}\right\} \tag{5.26}$$

$$(k=2,\ 3,\ 4)$$

Evidently (5.26) satisfies (5.23). If P_0 and Q_0 in (5.26) are not simultaneously equal to zero for the integer ν ($\nu\neq 1$), and if the quantities

$$\left.\begin{aligned} &X_{11}=P_1\cos t_1+Q_1\sin t_1+W_{11}(t), \qquad X_{k1}=W_{k1}(t_1),\\ &X_{1n}=P_n\cos t_1+Q_n\sin t_1+W_{1n}(t_1), \qquad X_{kn}=W_{kn}(t_1),\end{aligned}\right\} \tag{5.27}$$

which are led from (5.24) and (5.25) satisfy the conditions

$$\left.\begin{aligned} &X_{11}(2\pi)=X_{11}(0), \qquad X_{11}'(2\pi)=X_{11}'(0),\\ &X_{k1}(2\pi)=X_{k1}(0), \qquad X_{k1}'(2\pi)=X_{k1}'(0),\\ &X_{1n}(2\pi)=X_{1n}(0), \qquad X_{1n}'(2\pi)=X_{1n}'(0),\\ &X_{kn}(2\pi)=X_{kn}(0), \qquad X_{kn}'(2\pi)=X_{kn}'(0),\end{aligned}\right\} \tag{5.28}$$

then $X_i(t_1)$ in (5.19) becomes the periodic function with period 2π which is ν times the period $2\pi/\nu$ of disturbing force. Consequently X_i is the sub-harmonic oscillations of order $1/\nu$ and x_i becomes the sub-harmonic oscillation having period ω/ν. In (5.27), the terms W_{i1} and W_{in} represent the forced vibrations. Eq. (5.28) expresses the periodicity conditions for X_i which require that the terms $\sin t_1$ and

$\cos t_1$ are not present in the right-hand side of the 1st equation of (5.24) and of (5.25), since otherwise terms $t_1 \sin t_1$ and $t_1 \cos t_1$ would arise in the solutions which present an exponential resonance case. Therefore the coefficients of $\sin t_1$ and $\cos t_1$ should be zero, and through this condition, P_0, Q_0, P_n and Q_n are determined. Since p_2, p_3 and p_4 are not integral multiples of p_1, *viz.*, λ_k is not an integer, and since the frequencies of disturbing forces in the right-hand side of the 2nd equations of (5.23), (5.24) and (5.25) are integers, resonance does not occur and the periodicity condition can be satisfied.

Setting

$$C_i(X_1', X_2', X_3', X_4') = C_{i1}X_1' + C_{i2}X_2' + C_{i3}X_3' + C_{i4}X_4', \tag{5.29}$$

and considering that the terms $\sin t_1$ and $\cos t_1$ are not contained in the right-hand side of the 1st equation of (5.24), and using the relation (5.26), we have

$$\left.\begin{aligned} &\frac{1}{\varepsilon}(1-\lambda_1^2)P_0 + C_{11}Q_0 + g_0(P_0, Q_0) = 0, \\ &-C_{11}P_0 + \frac{1}{\varepsilon}(1-\lambda_1^2)Q_0 + h_0(P_0, Q_0) = 0, \end{aligned}\right\} \tag{5.30}$$

where

$$g_0 = \frac{1}{\pi}\int_{-\pi}^{\pi} \Phi_1(X_{10}, X_{20}, X_{30}, X_{40}) \cos t_1 \, dt_1, \qquad h_0 = \frac{1}{\pi}\int_{-\pi}^{\pi} \Phi_1(X_{j0}) \sin t_1 \, dt_1. \tag{5.31}$$

Using (5.30) we can determine P_0 and Q_0. Observing (5.30), we can see that when $\Phi_1(X_{j0})$ does not contain the terms $\sin t_1$ and $\cos t_1$, the sub-harmonic oscillations do not take place, since $g_0 = h_0 = 0$ and $P_0 = Q_0 = 0$. In order to determine the values of P_0, Q_0, P_1, Q_1, P_n and Q_n etc., the condition given later in (5.33) is required. From (5.22) (5.24) and (5.25), we have

$$\begin{aligned} J_{1n} &= \frac{1}{\varepsilon}(1-\lambda_1^2)X_{1n} + C_1(X_{jn}') + G_{1n} \\ &= \frac{1}{\varepsilon}(1-\lambda_1^2)X_{1n} + C_1(X_{jn}') + \sum_{j=1}^{4} X_{jn}\left(\frac{\partial \Phi_1}{\partial X_j}\right)_{\varepsilon=0} + Z_{1n}(X_{j0}, X_{j1}, \ldots, X_{j,n-1}) \\ &= \sum_{j=1}^{4}\left\{X_{jn}'\left(\frac{\partial H_1}{\partial X_j'}\right)_{\varepsilon=0} + X_{jn}\left(\frac{\partial H_1}{\partial X_j}\right)_{\varepsilon=0}\right\} + Z_{1n} \\ &= \left\{X_{1n}'\left(\frac{\partial H_1}{\partial X_1'}\right)_{\varepsilon=0} + X_{1n}\left(\frac{\partial H_1}{\partial X_1}\right)_{\varepsilon=0}\right\} \\ &\quad + \left\{X_{2n}'\left(\frac{\partial H_1}{\partial X_2'}\right)_{\varepsilon=0} + X_{2n}\left(\frac{\partial H_1}{\partial X_2}\right)_{\varepsilon=0}\right\} + \ldots + Z_{1n}. \end{aligned}$$

As the only terms containing P_n and Q_n in the above equation are X_{1n} and X_{1n}', using (5.27), we have

$$\begin{aligned} J_{1n} = &\left\{(-P_n \sin t_1 + Q_n \cos t_1)\left(\frac{\partial H_1}{\partial X_1'}\right)_{\varepsilon=0} + (P_n \cos t_1 + Q_n \sin t_1)\left(\frac{\partial H_1}{\partial X_1}\right)_{\varepsilon=0}\right\} \\ &+ \sum_{l=0}^{n}(a_l \sin lt_1 + b_l \cos lt_1), \end{aligned}$$

in which known quantities a_l and b_l do not contain P_n and Q_n. Putting

$$\left.\begin{aligned} S_P &= \frac{1}{\pi}\int_{-\pi}^{\pi}\left\{-\sin t_1\left(\frac{\partial H_1}{\partial X_1'}\right)_{\varepsilon=0}+\cos t_1\left(\frac{\partial H_1}{\partial X_1}\right)_{\varepsilon=0}\right\}\sin t_1 dt_1,\\ C_P &= \frac{1}{\pi}\int_{-\pi}^{\pi}\left\{-\sin t_1\left(\frac{\partial H_1}{\partial X_1'}\right)_{\varepsilon=0}+\cos t_1\left(\frac{\partial H_1}{\partial X_1}\right)_{\varepsilon=0}\right\}\cos t_1 dt_1,\\ S_Q &= \frac{1}{\pi}\int_{-\pi}^{\pi}\left\{\cos t_1\left(\frac{\partial H_1}{\partial X_1'}\right)_{\varepsilon=0}+\sin t_1\left(\frac{\partial H_1}{\partial X_1}\right)_{\varepsilon=0}\right\}\sin t_1 dt_1,\\ C_Q &= \frac{1}{\pi}\int_{-\pi}^{\pi}\left\{\cos t_1\left(\frac{\partial H_1}{\partial X_1'}\right)_{\varepsilon=0}+\sin t_1\left(\frac{\partial H_1}{\partial X_1}\right)_{\varepsilon=0}\right\}\cos t_1 dt_1, \end{aligned}\right\} \tag{5.32}$$

the required conditions are

$$\left.\begin{aligned} C_P P_n + C_Q Q_n &= -b_1,\\ S_P P_n + S_Q Q_n &= -a_1, \end{aligned}\right\}$$

for the reason that J_{1n} does not have the terms of $\sin t_1$ and $\cos t_1$. Then the following condition which is required to make it possible to determine P_n and Q_n is

$$\begin{vmatrix} C_P & C_Q \\ S_P & S_Q \end{vmatrix} \neq 0. \tag{5.33}$$

Amplitudes of sub-harmonic oscillation can be obtained from (5.30).

Observing the transformation (5.7), we can see that the sub-harmonic oscillations are not rectilinear vibrations but are the whirling motions in which angular velocity is equal to ω/ν, in this system having gyroscopic terms.

4. Stability of sub-harmonic oscillations

Even if the solutions of sub-harmonic oscillations are obtained as stated in the preceding section, such vibrations do not actually occur unless they are stable solutions. In the present section, the treatment of stability of sub-harmonic oscillation in the system having multiple degrees of freedom is discussed in a manner similar to that devised by Andronow and Witt.[9]

After observing (5.26), we take for the solutions of (5.18) the forms

$$\left.\begin{aligned} X_1 &= U_1(t_1)\cos t_1 + V_1(t_1)\sin t_1 + \frac{A_1}{1-\nu^2}\cos \nu t_1 + \frac{B_1}{1-\nu^2}\cos(\nu t_1+\beta),\\ X_k &= U_k(t_1)\cos \lambda_k t_1 + V_k(t_1)\sin \lambda_k t_1 + \frac{A_k}{\lambda_k^2-\nu^2}\cos \nu t_1 + \frac{B_k}{\lambda_k^2-\nu^2}\cos(\nu t_1+\beta), \end{aligned}\right\} \tag{5.34}$$

$$(k=2,\ 3,\ 4)$$

in which U_1 and V_1 are slowly varying functions of time t_1, and U_k, V_k, U_1', V_1', U_k', V_k', U_k'' and V_k'' are small quantities of the same order of ε, and U_1'' and V_1'' have the same order of magnitude ε^2. By differentiation of (5.34) we find

$$\left.\begin{aligned} X_1' &= (U_1' + V_1)\cos t_1 + (V_1' - U_1)\sin t_1 - \frac{A_1\nu}{1-\nu^2}\sin \nu t_1 - \frac{B_1\nu}{1-\nu^2}\sin(\nu t_1 + \beta), \\ X_1'' &= (U_1'' + 2V_1' - U_1)\cos t_1 + (V_1'' - 2U_1' - V_1)\sin t_1 - \frac{A_1\nu^2}{1-\nu^2}\cos \nu t_1 \\ &\quad - \frac{B_1\nu^2}{1-\nu^2}\cos(\nu t_1 + \beta). \end{aligned}\right\} \quad (5.35)$$

Observing (5.24) we have

$$H_1(X_j, X_j') = \frac{1}{\varepsilon}(1-\lambda_1^2)X_1 + C_1(X_j') + \Phi_1(X_j). \quad (5.36)$$

Substituting (5.34) and (5.35) into (5.36), we obtain

$$\begin{aligned} \varepsilon H_1(X_j, X_j') &= \varphi_0(U_1, V_1)\cos t_1 + \Phi_0(U_1, V_1)\sin t_1 + \psi_1(U_1, V_1, U_1', V_1')\cos t_1 \\ &\quad + \varphi_2(U_1, V_1, U_1', V_1')\sin t_1 + \psi_3(U_1, V_1, U_1', V_1', U_k, V_k, U_k', V_k'), \end{aligned} \quad (5.37)$$

where

$$\left.\begin{aligned} \varphi_0 + \psi_1 &= \frac{1}{\pi}\int_{-\pi}^{\pi} \varepsilon H_1 \cos t_1\, dt_1, \\ \Phi_0 + \psi_2 &= \frac{1}{\pi}\int_{-\pi}^{\pi} \varepsilon H_1 \sin t_1\, dt_1. \end{aligned}\right\} \quad (5.38)$$

Since p_k is not an integral multiple of p_1, *viz.*, λ_k is not an integer, U_k and V_k are not contained in φ_0, Φ_0, ψ_1 and ψ_2. In (5.37) φ_0, Φ_0 are the same small order of ε, and ψ_1, ψ_2 are small quantities of the same order of ε^2, ψ_3 is the term in which the period is not equal to 2π. Clearly U_1', V_2' are not contained in φ_0 and Φ_0 since φ_0, Φ_0 are small quantities of the same order of ε. Inserting (5.34), (5.35) and (5.37) into the 1st equation of (5.18), and assuming the higher powers of small quantities to be negligible, we have

$$2V_1' = \varphi_0, \qquad -2U_1' = \Phi_0. \quad (5.39)$$

When we put $U_1' = V_1' = 0$ in (5.39), then U_1 and V_1 obtained from (5.39) obviously coincide with P_0 and Q_0 taken from (5.30). Let U_1 and V_1 in a steady state ($U_1' = V_1' = 0$) be $U_{10}(=P_0)$ and $V_{10}(=Q_0)$ respectively, and then we replace U_1 and V_1 in (5.39) with $U_{10}+\xi$ and $V_{10}+\eta$, or

$$U_1 = U_{10} + \xi, \qquad V_1 = V_{10} + \eta$$

where ξ and η are small deviations from a steady state, and then we develope (5.39) in powers ξ and η and reject all but the linear terms in ξ and η, obtaining

$$\left.\begin{aligned} 2\eta' &= \xi\frac{\partial \varphi_0}{\partial U_1} + \eta\frac{\partial \varphi_0}{\partial V_1}, \\ -2\xi' &= \xi\frac{\partial \Phi_0}{\partial U_1} + \eta\frac{\partial \Phi_0}{\partial V_1}, \end{aligned}\right\} \quad (5.40)$$

where $\frac{\partial\varphi_0}{\partial U_1}$, $\frac{\partial\varphi_0}{\partial V_1}$, $\frac{\partial\Phi_0}{\partial U_1}$ and $\frac{\partial\Phi_0}{\partial V_1}$ take the values in a steady state ($U_1' = V_1' = 0$). From (5.40), we get

$$\frac{d\eta}{d\xi} = \frac{\xi\frac{\partial\varphi_0}{\partial U_1} + \eta\frac{\partial\varphi_0}{\partial V_1}}{-\xi\frac{\partial\Phi_0}{\partial U_1} - \eta\frac{\partial\Phi_0}{\partial V_1}} = \frac{A\xi + B\eta}{C\xi + D\eta}.$$

Required conditions for stability of motion are as follows[10]:

$$\left.\begin{aligned} AD - BC &= \frac{\partial\varphi_0}{\partial V_1}\frac{\partial\Phi_0}{\partial U_1} - \frac{\partial\varphi_0}{\partial U_1}\frac{\partial\Phi_0}{\partial V_1} < 0, \\ B + C &= \frac{\partial\varphi_0}{\partial V_1} - \frac{\partial\Phi_0}{\partial U_1} < 0. \end{aligned}\right\} \tag{5.41}$$

5. In the case in which p_2, p_3 etc. are integral multiples of p_1

In sections 3 and 4, we treat with occurrence and stability criteria of sub-harmonic oscillations on the assumption that p_2, p_3 and p_4 are not integral multiples of p_1. In the present section we discuss sub-harmonic oscillations when p_2 is integral multiple of p_1. Let us suppose that p_2 is κ times p_1, *i.e.*, $p_2/p_1 = \kappa$ (κ is an integer).

We replace (5.18) with the following equations:

$$\left.\begin{aligned} X_1'' + X_1 &= \{(1-\lambda_1^2)X_1 + \varepsilon C_1(X_j') + \varepsilon\Phi_1(X_j) + A_1\cos\nu t_1 + B_1\cos(\nu t_1+\beta)\} \\ &= H_1(X_j, X_j') + A_1\cos\nu t_1 + B_1\cos(\nu t_1+\beta), \\ X_2'' + \kappa^2 X_2 &= \{(\kappa^2-\lambda_2^2)X_2 + \varepsilon C_2(X_j') + \varepsilon\Phi_2(X_j)\} + A_2\cos\nu t_1 + B_2\cos(\nu t_1+\beta) \\ &= H_2(X_j, X_j') + A_2\cos\nu t_1 + B_2\cos(\nu t_1+\beta), \\ X_{3,4}'' + \lambda_{3,4}^2 X_{3,4} &= \varepsilon C_{3,4}(X_j') + \varepsilon\Phi_{3,4}(X_j) + A_{3,4}\cos\nu t_1 + B_{3,4}\cos(\nu t_1+\beta). \end{aligned}\right\} \tag{5.18a}$$

In (5.18a), $(\kappa^2 - \lambda_2^2) = \kappa^2(1-\lambda_1^2)$ is also a small quantity of the same order of ε, as well as of $(1-\lambda_1^2)$. The 1st approximation is as follows:

$$\left.\begin{aligned} X_{10} &= P_0\cos t_1 + Q_0\sin t_1 + \frac{A_1}{1-\nu^2}\cos\nu t_1 + \frac{B_1}{1-\nu^2}\cos(\nu t_1+\beta), \\ X_{20} &= R_0\cos\kappa t_1 + S_0\sin\kappa t_1 + \frac{A_2}{\kappa^2-\nu^2}\cos\nu t_1 + \frac{B_2}{\kappa^2-\nu^2}\cos(\nu t_1+\beta), \\ X_{30,40} &= \frac{A_{3,4}}{\lambda_{3,4}^2-\nu^2}\cos\nu t_1 + \frac{B_{3,4}}{\lambda_{3,4}^2-\nu^2}\cos(\nu t_1+\beta). \end{aligned}\right\} \tag{5.26a}$$

In the first place, it is required that X_{1n}, X_{2n}, X_{3n} and X_{4n} represented in the following equations

$$\left.\begin{aligned} X_{1n} &= P_n\cos t_1 + Q_n\sin t_1 + W_{1n}(t_1), \\ X_{2n} &= R_n\cos\kappa t_1 + S_n\sin\kappa t_1 + W_{2n}(t_1), \\ X_{3n,4n} &= W_{3n,4n}(t_1), \end{aligned}\right\} \tag{5.27a}$$

satisfy the relations (5.28) for positive integers but $\nu=1$. Consequently the components of $\sin t_1$ and $\cos t_1$ must not be contained in the right-hand side of the equations of X_{11} and X_{1n} and, furthermore, the terms of $\sin \kappa t_1$ and $\cos \kappa t_1$ should not be included in the right-hand side of the equations of the motions of X_{21} and X_{2n}. Required relations induced by these conditions are

$$\left.\begin{aligned}
&\frac{1}{\varepsilon}(1-\lambda_1^2)P_0+C_{11}Q_0+g_0(P_0,\ Q_0,\ R_0,\ S_0)=0,\\
&-C_{11}P_0+\frac{1}{\varepsilon}(1-\lambda_1^2)Q_0+h_0(P_0,\ Q_0,\ R_0,\ S_0)=0,\\
&\frac{\kappa^2}{\varepsilon}(1-\lambda_1^2)R_0+C_{22}\kappa S_0+u_0(P_0,\ Q_0,\ R_0,\ S_0)=0,\\
&-C_{22}\kappa R_0+\frac{\kappa^2}{\varepsilon}(1-\lambda_1^2)S_0+v_0(P_0,\ Q_0,\ R_0,\ S_0)=0,
\end{aligned}\right\} \tag{5.30a}$$

in which

$$\left.\begin{aligned}
u_0&=\frac{1}{\pi}\int_{-\pi}^{\pi}\Phi_2(X_{j0})\cos\kappa t_1\,dt_1,\\
v_0&=\frac{1}{\pi}\int_{-\pi}^{\pi}\Phi_2(X_{j0})\sin\kappa t_1\,dt_1,
\end{aligned}\right\} \tag{5.31a}$$

and in which g_0, h_0 are given by (5.31). We can determine P_0, Q_0, R_0 and S_0 by (5.30a). Even if $R_0=0$, $S_0=0$, sub-harmonic oscillations can appear, provided that P_0 and Q_0 are not equal to zero at the same time. According to a procedure similar to that in section 3, the condition to be able to determine P_n, Q_n, R_n and S_n is obtained as follows:

$$\begin{vmatrix} C_P & C_Q & C_R & C_S\\ S_P & S_Q & S_R & S_S\\ C_{P\kappa} & C_{Q\kappa} & C_{R\kappa} & C_{S\kappa}\\ S_{P\kappa} & S_{Q\kappa} & S_{R\kappa} & S_{S\kappa}\end{vmatrix}\neq 0, \tag{5.33a}$$

where

$$\left.\begin{aligned}
C_R&=\frac{1}{\pi}\int_{-\pi}^{\pi}\left\{-\kappa\sin\kappa t_1\left(\frac{\partial H_1}{\partial X_2'}\right)_{\varepsilon=0}+\cos\kappa t_1\left(\frac{\partial H_1}{\partial X_2}\right)_{\varepsilon=0}\right\}\cos t_1\,dt_1,\\
S_R&=\frac{1}{\pi}\int_{-\pi}^{\pi}\left\{-\kappa\sin\kappa t_1\left(\frac{\partial H_1}{\partial X_2'}\right)_{\varepsilon=0}+\cos\kappa t_1\left(\frac{\partial H_1}{\partial X_2}\right)_{\varepsilon=0}\right\}\sin t_1\,dt_1,\\
C_S&=\frac{1}{\pi}\int_{-\pi}^{\pi}\left\{\kappa\cos\kappa t_1\left(\frac{\partial H_1}{\partial X_2'}\right)_{\varepsilon=0}+\sin\kappa t_1\left(\frac{\partial H_1}{\partial X_2}\right)_{\varepsilon=0}\right\}\cos t_1\,dt_1,\\
S_S&=\frac{1}{\pi}\int_{-\pi}^{\pi}\left\{\kappa\cos\kappa t_1\left(\frac{\partial H_1}{\partial X_2'}\right)_{\varepsilon=0}+\sin\kappa t_1\left(\frac{\partial H_1}{\partial X_2}\right)_{\varepsilon=0}\right\}\sin t_1\,dt_1,\\
C_{P\kappa}&=\frac{1}{\pi}\int_{-\pi}^{\pi}\left\{-\sin t_1\left(\frac{\partial H_2}{\partial X_1'}\right)_{\varepsilon=0}+\cos t_1\left(\frac{\partial H_2}{\partial X_1}\right)_{\varepsilon=0}\right\}\cos\kappa t_1\,dt_1,\\
S_{P\kappa}&=\frac{1}{\pi}\int_{-\pi}^{\pi}\left\{-\sin t_1\left(\frac{\partial H_2}{\partial X_1'}\right)_{\varepsilon=0}+\cos t_1\left(\frac{\partial H_2}{\partial X_1}\right)_{\varepsilon=0}\right\}\sin\kappa t_1\,dt_1,
\end{aligned}\right\} \tag{5.32a}$$

$$
\left.\begin{aligned}
C_{Q\kappa} &= \frac{1}{\pi}\int_{-\pi}^{\pi}\left\{\cos t_1\left(\frac{\partial H_2}{\partial X_1'}\right)_{\varepsilon=0}+\sin t_1\left(\frac{\partial H_2}{\partial X_1}\right)_{\varepsilon=0}\right\}\cos \kappa t_1\, dt_1,\\
S_{Q\kappa} &= \frac{1}{\pi}\int_{-\pi}^{\pi}\left\{\cos t_1\left(\frac{\partial H_2}{\partial X_1'}\right)_{\varepsilon=0}+\sin t_1\left(\frac{\partial H_2}{\partial X_1}\right)_{\varepsilon=0}\right\}\sin \kappa t_1\, dt_1,\\
C_{R\kappa} &= \frac{1}{\pi}\int_{-\pi}^{\pi}\left\{-\kappa\sin \kappa t_1\left(\frac{\partial H_2}{\partial X_2'}\right)_{\varepsilon=0}+\cos \kappa t_1\left(\frac{\partial H_2}{\partial X_2}\right)_{\varepsilon=0}\right\}\cos \kappa t_1\, dt_1,\\
S_{R\kappa} &= \frac{1}{\pi}\int_{-\pi}^{\pi}\left\{-\kappa\sin \kappa t_1\left(\frac{\partial H_2}{\partial X_2'}\right)_{\varepsilon=0}+\cos \kappa t_1\left(\frac{\partial H_2}{\partial X_2}\right)_{\varepsilon=0}\right\}\sin \kappa t_1\, dt_1,\\
C_{S\kappa} &= \frac{1}{\pi}\int_{-\pi}^{\pi}\left\{\kappa\cos \kappa t_1\left(\frac{\partial H_2}{\partial X_2'}\right)_{\varepsilon=0}+\sin \kappa t_1\left(\frac{\partial H_2}{\partial X_2}\right)_{\varepsilon=0}\right\}\cos \kappa t_1\, dt_1,\\
S_{S\kappa} &= \frac{1}{\pi}\int_{-\pi}^{\pi}\left\{\kappa\cos \kappa t_1\left(\frac{\partial H_2}{\partial X_2'}\right)_{\varepsilon=0}+\sin \kappa t_1\left(\frac{\partial H_2}{\partial X_2}\right)_{\varepsilon=0}\right\}\sin \kappa t_1\, dt_1.
\end{aligned}\right\}
$$

The procedure to obtain conditions of stability of motion is given below. In this case, in place of (5.34), we may put the solutions of (5.18) as follows:

$$
\left.\begin{aligned}
X_1 &= U_1(t_1)\cos t_1+V_1(t_1)\sin t_1+\frac{A_1}{1-\nu^2}\cos \nu t_1+\frac{B_1}{1-\nu^2}\cos(\nu t_1+\beta),\\
X_2 &= U_2(t_1)\cos \kappa t_1+V_2(t_1)\sin \kappa t_1+\frac{A_2}{\kappa^2-\nu^2}\cos \nu t_1+\frac{B_2}{\kappa^2-\nu^2}\cos((\nu t_1+\beta),\\
X_{3,4} &= U_{3,4}(t_1)\cos \lambda_{3,4}t_1+V_{3,4}(t_1)\sin \lambda_{3,4}t_1+\frac{A_{3,4}}{\lambda_{3,4}^2-\nu^2}\cos \nu t_1\\
&\quad+\frac{B_{3,4}}{\lambda_{3,4}^2-\nu^2}\cos(\nu t_1+\beta).
\end{aligned}\right\}\qquad(5.34a)
$$

We suppose that U_3, U_4, V_3, V_4, U_1', U_2', U_3', U_4', V_1', V_2', V_3', V_4', U_3'', U_4'', V_3'' and V_4'' are small quantities of the same order as that of ε and that U_1'', U_2'', V_1'' and V_2'' are quantities of the same order as that of ε^2. Inserting (5.34a) into H_1 and H_2 in (5.18a), we put

$$
\left.\begin{aligned}
\varphi_{10}+\psi_1 &= \frac{1}{\pi}\int_{-\pi}^{\pi}\varepsilon H_1(X_j,\ X_j')\cos t_1\, dt_1,\\
\Phi_{10}+\psi_2 &= \frac{1}{\pi}\int_{-\pi}^{\pi}\varepsilon H_1(X_j,\ X_j')\sin t_1\, dt_1,\\
\varphi_{20}+\psi_{12} &= \frac{1}{\pi}\int_{-\pi}^{\pi}\varepsilon H_2(X_j,\ X_j')\cos \kappa t_1\, dt_1,\\
\Phi_{20}+\psi_{22} &= \frac{1}{\pi}\int_{-\pi}^{\pi}\varepsilon H_2(X_j,\ X_j')\sin \kappa t_1\, dt_1,
\end{aligned}\right\}\qquad(5.38a)
$$

in which φ_{10}, φ_{20}, Φ_{10} and Φ_{20} are the small quantities of the 1st order, and ψ_1, ψ_2, ψ_{12} and ψ_{22} small quantities of the 2nd. Substituting (5.34a) and (5.38a) into the 1st and 2nd equations of (5.18a), and rejecting all terms of order higher than the 1st, we obtain

$$
-2U_1'=\Phi_{10},\quad 2V_1'=\varphi_{10},\quad -2\kappa U_2'=\Phi_{20},\quad 2\kappa V_2'=\varphi_{20}.\qquad(5.39a)
$$

Generally φ_{10}, φ_{20}, Φ_{10} and Φ_{20} obtained from (5.38a) are functions of U_1, U_2, V_1

and V_2, since κ is integer.

Putting

$$\left.\begin{aligned} U_1 &= U_{10}+\xi_1, \\ U_2 &= U_{20}+\xi_2, \end{aligned}\right\} \qquad \left.\begin{aligned} V_1 &= V_{10}+\eta_1, \\ V_2 &= V_{20}+\eta_2, \end{aligned}\right\}$$

and neglecting higher powers of ξ_1, ξ_2, η_1 and η_2, we get

$$\left.\begin{aligned} 2\eta_1' &= \sum_{i=1}^{2}\left(\xi_i\frac{\partial\varphi_{10}}{\partial U_i}+\eta_i\frac{\partial\varphi_{10}}{\partial V_i}\right), \\ -2\xi_1' &= \sum_{i=1}^{2}\left(\xi_i\frac{\partial\Phi_{10}}{\partial U_i}+\eta_i\frac{\partial\Phi_{10}}{\partial V_i}\right), \\ 2\kappa\eta_2' &= \sum_{i=1}^{2}\left(\xi_i\frac{\partial\varphi_{20}}{\partial U_i}+\eta_i\frac{\partial\varphi_{20}}{\partial V_i}\right), \\ -2\kappa\xi_2' &= \sum_{i=1}^{2}\left(\xi_i\frac{\partial\Phi_{20}}{\partial U_i}+\eta_i\frac{\partial\Phi_{20}}{\partial V_i}\right), \end{aligned}\right\} \qquad (5.40\text{a})$$

where $\partial\varphi_{10,20}/\partial U_{1,2}$ and $\partial\Phi_{10,20}/\partial V_{1,2}$ take the values in steady state of motion which are already known. As we can transform simultaneous differential equations of the 1st order (5.40a) into the differential equation of the 4th order, which is

$$A_0Z^{(4)}+A_1Z'''+A_2Z''+A_3Z'+A_4Z=0,$$

then stability conditions of Hurvitz can be applied. Coefficients A_0, A_1, A_2, A_3, A_4 are the sum of the minor determinants of the determinant consisting of coefficients of (5.40a).

For the case in which not only p_2 but also p_3 and p_4 are integral multiples of p_1, a method such as mentioned in the present section can be employed.

6. Occurrence of "summed and differentical harmonic oscillations"

In this section, the prime in the quantity does not mean differentiation with respect to t_1; the prime here is used only to distingish notations. Now we consider the quantities ω_1 and ω_2 represented by

$$\omega_1(p_1\pm p_2)=p_1\omega, \qquad \omega_2(p_1\pm p_2)=p_2\omega,$$
$$\therefore\quad \omega_1\pm\omega_2=\omega, \qquad (5.42)$$

and rewrite (5.16) as follows:

$$\left.\begin{aligned} \ddot{X}_1+\omega_1^2X_1 &= (\omega_1^2-p_1^2)X_1+\varepsilon C_1'(\dot{X}_j)+\varepsilon\Phi_1'(X_j)+A_1'\cos\omega t+B_1'\cos(\omega t+\beta). \\ \ddot{X}_2+\omega_2^2X_2 &= (\omega_2^2-p_2^2)X_2+\varepsilon C_2'(\dot{X}_j)+\varepsilon\Phi_2'(X_j)+A_2'\cos\omega t+B_2'\cos(\omega t+\beta), \\ \ddot{X}_{3,4}+p_{3,4}^2X_{3,4} &= \varepsilon C_{3,4}'(\dot{X}_j)+\varepsilon\Phi_{3,4}'(X_j)+A_{3,4}'\cos\omega t+B_{2,4}'\cos(\omega t+\beta). \end{aligned}\right\} \qquad (5.43)$$

When we assume that

$$\omega_1\fallingdotseq p_1, \qquad \omega_2\fallingdotseq p_2, \qquad (5.44)$$

then $(\omega_1^2-p_1^2)$ and $(\omega_2^2-p_2^2)$ are small quantities of the 1st order, and we now treat with vibrations in rotating speed ω satisfying the relation

$$\omega = \omega_1 \pm \omega_2 \fallingdotseq p_1 \pm p_2. \tag{5.45}$$

Inserting (5.19) into (5.43), we obtain

$$\left.\begin{aligned}
&\ddot{X}_{10} + \omega_1^2 X_{10} = A_1' \cos \omega t + B_1' \cos(\omega t + \beta),\\
&\ddot{X}_{20} + \omega_2^2 X_{20} = A_2' \cos \omega t + B_2' \cos(\omega t + \beta),\\
&\ddot{X}_{30,40} + p_{3,4}^2 X_{30,40} = A_{3,4}' \cos \omega t + B_{3,4}' \cos(\omega t + \beta),
\end{aligned}\right\} \tag{5.46}$$

$$\left.\begin{aligned}
&\ddot{X}_{11} + \omega_1^2 X_{11} = \frac{1}{\varepsilon}(\omega_1^2 - p_1^2) X_{10} + C_1'(\dot{X}_{j0}) + \Phi_1'(X_{j0}),\\
&\ddot{X}_{21} + \omega_2^2 X_{21} = \frac{1}{\varepsilon}(\omega_2^2 - p_2^2) X_{20} + C_2'(\dot{X}_{j0}) + \Phi_2'(X_{j0}),\\
&\ddot{X}_{31,41} + p_{2,4}^2 X_{31,41} = C_{3,4}'(\dot{X}_{j0}) + \Phi_{3,4}'(X_{j0}),
\end{aligned}\right\} \tag{5.47}$$

$$\left.\begin{aligned}
&\ddot{X}_{1n} + \omega_1^2 X_{1n} = \frac{1}{\varepsilon}(\omega_1^2 - p_1^2) X_{1,n-1} + C_1'(\dot{X}_{j,n-1}) + G_{1,n-1}',\\
&\ddot{X}_{2n} + \omega_2^2 X_{2n} = \frac{1}{\varepsilon}(\omega_2^2 - p_2^2) X_{2,n-1} + C_2'(\dot{X}_{j,n-1}) + G_{2,n-1}',\\
&\ddot{X}_{3n,4n} + p_{3,4}^2 X_{3n,4n} = C_{3,4}'(\dot{X}_{j,n-1}) + G_{3,n-1;4,n-1}',
\end{aligned}\right\} \tag{5.48}$$

in which

$$\Phi_i'(X_1, X_2, X_3, X_4) = \Phi_i'(X_{10}, X_{20}, X_{30}, X_{40}) + \varepsilon G_{i1}' + \varepsilon^2 G_{i2}' + \cdots, \tag{5.21a}$$

and G_{in}' is given by an expression similar to (5.22). The solutions of 1st approximation are

$$\left.\begin{aligned}
X_{10} &= P_0 \cos \omega_1 t + Q_0 \sin \omega_1 t + \frac{A_1'}{\omega_1^2 - \omega^2} \cos \omega t + \frac{B_1'}{\omega_1^2 - \omega^2} \cos(\omega t + \beta),\\
X_{20} &= R_0 \cos \omega_2 t + S_0 \sin \omega_2 t + \frac{A_2'}{\omega_2^2 - \omega^2} \cos \omega t + \frac{B_2'}{\omega_2^2 - \omega^2} \cos(\omega t + \beta),\\
X_{30,40} &= \frac{A_{3,4}'}{p_{3,4}^2 - \omega^2} \cos \omega t + \frac{B_{3,4}'}{p_{3,4}^2 - \omega_2} \cos(\omega t + \beta).
\end{aligned}\right\} \tag{5.49}$$

Occurrence of two vibrations with frequencies $\omega_1 (\fallingdotseq p_1)$ and $\omega_2 (\fallingdotseq p_2)$ is possible provided that P_0, Q_0, R_0 and S_0 have definite values and that $P_0^2 + Q_0^2 \neq 0$, $R_0^2 + S_0^2 \neq 0$. Values of P_n, Q_n, R_n and S_n are determined by using the condition that periodicity of solutions is held, namely, that terms exciting resonance are not contained in the right-hand side of (5.47) and (5.48). Inserting (5.49) into (5.47), and denoting the coefficients of terms $\cos \omega_1 t$, $\sin \omega_1 t$ in Φ_1' as a_0, b_0 and coefficients of $\cos \omega_2 t$, $\sin \omega_2 t$ in Φ_2' as c_0, d_0, the above conditions lead to

$$\left.\begin{aligned}
&\frac{1}{\varepsilon}(\omega_1^2 - p_1^2) P_0 + C_{11} \omega_1 Q_0 + a_0(P_0, Q_0, R_0, S_0) = 0,\\
&\frac{1}{\varepsilon}(\omega_1^2 - p_1^2) Q_0 - C_{11} \omega_1 P_0 + b_0(P_0, Q_0, R_0, S_0) = 0,\\
&\frac{1}{\varepsilon}(\omega_2^2 - p_2^2) R_0 + C_{22} \omega_2 S_0 + c_0(P_0, Q_0, R_0, S_0) = 0,\\
&\frac{1}{\varepsilon}(\omega_2^2 - p_2^2) S_0 - C_{22} \omega_2 R_0 + d_0(P_0, Q_0, R_0, S_0) = 0.
\end{aligned}\right\} \tag{5.50}$$

Using (5.50), we can determine P_0, Q_0, R_0 and S_0. Since the relations

$$\omega_1 = \frac{p_1}{p_1 \pm p_2}\omega, \qquad \omega_2 = \frac{p_2}{p_1 \pm p_2}\omega,$$

are obtained by (5.42) and (5.45), if we put $p_1 \pm p_2 = p$, $p/\omega = \lambda$, then (5.50) can be transformed into the same equations as (5.30a) which is the equation of response curve of sub-harmonic oscillations. Although $a_0 = b_0 = 0$ leads to $P_0 = Q_0 = 0$ and $R_0 = S_0 = 0$ when $c_0 = d_0 = 0$ then vibrations of this kind do not appear, but when the components $\cos(\omega \mp \omega_2)$ $t$and $\sin(\omega \mp \omega_2)t$ are contained in Φ_1', and when Φ_2' includes the terms of $\cos\{\pm(\omega - \omega_1)t\}$ and $\sin\{\pm(\omega - \omega_1)t\}$, then a_0, b_0, c_0 and d_0 are not equal to zero; thus occurrence of these vibrations is possible. Values C_{11} and C_{22} in (5.50) are representations similar to (5.29). Conditions to make it possible to determine P_n, Q_n, R_n and S_n and to establish stability of motion are given by the same procedure as stated in section 5. When these conditions are satisfied, two vibrations with frequencies ω_1 and ω_2, the sum of which, or the difference between which is almost equal to frequency ω of external force, can take place simultaneously at the rotating speed of shaft ω which is almost equal to the absolute value of sum of or difference in the natural frequencies of p_i and p_k ($i = 1, 2, 3, 4$; $k = 1, 2, 3, 4$; $i \neq k$). Furthermore, the frequencies ω_1, ω_2 of these two vibrations are almost equal to the natural frequencies p_i and p_k. When the relation

$$p_{3,4} = lp_1 + kp_2$$

(l and k are positive or negative integers)

is held, we may well be apprehensive that at some step in the progress of successive approximations, $G_{3,n-1}$ and $G_{4,n-1}$ in (5.48) have components inducing resonance, and that periodicity conditions could not be held. But only if we replace 3rd equation in (5.43) with

$$\ddot{X}_{2,4} + (l\omega_1 + k\omega_2)^2 X_{2,4} = \{(l\omega_1 + k\omega_2)^2 - p_{3,4}^2\} X_{3n,4n} + \varepsilon C_{3,4}' + \varepsilon \Phi_{3,4}' + A_{3,4}' \cos\omega t + B_{3,4}' \cos(\omega t + \beta), \tag{5.43a}$$

is there no need for apprehension. Since $\{(l\omega_1 + k\omega_2)^2 - p_{3,4}^2\}$ is small of 1st order, we should use

$$X_{30,40} = T_0 \cos(l\omega_1 + k\omega_2)t + U_0 \cos(l\omega_1 + k\omega_2)t + \frac{A_{3,4}'}{\{(l\omega_1 + k\omega_2)^2 - \omega^2\}} \cos\omega t + \frac{B_{3,4}'}{\{(l\omega_1 + k\omega_2)^2 - \omega^2\}} \cos(\omega t + \beta), \tag{5.49a}$$

instead of 3rd equation of (5.49). Treatment from now on is the same as that already mentioned. Even if T_0, U_0, T_n and U_n become zero, vibrations of "summed and differential harmonic oscillations" can occur.

When the non-linear term Φ_i' is complicated and has many terms with various frequencies, vibration consisting of various modes may take place at the rotation speed ω which satisfies the relation

$$n\omega = lp_i \pm mp_j, \tag{5.52}$$

or the more general expression

$$n\omega = l_1 p_1 + l_2 p_2 + l_3 p_3 + l_4 p_4. \tag{5.53}$$

In (5.52), (5.53), l, m, n, l_1, l_2, l_3 and l_4 are positive or negative integers. Since in (5.52) putting $i=j$ and $n=1$, vibrations become sub-harmonic oscillations, then we may consider sub-harmonic oscillations as special cases of vibrations of "summed and differential harmonic oscillations" modes of which are discussed in the present section.

When sub-harmonic oscillation has the higher order, occurrence of this vibration is more difficult; then we may state that occurrence of vibrations of the most simple type expressed by $|p_i \pm p_j| = \omega$ is the most probable.

If the ratio p_1/p_2 is a rational number, then the excitation in the right-hand sides of (5.47) and (5.48) is on the whole periodic, and a convergent successive approximation process can be furnished. If, however, the ratio p_1/p_2 be irrational and excitation is thus an almost periodic function of time t, the problem of "difficulty of the samall divisors" would come up in the present case where the perturbation method previously applied is to be continued in order to obtain an approximation of higher order. This difficulty may, however, be circumvented in the present case as well as in the case of combination oscillation in one degree of freedom system, at least if there is damping in the system.[10]

Incidentally it should be noted that vibrations of "summed and differential harmonic oscillations" discussed in the present section are not rectilinear vibrations, but are whirling motions of forward or backward precession, accordingly as p_i is positive or negative.

7. Multiple degrees of freedom system without gyroscopic terms

Differential equation of n degrees of freedom system without gyroscopic terms is

$$a_{k1}\ddot{x}_1 + a_{k2}\ddot{x}_2 + \ldots + c_{k1}x_1 + c_{k2}x_2 + \ldots = F_k(t), \qquad (k = 1, 2, \ldots, n) \tag{5.1a}$$

instead of (5.1). Using some linear transformation between coordinates represented by

$$x_k = \alpha_{k1}X_1 + \alpha_{k2}X_2 + \ldots + \alpha_{kn}X_n, \tag{5.7a}$$

we carry out transformation into normal coordinates which lead to

$$\ddot{X}_k + p_k^2 X_k = F_k'(t). \tag{5.10a}$$

Consequently the differential equation with damping term and non-linear term

$$a_{k1}\ddot{x}_1 + a_{k2}\ddot{x}_2 + \ldots + \varepsilon b_{k1}\dot{x}_1 + \varepsilon b_{k2}\dot{x}_2 + \ldots + c_{k1}x_k + c_{k2}x_2 + \ldots + \varepsilon f(x_1, x_2, \ldots, x_n) = F_k(t), \tag{5.15a}$$

can be rewritten as follows:

$$\ddot{X}_k + p_k^2 X_k = \varepsilon C_k(\dot{X}_1, \dot{X}_2, \ldots, \dot{X}_n) + \varepsilon \Phi_k(X_1, X_2, \ldots, X_n) + F_k'(t), \tag{5.16a}$$

by transformation (5.10a), where C_k is a linear equation of $X_1, X_2, \ldots, X_n$, and Φ_k is a non-linear term, and F_k' is external force. Equation (5.16a) is exactly the

same as (5.16), and for this reason all discussions in sections 3, 4, 5 and 6 can be applied to general systems without gyroscopic terms. But vibrations appearing in systems without gyroscopic terms are not the whirling motions which take place in systems with gyroscopic terms; they are rectilinear vibrations.

Chapter VI. On the Critical Speed of Synchronous Backward Precession[11]

1. Introduction

Although, as has already been reported by the author, resonance of synchronous backward precession can occur when bearing pedestals deflect, this resonance can also appear when pedestals have no flexibility and there is a loose fit of ball bearing in pedestal. Furthermore, the auther finds that this critical speed takes place when single-row radial ball bearings are used. When the deflection curve of shaft whirls with angular velocity the same as rotating speed of shaft ω, and direction of whirl is reverse to that of rotation of shaft, such precessional motion is called "synchronous backward precession." The relation between dry friction and this resonance is also discussed in the present chapter.

2. Effects of fit of ball bearing (the case where self-aligning double-row ball bearing is used)

Two kinds of pedestals are used in our experiments as shown in Fig. 38, one comparatively rigid, the other more flexible. Measuring deflections at top of pedestals, we find that the former, pedestal II, has a stiffness of about 9.8×10^5 kg/cm and that the later, pedestal 1, has 1.15×10^3 kg/cm in *OB* direction.

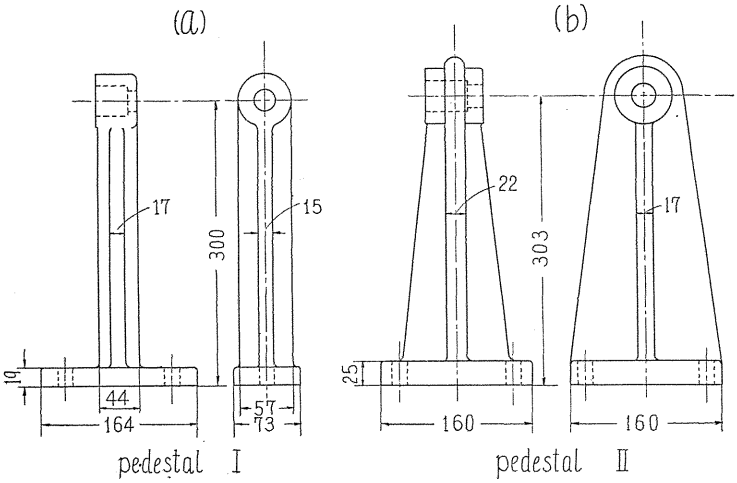

FIG. 38. Bearing pedestals.

When disc is not located at middle of shaft, *viz.*, $a \neq b$, as shown in Fig. 1, free vibrations with modes of backward precession can appear in the system, and the critical speed of synchronous backward precession can take place under certain

conditions. We can find that in such a vibratory system, critical speed of synchronous backward precession does not occur when rigid pedestal II is used and fit of ball bearing into bearing box is tight, and that it does take place when there is a loose fit.

As we have already reported, there are two critical speeds of synchronous backward precession, one is higher than the major critical speed ω_c, the other lower.[1)12)] We designate the former ω_{b1}, and the latter ω_{b2}.

The way of change in magnitudes of amplitudes at critical speed ω_{b2} accordingly as degree of fit is varied or different kinds of pedestals are used, is indicated in Fig. 39. In all experiments shown in Fig. 39, shaft No. 1 supported by self-aligning double-row ball bearings is used. In Fig. 39 (*a*), flexible pedestal I is used and fit of ball bearings is "medium fit"; in Fig. 39 (*b*) pedestal I and "wringing fit" is used; in Figs. 39 (*c*) and (*d*) pedestal II and "medium fit" is used, and in Fig. 39 (*e*) pedestal II and "wringing fit" is used. In the case of Fig. 39 (*e*) where rigid pedestal II is used and fit of ball bearing is tight, the peak of synchronous backward precession is smallest, and even though rigid pedestal II is used, amplitudes build up remarkably when fit is loose, as shown in Figs. 39 (*c*) and (*d*). Since stiffness of shaft considered together with pedestal in *OB* direction (see Fig. 1) is slightly smaller than that in *OA* direction, and non-uniformity of stiffness takes place when flexible pedestal I is used, rather high peaks of this critical speed can appear, as shown in Fig. 39 (*b*), even when fit of ball bearing is tight. Obviously,

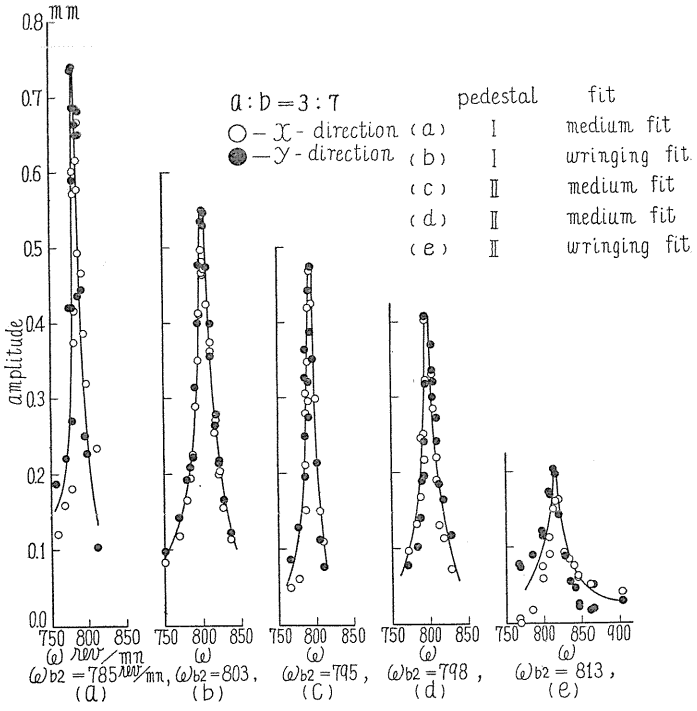

FIG. 39. Effect of fit of ball bearing and rigidity of pedestal at critical speed ω_{b2} (self-aligning double-row ball bearing, shaft No. 1, $a : b = 3 : 7$).

amplitudes in Fig. 39 (a) are largest when pedestal is flexible and fit is loose. The value of the critical speed ω_{b2} in Figs. 39 (a), (b), (c), (d) and (e) are 785, 803, 795, 798 and 813 r.p.m. respectively, and we can see that spring constants of shaft become large and the peak shifts to higher speed when pedestal is rigid or fit of ball bearing is tight. Fig. 40 is the result of using rigid pedestal II and "loose fit." In "loose fit" there is a somewhat large clearance between ball bearing and outer surface of outer ring of ball bearing. Fig. 40 shows that magnitude of amplitude does not increase accordingly as magnitude of clearance increases.

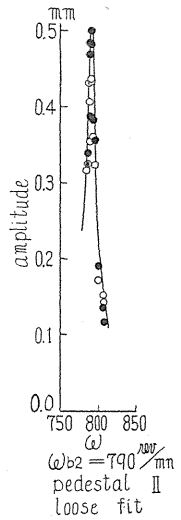

FIG. 40. Response curve for "loose fit" (shaft No. 1, self-aligning double-row ball bearing).

To vary fit of ball bearing, several kinds of bush are used, internal diameters of which differ slightly and are pressed into pedestal, as shown in Fig. 41.

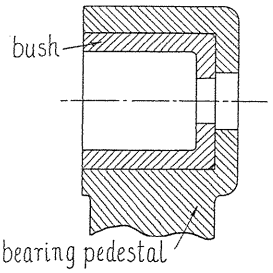

FIG. 41

Although the internal surface of bush is machined to a comparatively fine surface, it is not exactly a perfect circle. Furthermore, it is inevitable that flaws are created on the inner surface of bearing box when ball bearing is inserted into pedestal or is removed. Accordingly, as degree of fit of ball bearing into bush is not equal in all directions, thus stiffness of shaft considered together with pedestal is also not equal in all directions. This non-uniformity of stiffness results in occurrence of critical speeds of synchronous backward precession,[12] as just mentioned.

We can easily understand this behavior when we consider that, for example, if supporting condition of a cantilever becomes even slightly loose, its natural frequency is decreased remarkably. When we fix a cantilever tightly, increase in natural frequency does not become large beyond a certain limit, even if we support it more tightly. Similarly, when there is, to some extent, interference in all derections, non-uniformity of stiffness is comparatively small in spite of partial difference in interference; thus the peak of critical speed is small. From experiments we find that when rigid pedestal II is used and fit is "wringing fit," directional non-uniformity in natural frequency is only 0.5~1.0% and stiffness of shaft is almost equal in all directions. On the other hand, in the case of "medium fit" and "snug fit" where there is no clearance or there is a slight interference in a certain direction and clearance is present in other directions, directional non-uniformity may be largest. Since diameter of outer ring of ball bearing used in our experiment is 30 mm, there is clearance of $20 \sim 30\ \mu$ in "medium fit," and interference of $15 \sim 20\ \mu$ "wringing fit." As radial clearance between balls and inner ring or balls and outer ring is only several microns, interference can take place in all directions in "wringing fit." Directional difference in natural frequency p_0 when $\omega = 0$ is about

5% in experiments shown in Fig. 39 (*b*) and 0.9% in Fig. 39 (*e*), and these experimental results indicate that directional non-uniformity of stiffness becomes very small when pedestal is rigid and fit is tight.

Although directional difference in radial clearance results in the occurrence of critical speed of backward precession because of non-uniformity of stiffness, equal clearance in all derections does not result in appearance of this critical speed; it results in decrement of the critical speed because of decrease of stiffness. An analogy can be found in a discussion of the major critical speed in the system with radial backlash.[13] Consequently, the amplitude in Fig. 40, where considerable radial clearance exists in all directions, is almost equal to that in Fig. 39 (*b*) or (*c*). Owing to radial backlash, the peak in Fig. 40 is located at rotating speed lower than that in Figs. 39 (*c*) and (*d*).

Supposing a case where almost equal radial clearance is present in all directions and whirling motion of synchronous backward precession takes place, then the quetion comes up: Would friction in a ball bearing develop this whirling motion? If so, the actual occurrence of this critical speed can be attributed to a fricitional resisting force in bearing. Surely friction builds up that motion, but this effect is negligibly small. Energy given to shaft by frictional force is proportional to magnitude of deflection of shaft, while energy lost by viscous damping force is in proportion to square of deflection. Designating the former energy as E_1, the latter E_2, then we have

$$E_1 \propto \mu \cdot r \cdot s, \tag{6.1}$$

$$E_2 \propto c \cdot r^2, \tag{6.2}$$

where μ is coefficient of friction in ball bearing, r deflection of shaft, s radial clearance and c damping coefficient. As r is remarkably larger than s, ($r \gg s$) then $E_2 \gg E_1$ and E_1 only reduces damping action in the system. Therefore, frictional force in ball bearing can not introduce critical speeds of synchronous backward precession. Experimentally, we can artificially enlarge μ, but amplitude does not increase. Therefore, in Fig. 40 where s is large, the amplitude is almost equal to that in Fig. 39 (*c*), and is smaller than that in Fig. 39 (*a*).

The following experiment shown in Fig. 42 makes more clear the conclusion obtained in the present section. Fig. 42 (*a*) shows experimental result when rigid pedestal II is used and fit is "medium fit." Applying adhesive to inner surface of bush and outer surface of outer ring of ball bearing and then assembling the apparatus, we obtain experimental results shown in Fig. 42 (*b*) when adhesive has already dried, in about 3 or 4 days. Because adhesive does not make the fit tighter than "wringing fit," amplitude in Fig. 42 (*b*) is larger than that in Fig. 39 (*e*). However, since adhesive makes the amplitude markedly smaller, then the amplitude in Fig. 42 (*b*) is smaller than that in Fig. 42 (*a*).

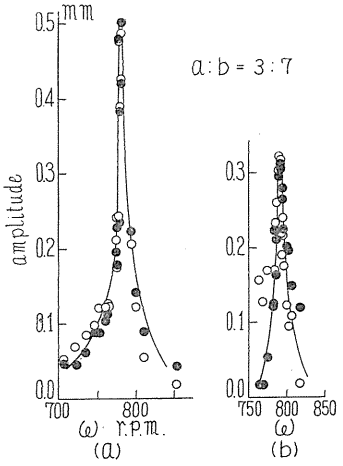

FIG. 42. Effect of fit at ω_{b2} (shaft No. 1, self-aligning double-row ball bearing).

In experiments shown in Figs. 39, 40 and 42, all conditions (eccentricity, ball bearing, shaft, etc.) except fit and pedestal are the same.

3. Where single-row radial ball bearins are used

Although spring characteristics are linear when the shaft is supported by self-aligning double-row ball bearings (see Chapter II), when the shaft is supported by single-row radial ball bearings, the non-linear, non-symmetrical characteristics induced by angular clearance of ball bearing and by out-of-alignment between center lines of upper and lower pedestals can take place. These characteristics also have directional non-uniformity, and thus rigidity of shaft itself is unequal in all directions. Therefore, critical speeds of synchronous backward precession take place in the shaft supported by single-row radial ball bearings even when rigid pedestal II is used and fit is tight.

Fig. 43 illustrates an experiment where upper and lower ball bearings have

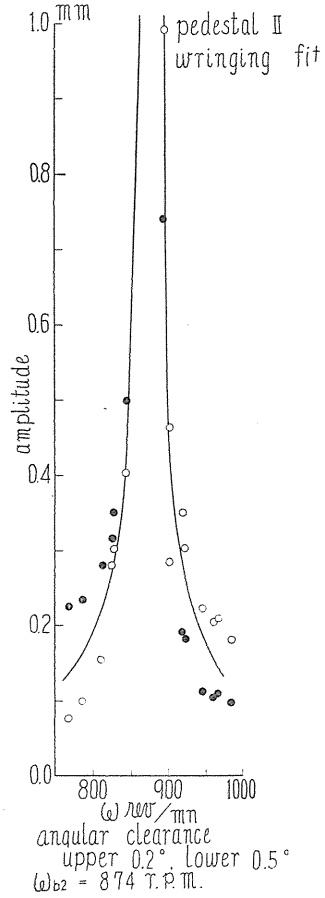

FIG. 43. Peak of synchronous backward precession appearing in shaft supported by single-row radial ball bearings (shaft No. 1, $a : b = 3 : 7$).

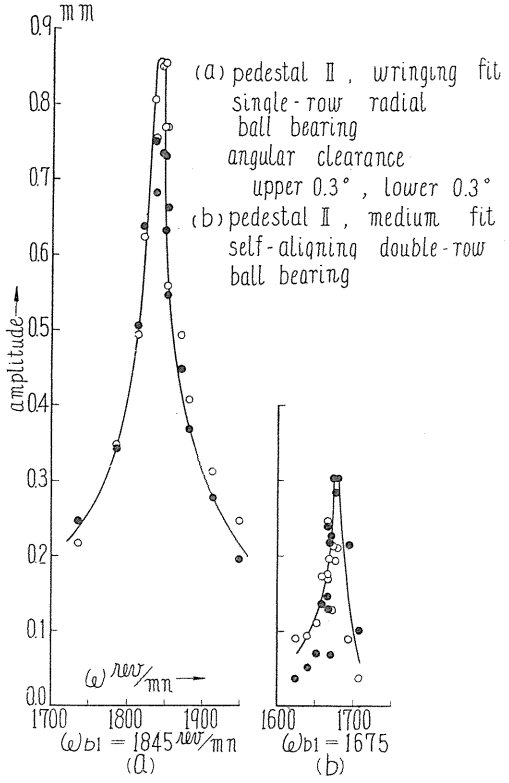

FIG. 44. Experimental results at the higher critical speed ω_{b1} of synchronous backward precession.

angular clearances 0.2° and 0.5°, where fit is "wringing fit" and rigid pedestal II is used. Here, amplitudes build up considerably larger than those in Figs. 39, 40 and 42 where self-aligning double-row ball bearings are used. In Fig. 43, where directional difference in natural frequency p_0 (when $\omega=0$) is about 8%, we can see that rigidity of shaft has considerable variation in all directions. Since single-row radial ball bearings are used, supporting condition of shaft is more rigid, and then critical speed ω_{b2} ($=874$ r.p.m.) is very much larger than that in Figs. 39, 40 and 42. In numerous experiments, we found that when single-row radial ball bearings are used it is inevitable that critical speeds ω_{b1} and ω_{b2} appear and that non-linearity takes place in spring characteristics.

Although Figs. 39, 40, 42 and 43 show results of experiments at lower critical speed ω_{b2}, similar results are also obtainable at higher critical speed ω_{b1}, as shown in Fig. 44. In experiment shown in Fig. 44 (a) where single-row radial ball bearings and rigid pedestal II are used and fit is "wringing fit," the peak is considerable. In experiment at ω_{b1} in which self-aligning double-row ball bearings and pedestal II are used and where fit is "wringing fit," the peak is so small as to be invisible. This experiment corresponds to that at ω_{b2} shown in Fig. 34 (e). On the other hand, when fit is "medium fit," the peak at ω_{b1} can appear, as shown in Fig. 44 (b).

4. Effect of guard ring

Use of guard ring G, shown in Fig. 1, to check the shaft-break is dangerous when critical speeds of synchronous backward precession take place, as we shall see later.

Checking increase of shaft deflections by guard ring with radial clearance 0.4 mm, results in the situation shown in Fig. 45. As rotating speed of shaft ω increases, the amplitude varies along curve AB and reaches point B where the shaft begins to touch inner surface of guard ring and "shaft whipping" due to dry friction exerting on the shaft then takes place. With further increase of ω, the amplitude varies along curve BC, and since the shaft keeps in touch with guard ring, we cannot accelerate ω more than C, and thus risk breakdown of the shaft. Then by stopping the whirling motion of "shaft whipping" to point D the motion changes along curve BD. When ω is retarded, the amplitude moves along D, B and A, thus no "shaft whipping" occurs. The reason the "shaft whipping" takes place only when ω is accelerated is clarified when we consider that at the time the shaft touches guard ring, the supporting condition of shaft changes and its stiffness is made more rigid; thus the resonance speed shifts to higher speed and point B becomes a rotating speed lower than resonance speed. As the motion at rotating speed lower than the resonance speed has the mode of synchronous backward precession in the case of "shaft whipping,"[14] the motions

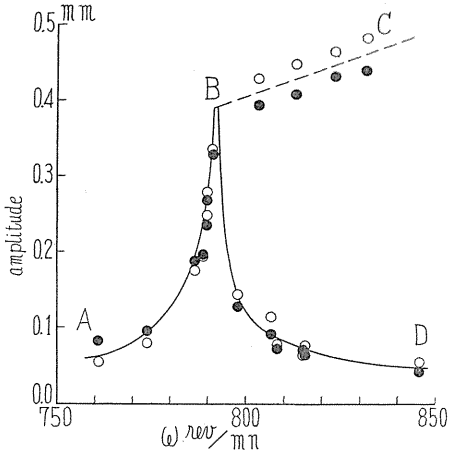

FIG. 45. "Shaft whipping" due to guard ring.

on curve BC as well as those on AB and BD are vibrations with synchronous backward precession $[-\omega]$.

When radial clearance is not considerable, "shaft whipping" does not occur, and if considerable is also difficult to make the shaft touch guard ring and cause appearance of frictional force, the only exception being when very large disturbing force is exerted. However, if whirling motion of synchronous backward precession exists, it is very easy to bring the system to "shaft whipping" condition. Accordingly, we can consider vibration of synchronous backward precession as a precondition for occurrence of "shaft whipping" induced by dry friction.

Vibratory waves of $[-\omega]$ as well as $[+\omega]$ are shown in Fig. 46. In Fig. 46 (c) transitions from $[+\omega]$ to $[-\omega]$ and vice versa are shown. In waves of $[-\omega]$, there is 180° difference in phase angle between x and y directions. In Fig. 46 (c), motion is rectilinear vibration appearing at both lower and higher speeds of peaks ω_{b1} and ω_{b2}, where whirling motion of shaft changes from backward to forward precession and vice versa.

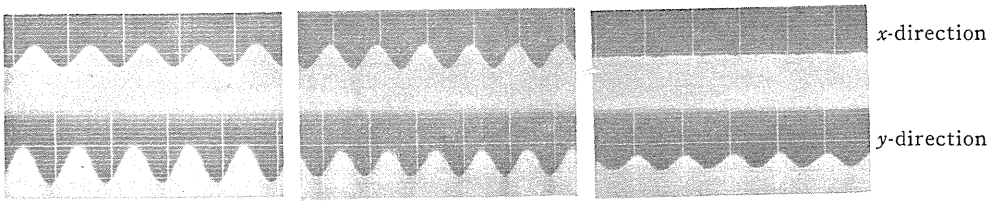

Synchronous forward precession $[+\omega]$. (a)

Synchronous backward precession $[-\omega]$. (b)

Tansition between $[+\omega]$ and $[-\omega]$. (c)

FIG. 46. Vibratory waves.

5. Forced vibrations of synchronous backward precession

As shown by curves I, II, III and V in Fig. 17, free vibrations of both forward and backward precession can take place in the system when $\omega \neq 0$ and $a \neq b$. Accordingly, designation of natural frequency p_i also describes its modes of vibration as represented by sign of p_i. Therefore, when we examine the nature of external disturbance in order to avoid resonant condition in such a system, we should find not only frequency of external force but also its modes of vibration. Assuming two kinds of external force with frequency ω_0, components of which in x and y directions are

$$P_x = A\cos\omega_0 t, \qquad P_y = A\sin\omega_0 t, \tag{6.3a}$$

and

$$P_x = A\cos\omega_0 t, \qquad P_y = B\sin\omega_0 t, \qquad (A \neq B), \tag{6.3b}$$

we find the dynamical effect of these two forces to be quite different. Although only one vibration of $[+\omega]$ takes place in the system by force shown by (6.3a), we can rewrite (6.3b) as follows:

$$\left.\begin{aligned} P_x &= \frac{1}{2}(A+B)\cos\omega_0 t + \frac{1}{2}(A-B)\cos\omega_0 t = C\cos\omega_0 t + D\cos\omega_0 t, \\ P_y &= \frac{1}{2}(A+B)\sin\omega_0 t - \frac{1}{2}(A-B)\sin\omega_0 t = C\sin\omega_0 t - D\sin\omega_0 t, \end{aligned}\right\} \quad (6.4)$$

and the force represented by (6.3a) or (6.4) can excite forced vibrations of both the forward and backward precession. As the locations of resonance speeds of these two forced vibrations are different, one exteral force of (6.3b) results in two kinds of critical speeds. Since, in practice, the disturbance exerted on the system shows that A is usually not equal to B, then we should consider one external force with frequency ω_0 as two disturbing forces and should treat with it in that way; otherwise, there would be occurrence of unexpected critical speed to cause trouble.

By exciting flexible pedestal I in the manner explained in section 4 of Chapter III, resonant conditions of backward precession take place along natural frequency curve $p-\omega$, as shown in Fig. 47, where p is the frequency of forced vibration, or natural frequency, and ω is rotating speed of shaft. Curve shown in Fig. 47 corresponds to curve III in Fig. 17 and to $p_3-\omega$ curve in Fig. 33 and 34. In Fig. 47, negative sign of p means backward precession.

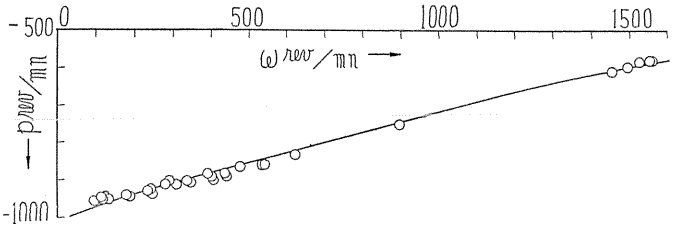

FIG. 47. Occurrence of forced vibrations of backward precession (shaft No. 1, $a:b=3:7$).

6. Conclusions

Conclusions arrived at in Chapter VI may be summarized as follows:

(1) When fit is loose, the critical speeds of synchronous backward precession can take place in spite of use of rigid pedestal.

(2) Directional non-uniformity of stiffness of shaft appears when fit is loose, resulting in these critical speeds.

(3) Since directional difference in shaft stiffness is considerable when single-row radial ball bearings are used, these critical speeds are remarkable.

(4) It is dangerous to check motion of synchronous backward precession by guard ring.

(5) The motion of synchronous backward precession can be considered a precondition to whirling motion of "shaft whipping" induced by dry friction.

(6) For the dynamic system with gyroscopic terms, one external force can excite forced vibrations of both forward and backward precession.

Chapter VII. On Critical Speeds of Shaft appearing at Lower Rotating Speeds[15]

1. Introduction

It has already been recognized that the secondary critical speed of a horizontal shaft can appear at a rotating speed equal to one-half the major critical speed.[16][17][18] We can prove that this critical speed can appear even if we use a vertical shaft.

Single-row radial ball bearings have small "angular clearance," therefore if bearing center lines of both bearing pedestals are not in alignment and if the shaft is not in a perfectly straight line, the statical deflection of shaft varies with angular position of the shaft. The statical deflection fluctuates with period $2\pi/\omega$ and it has components of $\sin n\omega t$ and $\cos n\omega t$, in which n is any integer. Under such conditions, when the periodic disturbing forces with frequencies $n\omega$ are applied to the disc supported by this shaft, then forced vibrations with frequencies 2ω, 3ω, 4ω etc. are induced. Accordingly, with even a vertical shaft, the secondary critical speed and other kinds of peaks can take place at rotating speeds lower than the major critical speed ω_c. Furthermore, these critical speeds of both forward and backward precession can take place since the system has gyroscopic terms.

2. Results of experiments

Two examples of experimental results are given in Fig. 48. In these experiments, shaft No. 1 ($a:b=3:7$) and single-row radial ball bearings with small angular clearances are used. Here peak $[+2\omega]$ shows the secondary critical speed of forward precession in which whirling speed of the elastic curve of shaft is exactly twice the rotating speed of shaft ω and peak $[-2\omega]$ indicates the secondary critical speed of backward precession. In Fig. 48 (a), peak $[-2\omega]$ is larger than that of $[+2\omega]$; in Fig. 48 (b) peak $[+2\omega]$ is larger than that of $[-2\omega]$. Over numerous experiments we were not able to determine which of the two is larger. Peaks $[+2\omega]$ and $[-2\omega]$ almost always appear remarkably when single-row radial ball bearings are used. When we change ball bearings from single-row radial ball bearings to self-aligning double-row ball bearings, however, all other conditions still remain the same as in Fig. 48, behavior of vibrations varies as shown in Fig. 49 where peak $[-2\omega]$ disappears and peak $[+2\omega]$ becomes considerably smaller and shifts to lower rotating speed. For the case where shaft No. 3 is used and ratio $a:b$ is changed, similar results to the above are obtained, as shown in Fig. 50 where peak $[-\omega]$ takes place because of directional non-uniformity of stiffness, as already explained in Chapter VI. In Fig. 50, amplitude of vibration of $[+2\omega]$ is almost equal to that of $[-2\omega]$. Changing from single-row radial ball bearings to self-aligning double-row ball bearings in Fig. 50, results in vibrations indicated in Fig. 51, in which neither peak $[+2\omega]$ nor $[-2\omega]$ takes place. Incidentally, peak $[-\omega]$ also does not appear because directional non-uniformity of spring characteristics vanishes. Thus we can see that peaks $[+2\omega]$ and $[-2\omega]$ do not usually occur when self-aligning double-row ball bearings are used, or if they do appear, they are very small. A remarkable occurrence of the whirling motions of $[+2\omega]$ and $[-2\omega]$ is possible in the vertical shaft only when the shaft is supported by single-row radial ball bearings.

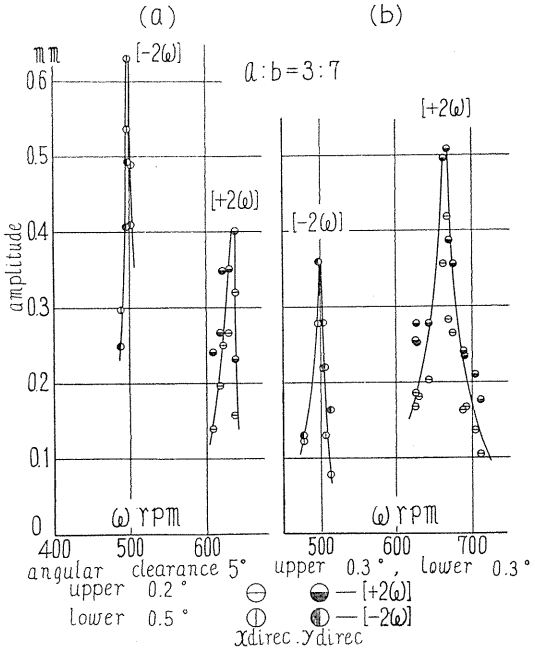

FIG. 48. Peak $[+2\omega]$ and peak $[-2\omega]$ (single-row radial ball bearing, shaft No. 1).

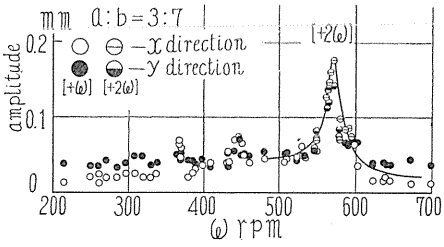

FIG. 49

FIG. 49. Peak of $[+2\omega]$ (self-aligning double-row ball bearing, shaft No. 1).

FIG. 50. Peaks of $[+2\omega]$ and $[-2\omega]$ (single-row radial ball bearing, shaft No. 3, $a:b=1:4$).

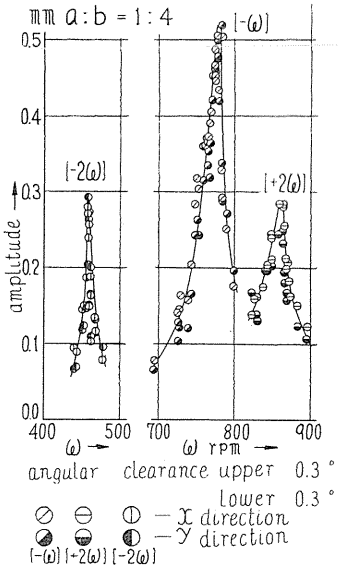

FIG. 50

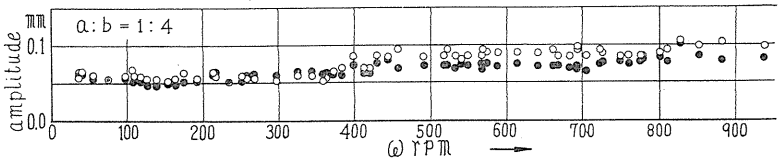

FIG. 51. Response curve (self-aligning double-row ball bearing, shaft No. 3).

3. Cause of occurrence of critical speeds of $[+2\omega]$ *and* $[-2\omega]$

Since the center lines of both upper and lower bearing pedestals are not in alignment, as mentioned in Chapter II, when the shaft is not deflected by any external force or moment and is located at equilibrium position (resting position), the shaft has already deflected under bending moment induced by out-of-alignment of center lines of pedestals when it is supported by single-row radial ball bearings. This statical deflection caused by bending moment appears on the plane where out-of-alignment exists.

Furthermore, because the shaft is not made exactly straight, its center line is not perfectly straight even when there is no stress, as shown in Fig. 52 (a_2). Fig. 52 (a_1) shows a straight shaft, but at neither journal end is the center line in alignment. In Figs. 52 (b) and (c), center lines of bearing pedestals are shown by chain lines, and center line of shaft when no bending action is exerted on shaft is represented by dotted line. When shafts such as shown in Figs. 52 (a_1) and (a_2) rotate, the situation becomes as indicated in Figs. 52 (b) and (c). When direction of bend of shaft coincides with direction of out-of-alignment of center lines of pedestals, as shown in Fig. 52 (c), bending action on the shaft by pedestals is smaller than bending action from any other angular position of the shaft, and stress in shaft due to bending takes the minimum value. On the other hand, when the shaft rotates by 180°, the situation becomes as shown in Fig. 52 (b) and the maximum bending action is exerted on the shaft. Consequently the statical deflection varies with period $2\pi/\omega$. If ball bearings have angular clearances, fluctuation of statical deflection is represented by Fourier's series having period $2\pi/\omega$, components of $\sin n\omega t$ and $\cos n\omega t$ (n is integer) as well as $\sin \omega t$ and $\cos \omega t$.

When ball bearings are not inserted correctly into journal of shaft, or groove on the inner ring of ball bearing is not machined exactly orthogonal to the center line of the inner ring, conditions become the same as outlined in the previous paragraph even if shaft is made perfectly straight.

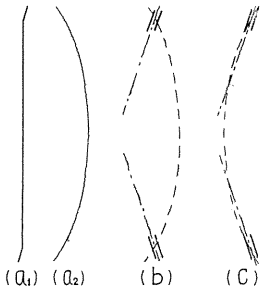

FIG. 52

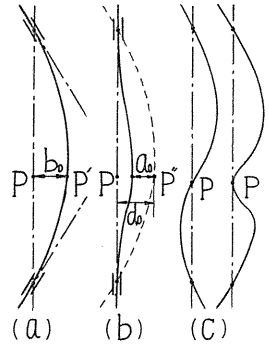

FIG. 53

In Fig. 53 (a), assuming the shaft which is made exactly straight is bent through out-of-alignment of pedestals, then disc center P is displaced to point P', and now we represent this deflection PP' as b_0. The displacement of disc is $d_0 = PP''$ when the shaft is not straight and is supported freely at both ends, as shown in Fig. 53 (b) where dotted line indicates center line of bent shaft when no

bending action is exerted on it. When the supporting condition changes and the shaft becomes fixed, the deflection decreases by a_0 and its value changes from d_0 to $d_0 - a_0$.

We assume, for brevity, that both center lines of upper and lower pedestals are present on the same plane and the elastic curve of deflection curve of shaft is a plane curve. Let $\bar{e}_0$ be deflection of disc when both pedestals are not in alignment and when shaft is not made exactly straight, then vector $\bar{e}_0$ of statical deflection is represented by

$$\bar{e}_0 = b_0 + (d_0 - a_0)\, e^{i\theta}, \tag{7.1}$$

where direction of out-of-alignment of pedestals $\overrightarrow{PP'}$ is positive direction of the real axis (x direction) and $\theta = \omega t$ is rotating angle of shaft.

The center line of shaft which is not exactly straight is in one or the other shapes as shown in Fig. 53 (c) when no stress appears in shaft; in such a case, d_0 in (7.1) is obviously equal to zero. As we shall see later, in the sense of dynamical effect, changing the balancing condition, namely, changing the value of eccentricity e or deviational angle τ, is equivalent to varying the magnitude of d_0. Since the value of d_0 will have no connection with our discussion from now on, we put $d_0 = 0$ for simplicity of treatment. Then (7.1) is rewritten

$$\bar{e}_0 = b_0 - a_0 e^{i\theta} = b_0 + a_0 e^{i(\omega t - \pi)} = R e^{i\delta_0}, \tag{7.1a}$$

where

$$R = \sqrt{a_0^2 + b_0^2 - 2 a_0 b_0 \cos \omega t}, \qquad \delta_0 = \tan^{-1}\left(\frac{-a_0 \sin \omega t}{b_0 - a_0 \cos \omega t}\right).$$

Because a single-row radial ball bearing has angular clearance, the relation (7.1a) is not always held. Now we suppose that when we change the inclination angle of elastic curve of the shaft at shaft ends by one-half angular clearance, the displacement varies by $c_0 (c_0 > 0)$. Consequently

$$\left.\begin{aligned} &\text{for} \quad R > c_0, \qquad \bar{e}_0 = (R - c_0)\, e^{i\delta_0}, \\ &\text{for} \quad R < c_0, \qquad \bar{e}_0 = 0. \end{aligned}\right\} \tag{7.2}$$

How to obtain $\bar{e}_0$ graphically is shown in Fig. 54. On the plane $z = x + iy$, putting $\bar{b}_0 = \overline{OA}$ on x-axis and drawing $-\bar{a}_0 = \overline{AB}$ as shown in the figure, thus $\overline{OB} = \overline{OA} + \overline{AB} = Re^{i\delta_0}$. Marking point D and extending $BD = c_0$, then $\overline{OD} = \bar{e}_0 = (R - c_0)e^{i\delta_0}$; thus we can obtain the position D of disc center for any angular position of shaft $\theta = \omega t$. When we rotate the shaft and θ is changed from 0 to 2π, we get a locus of point D, for example as shown in Fig. 54. The locus of D for the case of $a_0 : b_0 : c_0 = 1 : 2 : 1$ is shown in Fig. 54. Obviously the shape of locus is modified accordingly as ratio $a_0 : b_0 : c_0$ varies. Designating components of $\bar{e}_0$ in x and y directions as e_{0x} and e_{0y} respectively, for the simple case $a = b$ (see Fig. 1) the

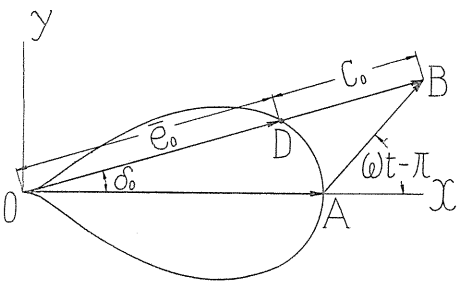

FIG. 54. Locus of shaft center ($a_0 : b_0 : c_0 = 1 : 2 : 1$).

differential equations of motion of disc are

$$\left.\begin{aligned} m\ddot{x}+\alpha x &= me\omega^2\cos(\omega t+\beta)+\alpha e_{0x},\\ m\ddot{y}+\alpha y &= me\omega^2\sin(\omega t+\beta)+\alpha e_{0y},\end{aligned}\right\} \tag{7.3}$$

For the general case of $a \neq b$ they are

$$\left.\begin{aligned} m\ddot{x}+\alpha x+\gamma\theta_x &= me\omega^2\cos(\omega t+\beta)+\alpha e_{0x}+\gamma\tau_{0x},\\ m\ddot{y}+\alpha y+\gamma\theta_y &= me\omega^2\sin(\omega t+\beta)+\alpha e_{0y}+\gamma\tau_{0y},\\ I\ddot{\theta}_x+I_p\omega\dot{\theta}_y+\gamma x+\delta\theta_x &= (I_p-I)\tau\omega^2\cos(\omega t+\beta+\varepsilon)+\gamma e_{0x}+\delta\tau_{0x},\\ I\ddot{\theta}_y-I_p\omega\dot{\theta}_x+\gamma y+\delta\theta_y &= (I_p-I)\tau\omega^2\sin(\omega t+\beta+\varepsilon)+\gamma e_{0y}+\delta\tau_{0y},\end{aligned}\right\} \tag{7.4}$$

where τ_{0x} and τ_{0y} are inclination angles of disc induced by e_{0x} and e_{0y} respectively, and β is angle between $\bar{e}_0$ and eccentricity e, and ε is angle between e and τ. Observing locus in Fig. 54 or Fig. 55, we can represent e_{0x} and e_{0y} as follows:

$$\left.\begin{aligned} e_{0x} &= a_0+A_1\cos\omega t+A_2\cos 2\omega t\\ &\quad +A_3\cos 3\omega t+\ldots,\\ e_{0y} &= B_1\sin\omega t+B_2\sin 2\omega t\\ &\quad +B_3\sin 3\omega t+\ldots,\end{aligned}\right\} \tag{7.5}$$

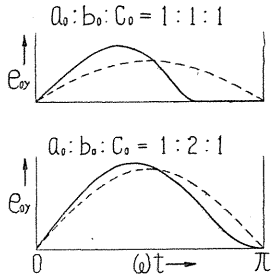

FIG. 55. $e_{0y}-\theta$ diagram.

or as

$$\left.\begin{aligned} e_{0x} &= a_0+\frac{1}{2}(A_1+B_1)\cos\omega t+\frac{1}{2}(A_2+B_2)\cos 2\omega t+\frac{1}{2}(A_3+B_3)\cos 3\omega t+\ldots\\ &\quad +\frac{1}{2}(A_1-B_1)\cos\omega t+\frac{1}{2}(A_2-B_2)\cos 2\omega t+\frac{1}{2}(A_3-B_3)\cos 3\omega t+\ldots\\ &= a_0+a_1\cos\omega t+a_2\cos 2\omega t+a_3\cos 3\omega t+\ldots\\ &\quad +a_{-1}\cos\omega t+a_{-2}\cos 2\omega t+a_{-3}\cos 3\omega t+\ldots,\\ e_{0y} &= \frac{1}{2}(A_1+B_1)\sin\omega t+\frac{1}{2}(A_2+B_2)\sin 2\omega t+\frac{1}{2}(A_3+B_3)\sin 3\omega t+\ldots\\ &\quad -\frac{1}{2}(A_1-B_1)\sin\omega t-\frac{1}{2}(A_2-B_2)\sin 2\omega t-\frac{1}{2}(A_3-B_3)\sin 3\omega t-\ldots\\ &= a_1\sin\omega t+a_2\sin 2\omega t+a_3\sin 3\omega t+\ldots\\ &\quad -a_{-1}\sin\omega t-a_{-2}\sin 2\omega t-a_{-3}\sin 3\omega t-\ldots.\end{aligned}\right\} \tag{7.5a}$$

Evidently coefficients a_n and a_{-m} in (7.5a) vary with ratio $a_0 : b_0 : c_0$ and are modified by magnitudes of a_0, b_0 and c_0. As we have already remarked in section 5 of Chapter VI, since the system with gyroscopic terms represented by (7.4) has free vibrations of both forward and backward precession, a_n and a_{-m} in (7.5a) excite forced vibrations of modes of $[+n\omega]$ and $[-m\omega]$ respectively. Forced vibration of mode of $[+\omega]$ induced by a_1 can be vanished by adjustment of eccentricity e and deviational angele τ, but vibrations of other modes cannot be vanished

by modification of balancing conditions of disc.

We can consider that magnitudes of a_0, b_0 and c_0 have values of the same order. Magnitudes of a_n and a_{-m} for several values of ratio $a_0 : b_0 : c_0$ are shown in the following table.

$a_0 : b_0 : c_0$	a_2/a_0	a_{-2}/a_0	a_3/a_0	a_{-3}/a_0	a_4/a_0	a_{-4}/a_0
1 : 1 : 1	0.1382	0.0274	0.0289	0.0111	0.0106	0.0135
1 : 2 : 1	0.0428	0.0915	0.0072	0.0346	0.0032	0.0157
1 : 2 : 1.25	0.0634	0.0871	0.0181	0.0298	0.0120	0.0046
1 : 4 : 3	0.0258	0.0692	0.0023	0.0159	0.0046	0.0069

Since values decrease in order of $a_{\pm 2}$, $a_{\pm 3}$, $a_{\pm 4}$, peaks $[\pm 2\omega]$ appear most strongly and those of $[\pm 3\omega]$ and $[\pm 4\omega]$ less strongly. As we can see by the above table, since a_{-2} is larger than a_2 when $a_0 < b_0$, and a_{-2} is smaller than a_2 for $a_0 > b_0$, then both cases in which peak $[-2\omega]$ is either larger or smaller than peak $[+2\omega]$, are possible, as shown in Fig. 48. When a_0 is 0.1 mm $\sim$ 1.0 mm, a_2 and a_{-2} become several microns $\sim$ 0.1 mm and these values are sufficient to generate remarkable peaks of $[+2\omega]$ and $[-2\omega]$.

Fig. 55 shows $e_{0y} - \theta$ diagrams for the case of $a_0 : b_0 : c_0 = 1 : 1 : 1$ and $1 : 2 : 1$, where the dotted line indicates a component of $\sin \omega t$. Clearly in Fig. 55, the component of $\sin 2\omega t$ predominates over all other components. In Fig. 56, the occurrence of peaks $[\pm 2\omega]$, $[\pm 3\omega]$ and $[\pm 4\omega]$ is shown; here shaft No. 1 ($a : b = 3 : 7$) and upper and lower single-row radial ball bearings with angular clearances 0.6° and 1.5° are used. These critical speeds can be obtained by drawing a straight lines $p = \pm n\omega$ in $p - \omega$ diagram and getting intersecting points of $p - \omega$ curves and line $p = \pm n\omega$, as shown, for example, in Fig. 17 or Fig. 33. Over numerous ex-

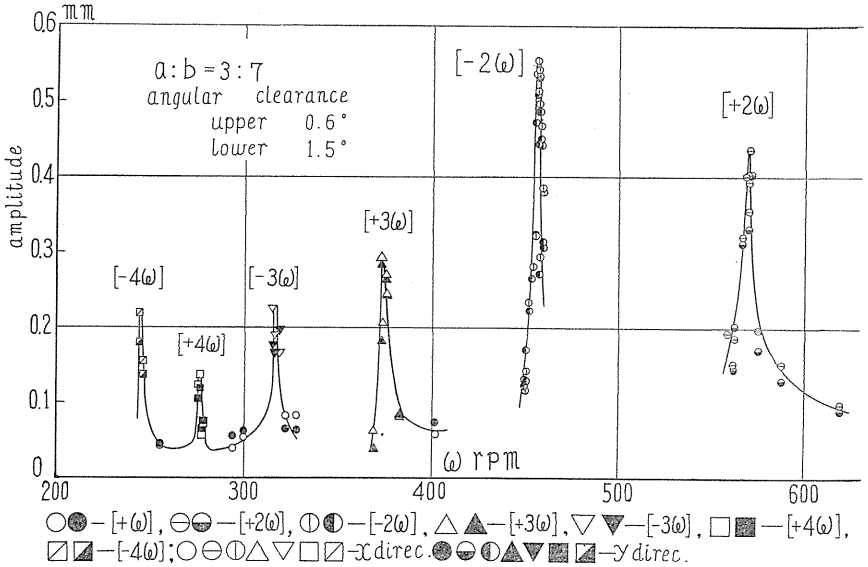

FIG. 56. Response curve (shaft No. 1).

periments, peaks $[\pm 3\omega]$ and $[\pm 4\omega]$ are not very large and peaks $[\pm 2\omega]$ are considerable.

For the case of self-aligning double-row ball bearings, in spite of their use, there is a somewhat small peak of $[+2\omega]$ in Fig. 49. As is already well-known, occurrence of vibration with frequency $(\nu \pm 1)\omega$ is possible provided that coupling is incorrectly assembled and bending moment varying with frequency $\nu\omega$ is applied to shaft end.[17)19)] When spring coupling S in Fig. 1 and shaft are not in alignment and S is somewhat bent, periodic bending moment with period $2\pi/\omega$ can be exerted on shaft end which induces forced vibration $[+2\omega]$ as shown in Fig. 49. To prove this point, we performed the following experiment. In the apparatus of Fig. 49, we remove spring coupling S at a certain rotating speed and cut off connection between driver and shaft. Then the shaft is gradually retarded and passes through critical speed of $[+2\omega]$. Fig. 57 shows experimental result when shaft is retarded. Since the effect of spring coupling S is eliminated, peak $[+2\omega]$ does not appear in Fig. 57. On the other hand, because peaks $[+2\omega]$ and $[-2\omega]$ shown in Fig. 56 are induced by $\bar{e}_0$ and not by spring coupling S, then even if we remove spring coupling S in experiment of Fig. 56, peaks $[+2\omega]$ and $[-2\omega]$ still exist in experiment under retarded condition, as shown in Fig. 58. Owing to retardation, the peaks $[+2\omega]$ and $[-2\omega]$ in Fig. 58 are somewhat smaller than those in Fig. 56.[22)]

In Fig. 59 vibratory waves of $[+2\omega]$ and $[-2\omega]$ are shown. Loci of shaft center S in motion of $[+2\omega]$ and $[-2\omega]$ are indicated in Fig. 60. Since the motion of $[+\omega]$ with rather small amplitude is superposed on those of $[+2\omega]$ and $[-2\omega]$, locus of $[+2\omega]$ is an epitrochoid and that of $[-2\omega]$ is a hypotrochoid. In Fig. 60 the interval between mark ○ and the next shows one revolution of shaft.

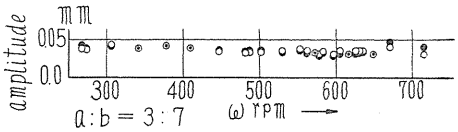

FIG. 57. Response curve under retarded condition (self-aligning double-row ball bearing).

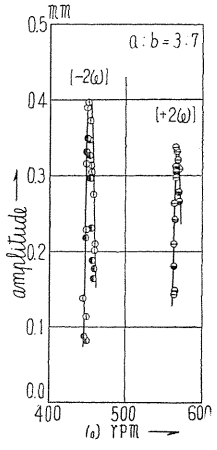

FIG. 58. Response curve under retarded condition (single-row radial ball bearing).

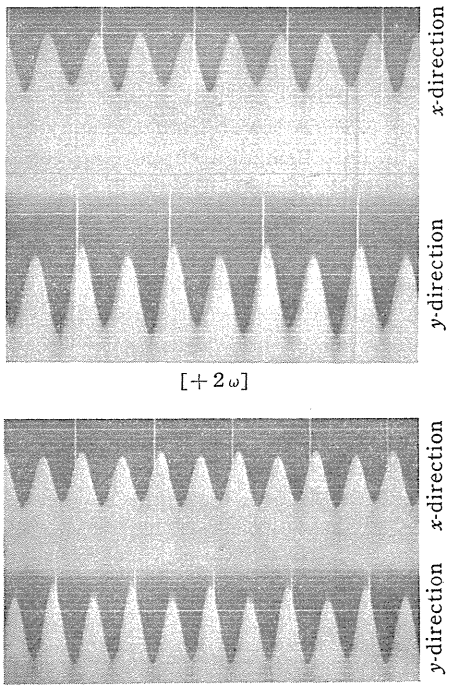

FIG. 59. Vibratory waves.

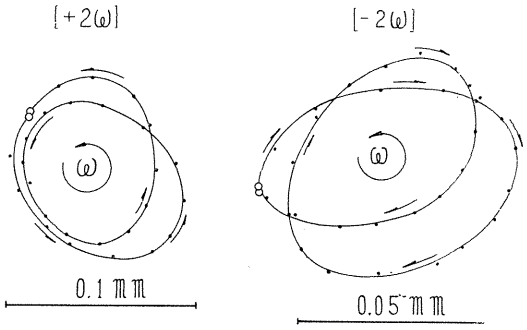

FIG. 60. Locus of shaft center *S*.

4. Conclusion

Conclusions arrived at in the present chapter may be summarized as follows:

1) When single-row radial ball bearings are used, remarkable peaks of $[+2\omega]$ and $[-2\omega]$ can take place even in vertical shaft, since there exist out-of-alignment between both upper and lower bearing pedestals, and angular clearance in ball bearing, and because machining shaft is not perfectly straight.

2) Peaks $[\pm 3\omega]$ and $[\pm 4\omega]$ with rather small amplitudes also take place.

3) Provided that coupling is assembled correctly, peaks $[\pm 2\omega]$ do not appear when self-aligning double-row ball bearings are used.

Chapter VIII. On Critical Speeds Induced by Ball Bearings Appearing at Lower Rotating Speeds

1. Introduction

That several critical speeds with various modes of vibration can take place at rotating speeds lower than the major critical speed ω_c, because of motion of steel balls in ball bearings supporting the shaft, is experimentally proved. Depending on construction of ball bearings, these critical speeds appear. They are found only in the shafts spported by single-row radial ball bearings, and never when self-aligning double-row ball bearings are used. Modes of vibration of critical speeds are determined by value of the rotating speed ω_1 of precessional motion of the balls during rotation of shaft (rotating speed of ball center around center of inner ring of ball bearing). These critical speeds are not induced by irregularities in ball bearings or by errors in machining. The construction of the ball bearing itself is the cause of these critical speeds.

In the present chapter, we discuss cause of the critical speeds and behavior of vibrations at critical speeds.

In Fig. 61, one example is given of response curve obtained by experiment. In this experiment, shaft No. 1 ($a:b=3:7$) supported by single-row radial ball bearing is used. Here response curves in $\omega = 300$ r.p.m. $\sim$ 1,100 r.p.m. and six peaks appearing at rotating speeds lower that the major critical speed $\omega_c = 1{,}200$ r.p.m. are indicated. Peak I of the motion $[+7/6 \cdot \omega]$ occurs in 1,020 r.p.m.; Peak II of $[-7/6 \cdot \omega]$ in 700 r.p.m.; Peak III of $[+13/6 \cdot \omega]$ in 525 r.p.m.; Peak IV of $[-13/6 \cdot \omega]$ in 420 r.p.m.; Peak V of $[+19/6 \cdot \omega]$ in 350 r.p.m., and Peak VI of $[-19/6 \cdot \omega]$ in 300 r.p.m. Peaks $[+7/6 \cdot \omega]$, $[+13/6 \cdot \omega]$ and $[+19/6 \cdot \omega]$ are

motions of forward precession; peaks $[-7/6 \cdot \omega]$, $[-13/6 \cdot \omega]$ and $[-19/6 \cdot \omega]$ are motions of backward precession. In the region 300 r.p.m.$\sim$1,100 r.p.m. there are critical speed ω_{b2} ($=800$ r.p.m.) of synchronous backward precession and others, discussed in Chapters VI and VII. The only critical speeds discussed in the present chapter are indicated in Fig. 61.

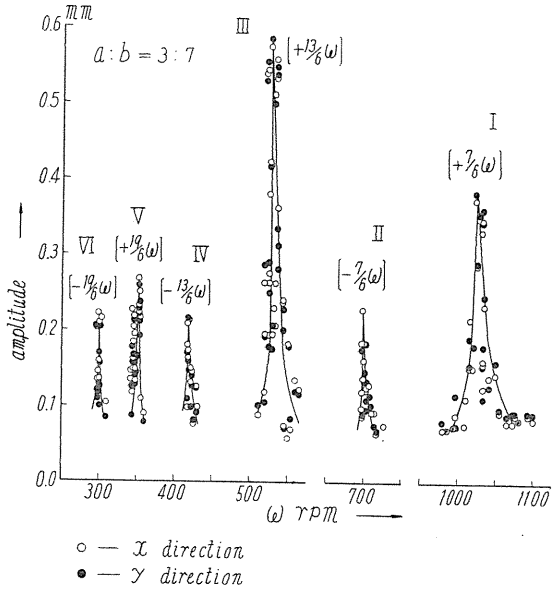

FIG. 61. Resonance curves at lower rotating speed.

2. Cause of occurrence of critical speeds

Noting the modes of vibrations, we see that the six critical speeds shown in Fig. 61 are furnished by precessional motion of balls in the ball bearing and by construction of the ball bearing itself.

a) Critical speed of $[+13/6 \cdot \omega]$ (Peak III)

By observing the motion of steel balls in a ball bearing during rotation of shaft, we can reveal the cause of occurrence of the critical speed, which we now explain.

An accepted rule is that the motion of the balls is carried out under the condition that the rolling contact is kept between balls and inner and outer rings. From a study of the motion of balls, it is concluded that as far as precessional motion of balls is concerned, that rule holds rigorously, independant of load, rotating speed of ω and lubrication,[20)23)] then we put

$$\alpha_1 = \omega_1/\omega, \tag{8.1}$$

where ω_1 is the angular velocity of precessional motion of balls, the value α_1 is a constant. When outer ring is fixed and inner ring rotates, we obtain the following relation[20)]

$$\alpha_1 = \frac{D}{2(D+d)} \tag{8.2}$$

because the motion of steel balls is in the state of rolling contact. In (8.2), D is diameter of inner ring and d is that of ball. For the single-row radial ball bearing used in our experiment, the value of

$$\left.\begin{aligned} &\alpha_1 = 0.3613 \fallingdotseq 13/36 = 0.3611, \\ \text{or}\quad &\omega_1 = 0.3613\,\omega \fallingdotseq 13/36 \cdot \omega, \end{aligned}\right\} \tag{8.3}$$

is obtained by actual measurement and the number of balls z put in one ball bearing is six. In a horizontal shaft system, radial load in vertical direction induced by gravitational force is exerted on ball bearing, and the journal of shaft moves slightly in vertical direction whenever a ball passes the point just under the shaft. Consequently disturbance having circular frequency

$$z\omega_1 = z\alpha_1\omega = 6 \times 13/36 \cdot \omega = 13/6 \cdot \omega \tag{8.4}$$

can be exerted on both ends of the shaft. External force caused by precessional motion of balls may be approximately put as follows:

$$F = A\cos z\omega_1 t = A\cos z\alpha_1\omega t = A\cos 13/6 \cdot \omega t, \tag{8.5}$$

and then occurrence of the critical speed of $[+13/6 \cdot \omega]$ becomes possible.

In our experiment, however, we use a vertical shaft. The reason for occurrence of peak $[+13/6 \cdot \omega]$ in the vertical shaft will now be explained.

As remarked in Chapter II, it is impossible for both upper and lower bearing pedestals to be in exact alignment; thus on the shaft there is always applied a bending action by the pedestals. Accordingly, in the direction where out-of-alignment is present between bearing center lines of both upper and lower pedestals, radial load induced by bending moment takes place, and then the critical speed $[+13/6 \cdot \omega]$ can occur as shown in Fig. 61.

When ball bearing is not accurately inserted into bearing box, or groove on outer ring is not correctly machined, the circumstances are the same even with alignment between both bearing center lines of pedestals.

b) Critical speed $[-13/6 \cdot \omega]$ (Peak IV)

The magnitude of disturbance A in (8.5) caused by precessional motion of steel balls varies with magnitude of radial load applying on ball bearing. Radial load induced by out-of-alignment between bearing center lines of pedestals is the largest in the direction in which out-of-alignment is present and the smallest in the direction perpendicular there-to. Accordingly, the disturbance through precessional motion of balls is not represented by (6.3a), but by (6.4). As explained in Chapter VI, in our experimental apparatus with gyroscopic effects, the external force having directional non-uniformity in magnitude as expressed by (6.4) results not only in forced vibration of forward precession, but also in that of backward precession, and thus the critical speed $[-13/6 \cdot \omega]$ can take place. Assuming that radial load takes place in x-direction caused by out-of-alignment of center lines, let e_0 be small deviation of shaft end in x-direction through passing of balls, as shown in Fig. 62. Magnitude of

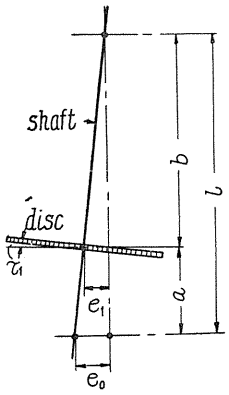

FIG. 62

deviation of disc center S and inclination angle of disc through e_0 are represented by e_1 and τ_1 respectively which are decided according to e_0 and $a:b$ (see Fig. 1). Now we assume that there is no deviation and no inclination angle in y-direction. In this rather simple case, the external forces

$$\left.\begin{aligned} F_x &= \frac{1}{2}(\alpha e_1+\gamma\tau_1)\cos\frac{13}{6}\omega t+\frac{1}{2}(\alpha e_1+\gamma\tau_1)\cos\frac{13}{6}\omega t,\\ F_y &= \frac{1}{2}(\alpha e_1+\gamma\tau_1)\sin\frac{13}{6}\omega t-\frac{1}{2}(\alpha e_1+\gamma\tau_1)\sin\frac{13}{6}\omega t,\\ F_{\theta x} &= \frac{1}{2}(\gamma e_1+\delta\tau_1)\cos\frac{13}{6}\omega t+\frac{1}{2}(\gamma e_1+\delta\tau_1)\cos\frac{13}{6}\omega t,\\ F_{\theta y} &= \frac{1}{2}(\gamma e_1+\delta\tau_1)\sin\frac{13}{6}\omega t-\frac{1}{2}(\gamma e_1+\delta\tau_1)\sin\frac{13}{6}\omega t, \end{aligned}\right\} \tag{8.6}$$

are added in the right-hand side of the first, second, third and fourth equations of (2.1) respectively, and the first terms in the right-hand side of (8.6) furnish peak $[+13/6\cdot\omega]$ and the second terms result in $[-13/6\cdot\omega]$.

c) Critical speeds of $[\pm 7/6\cdot\omega]$ and $[\pm 19/6\cdot\omega]$

As remarked in Chapter VII, the shaft is not made exactly straight, the center line not being a perfectly straight line even when there is no stress in the shaft. Therefore the magnitude of bending action through out-of-alignment between bearing center lines of both pedestals varies according to rotating angular postion of shaft, and radial load induced by bending moment changes periodically with period $2\pi/\omega$. Consequently, the small deviation e_0 in Fig. 62 fluctuates with period $2\pi/\omega$ and magnitude A of external force in (8.5) also varies; thus the disturbing force F in (8.5) can be approximately rewritten

$$\begin{aligned} F &= A_1(a+b\cos\omega t)\cos z\alpha_1\omega t\\ &= F_1\cos z\alpha_1\omega t+F_2\cos(z\alpha_1-1)\omega t+F_2\cos(z\alpha_1+1)\omega t. \end{aligned} \tag{8.7}$$

Since $\alpha_1\fallingdotseq 13/36\cdot\omega$ and $z=6$, then $z_1\alpha-1\fallingdotseq 7/6$ and $z\alpha_1+1=19/6$, hence

$$F=F_1\cos\frac{13}{6}\omega t+F_2\cos\frac{7}{6}\omega t+F_2\cos\frac{19}{6}\omega t \tag{8.8}$$

where the external forces with circular frequencies $7/6\cdot\omega$ and $19/6\cdot\omega$ are exerted on the disc. The constant part of disturbance through precessional motion of balls furnishes the external force with frequency $13/6\cdot\omega$, and the fluctuated parts induced by bend of shaft give the exciting forces with frequencies $7/6\cdot\omega$ and $19/6\cdot\omega$.

When ball bearings are not accurately inserted into shaft, or groove on inner ring is not correctly machined, the same effect as that resulting from bend of shaft comes up even when a prefectly straight shaft is used.

Since the external forces given by (8.8) are not of equal magnitude in all directions and have directional non-uniformity, critical speeds $[+7/6\cdot\omega]$, $[19/6\cdot\omega]$ of forward precession as well as peaks of $[-7/6\cdot\omega]$, $[-19/6\cdot\omega]$ of backward precession can take place.

It is expected that in a horizontal shaft because of larger magnitude of radial load, critical speeds $[\pm 13/6\cdot\omega]$ appear more strongly than in a vertical shaft.

Eqs. (8.5), (8.7) and (8.8) give approximate expressions in which we assume that the change of deviation e_0 in Fig. 62 through precessional motion of balls and the fluctuation of A in (8.5) induced by slight bend of shaft, are well represented by one circular function. These modes of changes would be represented more rigorously by forms containing terms of higher harmonics. It is anticipated, however, that coefficients of higher harmonics are very small and the distrubing forces furnished by higher harmonics are also very small. When we take into consideration higher harmonics, we can expect forced vibrations other than those shown in Fig. 61; but in our experiment such vibrations do not appear because the terms of higher harmonics are very small.

In Fig. 63, arrangement of balls in single-row radial ball bearing and in self-aliging double-row ball bearing is shown. In the former, the number of balls z is six and in the latter, eighteen, each with one row of nine balls. Since the interval between one ball and the next is very small in self-aligning double-row ball bearing, the disturbance e_0 by precessional motion of balls in Fig. 62 becomes very small. For self-aligning double-row ball bearings with 10 ϕ bore, $\alpha_1 \fallingdotseq 0.377 \fallingdotseq 17/45$, $z=18$, then if critical speeds $[\pm z\alpha_1\omega]$ take place, they would have modes $[\pm 34/5 \cdot \omega]$; but in our experiments in which we use self-aligning double-row ball bearings, peaks $[\pm 34/5 \cdot \omega]$ do not appear even in horizontal shaft[1] because of small e_0. Since the shaft is always freely supported when self-aligning double-row ball bearings are used, neither the out-of-alignment between center lines of both pedestals nor the bend of shaft furnish any effect on the shaft, and then all critical speeds $[\pm z\alpha_1\omega]=[\pm 34/5 \cdot \omega]$, $[\pm(z\alpha_1+1)\omega]=[\pm 39/5 \cdot \omega]$ and $[\pm(z\alpha_1-1)\omega]=[\pm 29/5 \cdot \omega]$ do not occur in our experiment with vertical shaft supported by self-aligning double-row ball bearings.[1]

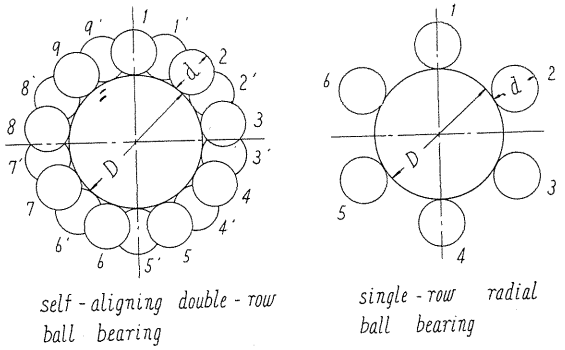

FIG. 63

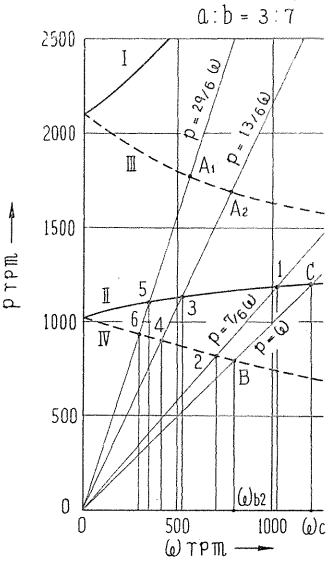

FIG. 64

FIG. 63. Arrangement of balls in ball bearings.

FIG. 64. Determination of critical speeds.

3. Location of critical speeds

We indicate in Fig. 64, $p-\omega$ curves of our experimental apparatus which is used in experiment shown in Fig. 61. Full line curves I and II represent natural

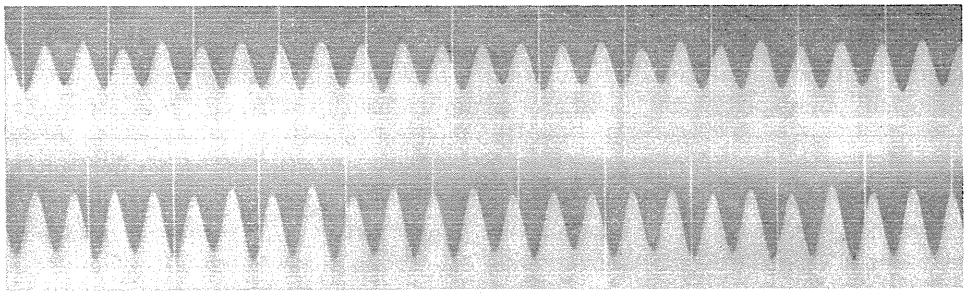

$[+13/6\,\omega]$

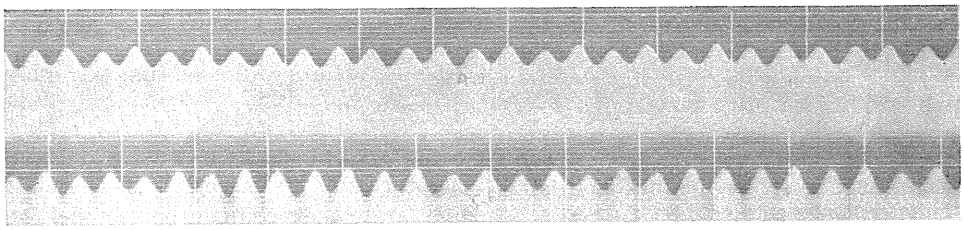

$[-13/6\,\omega]$

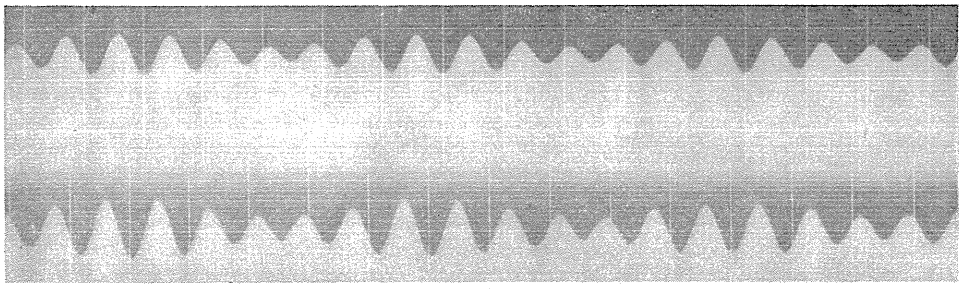

$[+7/6\,\omega]$

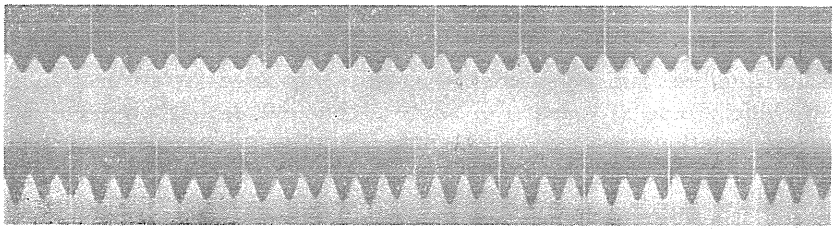

$[+19/6\,\omega]$

FIG. 65. Vibratory waves.

frequencies p of forward precession and dotted line curves III and IV express p of backward precession. Intersecting points C and B at which a straight line $p=\omega$ crosses curves II and IV respectively give the major critical speed ω_c of $[+\omega]$ and the critical speed ω_{b2} of synchronous backward precession $[-\omega]$. The abscissas of points 1, 3 and 5 where straight lines $p=7/6\cdot\omega$, $p=13/6\cdot\omega$ and $p=29/6\cdot\omega$ intersect curve II give the critical speeds of forward precession $[+7/6\cdot\omega]$ (Peak I), $[+13/6\cdot\omega]$ (Peak III) and $[+19/6\cdot\omega]$ (Peak V) respectively. Points 2, 4 and 6 at which these three straight lines intersect curve IV give the critical speeds of backward precession $[-7/6\cdot\omega]$ (Peak II), $[-13/6\cdot\omega]$ (Peak IV) and $[-19/6\cdot\omega]$ (Peak VI) respectively. Although these three straight lines can also intersect curve III, such vibrations, for example as represented by intersecting point A_1 or A_2 do not occur in our experiment. In one recording paper in Fig. 65 where several examples of vibratory waves are shown, the upper waves indicated are those in x-direction and the lower in y-direction. In the neighborhood of critical speed $[+7/6\cdot\omega]$, there is the strong major critical speed ω_c of $[+\omega]$, and superposition of two vibrations of $[+\omega]$ and $[+7/6\cdot\omega]$ results in the beating phenomena as shown in vibratory waves of $[+7/6\cdot\omega]$ in Fig. 65.

5. Conclusions

Obtained conclusoins in the present chapter may be summarized as follows:

1) When single-row radial ball bearings are used, critical speeds $[\pm z\alpha_1\omega]$ caused by precessional motion of balls appear even in a vertical shaft because of the presence of out-of-alignment between bearing center lines of both upper and lower pedestals.

2) Furthermore, peaks $[\pm(z\alpha_1\pm1)\omega]$ take place with bend of shaft.

3) Since disturbing forces induced by precessional motion of balls have directional non-uniformity in magnitude, critical speeds of backward precession $[-7/6\cdot\omega]$, $[-13/6\cdot\omega]$ and $[-19/6\cdot\omega]$ can appear.

4) Other critical speeds furnished by terms of higher harmonics do not appear.

5) When self-aligning double-row ball bearings are used, the deviation of e_0 in Fig. 62 is very small and the shaft is always freely supported, thus no critical speed excited by precessional motion of balls can occur.

Chapter IX. Vibrations of Rotating Shaft Generated by Passing through Critical Speed[22]

1. Introduction

The problem of critical speeds is usually discussed in connection with the system in which rotating speed ω of shaft is constant, *i.e.*, where neither acceleration nor retardation is present. Because there is no gyroscopic effect in the system where the disc is mounted in the middle of shaft ($a=b$ in Fig. 1), the critical speeds of backward precession (see Chapter VI) cannot take place even if the more flexible pedestal I (shown in Fig. 38) is used. Evidently the critical speed ω_{cA} in OA direction (Fig. 1) is slightly larger than that of ω_{cB} in OB direction because of flexibility of pedestal; response curves in both directions appear as shown in Fig. 66, where dotted lines represent the response curves in OA direction and full lines show those in OB direction. In the neighborhood of ω_{cA} or ω_{cB}, the path of shaft center S becomes an ellipse. When $\omega<\omega_{cB}$, gravitational center G

of disc locates outside of shaft center S, and inside when $\omega > \omega_{cA}$. In the region $\omega_{cB} < \omega < \omega_{cA}$, whirling motion of shaft center S is synchrounous backward precession with elliptical path, because G is outside of S in OA direction and inside in OB direction.

Clearly, this motion appears in the state of constant rotating speed. When the shaft is accelerated or retarded, *i.e.*, when ω is not constant, and the shaft passes through ω_{cA} and ω_{cB}, the motion becomes quite different and beating phenomena take place. In this chapter we study such complicated whirling motions and advance a method for balancing the rotating body by using beating phenomena.

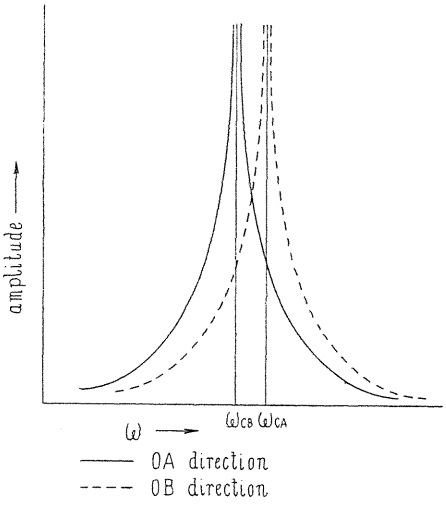

FIG. 66

2. Experimental apparatus

In so far as the experiment described in the present chapter is concerned, we use a horizontal shaft. The experimental apparatus has the following measurements: Diameter of disc 180 mm, thickness 12 mm, weight 2.126 kg; length of shaft 600 mm, diameter 12 mm, and $a = b$. Self-aligning double-row ball bearings are used in both pedestals in order to obtain linear spring characteristics of shaft, and flexible pedestals I are used.

At a certain rotating speed ω_0 higher than the major critical speeds ω_{cA} and ω_{cB}, we throw out the clutch and observe the motion in a state of retardation. Several kinds of lubrications are used in ball bearings and magnitude of retardation can be changed by magnitude of viscosity of grease.

3. Diagrams of retardation

State of retardation of the shaft is shown in Fig. 67 where we can see that retardation $d\omega/dt$ can be held in constant value during motion because potential energy due to deflection of shaft is smaller than 1% of kinetic energy of disc, even in rotating speed where maximum deflection appears. Mark ○ shows the speed where maximum deflection takes place.

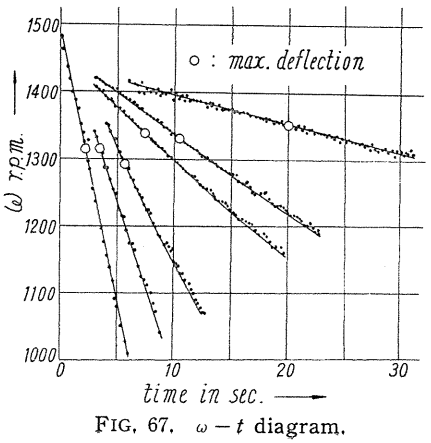

FIG. 67. $\omega - t$ diagram.

4. Motion of disc

In Fig. 68, vibration of retarded shaft in OA direction is given. After maximum deflection appears, remarkable beating phenomena set in. As we see later, superposition of forced vibration

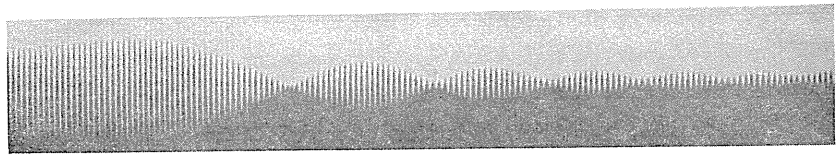

FIG. 68. Vibratory waves of beats.

due to eccentricity e and free vibration induced by angular retardation furnishes such beating phenomena. Maximum deflection appears after shaft passes critical speed and does not take place simultaneously in OA and OB directions. Since frequency of forced vibration coincides with rotating speed of shaft, and since natural frequency of free vibration agrees with critical speed, we can then understand that superposition of two vibrations in the neighborhood of the critical speed results in the beating phenomena. Furthermore, beating behavior varies accordingly as the magnitudes of retardation and the damping coefficient vary.

Analyzing records of motions in both OA and OB directions, the following facts are revealed.

1) Since location of maximum deflection of shaft and locations of loops and nodes of beating are different between OA and OB directions, locus of disc center S forms various shapes, *i.e.*, a circle, an ellipse or a straight line.

2) Diameter of circle of path of S and major or minor axis of ellipse change with time t.

3) Angular position of major or minor axis varies with time t and these axes revolve either in the same direction as rotation of shaft or in the opposite direction.

4) Whirling motion of shaft is sometimes forward precession and sometimes backward precession and at the transit point between forward and backward precession, and *vice versa*, the locus of shaft is a straight line and motion becomes a rectilinear vibration. For instance, the path of circle of forward precession gradually becomes thinner and changes into an ellipse; then magnitude of the minor axis decreases and finally equals zero when locus becomes a straight line and transit from forward precession to backward precession takes place, and the minor axis slowly becomes larger in the state of backward precession. Transit from backward to forward precession can be carried out in a similar manner. One example of changing from forward to backward precession is given in Fig. 69 where full lines represent loci of forward

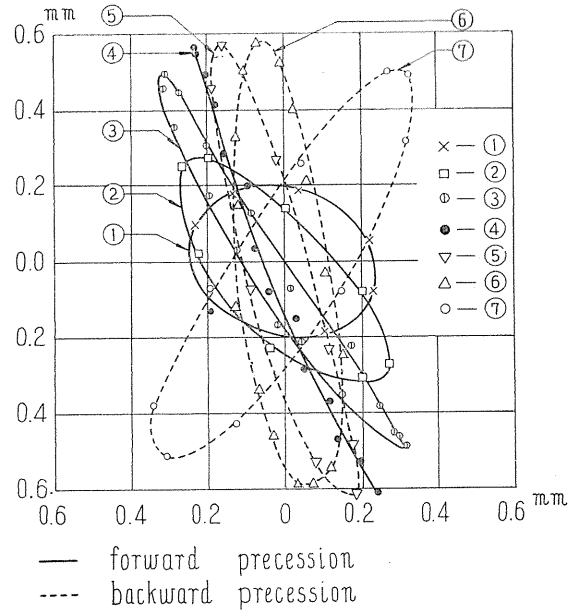

FIG. 69. Loci of path of shaft center S.

precession and dotted lines are those of backward precession and, numerals designating loci indicate the order of passing time.

This rather complicated motion of disc can be explained as follows. Consider the rectangular coordinate system o-xy in which the disc is located and let o be the position of the shaft center S when no deflection exists; let p be the natural frequency, let a and c be amplitudes of forced vibrations in x and y directions respectively, and let b and f be amplitudes of free vibrations in x and y directions respectively. The deflection of shaft center S consists of forced and free vibrations and can be represented as follows:

$$\left.\begin{aligned} x &= a\sin(\omega t+\varphi_a)+b\sin(pt+\varphi_b),\\ y &= c\sin(\omega t+\varphi_c)+f\sin(pt+\varphi_f),\end{aligned}\right\} \tag{9.1}$$

where φ_a, φ_b, φ_c and φ_d are phase angles at time $t=0$. Rewriting (9.1), we have

$$\left.\begin{aligned} x &= \sqrt{a^2+2ab\cos\{(p-\omega)t+(\varphi_b-\varphi_a)\}+b^2}\cdot\sin(\omega t+\varphi_a+\psi_x),\\ y &= \sqrt{c^2+2cf\cos\{(p-\omega)t+(\varphi_f-\varphi_c)\}+f^2}\cdot\sin(\omega t+\varphi_c+\psi_y),\end{aligned}\right\} \tag{9.2}$$

in which

$$\left.\begin{aligned} \tan\psi_x &= \frac{b\sin\{(p-\omega)t+(\varphi_b-\varphi_a)\}}{a+b\cos\{(p-\omega)t+(\varphi_b-\varphi_a)\}},\\ \tan\psi_y &= \frac{f\sin\{(p-\omega)t+(\varphi_f-\varphi_c)\}}{c+f\cos\{(p-\omega)t+(\varphi_f-\varphi_c)\}}.\end{aligned}\right\} \tag{9.3}$$

Concerning motions appearing in the neighborhood of critical speed, difference $(p-\omega)$ is small. Thereore the values $(p-\omega)t+(\varphi_b-\varphi_a)$ and $(p-\omega)t+(\varphi_f-\varphi_c)$ remain almost unchanged during one revolution of shaft $2\pi/\omega$; then putting

$$\left.\begin{aligned} \sqrt{a^2+2ab\cos\{(p-\omega)t+(\varphi_b-\varphi_a)\}+b^2} &= A,\\ \sqrt{c^2+2cf\cos\{(p-\omega)t+(\varphi_f-\varphi_c)\}+f^2} &= B,\\ \varphi_a+\psi_x &= \alpha,\\ \varphi_c+\psi_y &= \delta,\end{aligned}\right\} \tag{9.4}$$

A, B, α and δ do not change during one rotation $2\pi/\omega$. From (9.2) and (9.4), we have

$$x=A\sin(\omega t+\alpha),\qquad y=B\sin(\omega t+\delta). \tag{9.5}$$

So the relation between x and y

$$\frac{x^2}{A^2}+\frac{B^2}{y^2}-\frac{2xy}{AB}\cos(\delta-\alpha)=\sin^2(\delta-\alpha), \tag{9.6}$$

can be obtained from (9.5). The curve expressed by (9.6) is an ellipse. In (9.6), when $A=B$ and $\cos(\delta-\alpha)=0$, (9.6) is an equation of circle. Major axis D_1 of ellipse and minor axis D_2 are represented by

$$D_1,\ D_2=\frac{\sqrt{2}\,AB\sin(\delta-\alpha)}{A^2+B^2\pm\sqrt{(A^2+B^2)^2-4A^2B^2\sin^2(\delta-\alpha)}}, \tag{9.7}$$

in which the positive sign in denominator gives minor axis; negative sign furnishes major axis. Minor axis is equal to zero and motion becomes rectilinear vibration when $\sin(\delta-\alpha)=0$. Although both denominator and numerator become zero simultanuously when $\sin(\delta-\alpha)=0$, D_1 has a definite value.

By this we can clear up the cause of the phenomena of beating appearing after the shaft passing through the critical speed. Although D_1 and D_2 in (9.7) show almost no change in magnitude during one revloution of shaft $2\pi/\omega$, over a comparatively longer time they do vary slowly and this change results in a modification of form of path of shaft center. From (9.6), the angle Θ between x axis and major or minor axis of elliptical path is

$$\Theta=\frac{1}{2}\tan^{-1}\left\{\frac{2\cos(\delta-\alpha)\cdot AB}{A^2-B^2}\right\}. \qquad (9.8)$$

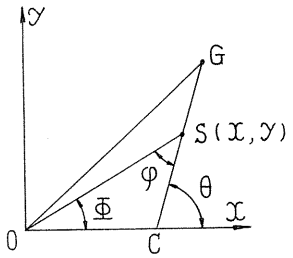

FIG. 70

Angle Θ is also a function of A, B, α and δ so that major or minor axis can rotate. As shown in Fig. 70, putting $x/y=\tan\Phi$, $d\Phi/dt$ is the angular velocity of disc center S around bearing center o. Clearly because

$$\tan\Phi=\frac{A\sin(\omega t+\alpha)}{B\sin(\omega t+\delta)},$$

then we have

$$\frac{d\Phi}{dt}=\cos^2\Phi\cdot\frac{A\omega\sin(\delta-\alpha)}{B\sin^2(\omega t+\delta)}. \qquad (9.9)$$

As A, B, $\cos^2\Phi$ and $\sin^2(\omega t+\delta)$ are positive, then when $\sin(\delta-\alpha)>0$, $d\Phi/dt$ has the same sign as that of $\Phi=d\theta/dt$ and whirling motion of shaft is forward precession. On the other hand, when $\sin(\delta-\alpha)<0$, the motion becomes backward precession. Fig. 71 is two diagrams of $\Theta-\omega/p$ curves obtained by experiment. Since value of retardation is constant as shown in Fig. 67, Fig. 71 is similar to

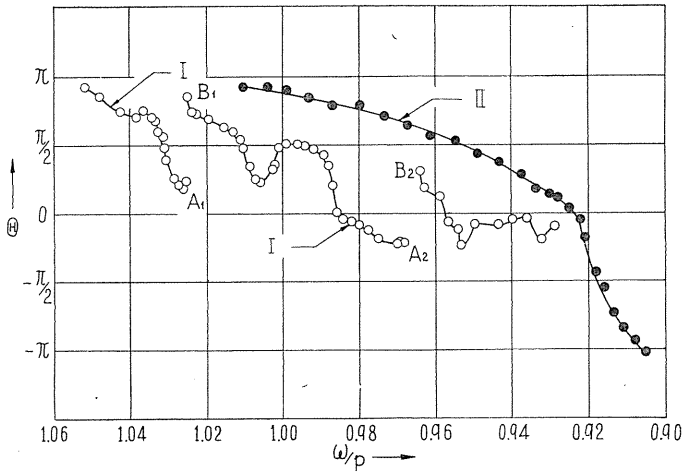

FIG. 71. $\Theta-\omega/p$ curves.

$\Theta - t$ diagram. In Fig. 71, Θ is the angle between x axis and major axis, and curve I is discontinuous because at these two discontinuous points, locus of path has become a circle and the distinction between the major and minor axis has vanished. Since there is a difference of about 270° between points A_1 and B_1; and between A_2 and B_2 in Fig. 71, we can see in the procedure of successive modification ellipse → circle → ellipse, that the direction of minor axis of the first ellipse coincides with that of major axis of the last ellipse. In the experiment given by curve II, since no circular locus is obtained, curve II has no discontinuous points. In Fig. 70, $\angle OSC = \varphi = \theta - \Phi$, and two diagrams of $\varphi - \omega/p$ obtained by experiments are shown in Fig. 72. Since $d\varphi/dt = d\theta/dt - d\Phi/dt = \omega - d\Phi/dt$, then the direction of tangent to curve shown in Fig. 72 is proportional to the difference between rotating speed of shaft ω and rotating speed $d\Phi/dt$ of disc center S. In Figs. 73 and 74, features of change of major and minor axes of locus are shown. In Fig. 73, mark ● shows the motion of synchronous backward precession and ○ represents motion of synchronous forward precession where we can see that locus of path of shaft center S can become a straight line even in transit from one forward precession to another forward precession as well as from backward to forward and from forward to backward. In Fig. 74, there is no backward precession.

Now we must note that maximum deflection takes place after shaft passes through the critical speed; therefore the rotating speed ω_m where the maximum deflection appears does not coincide with the critical speed p because of the existence of retardation. The value of $p - \omega_m$ is dependent upon magnitude of retardation and damping coefficient.

Two response curves are shown in Fig. 75 where r_1 and r_2 are amplitudes of vibrations, e is eccentricity, $\beta = d\omega/dt < 0$, $\gamma = \beta/p^2$ which is a dimensionless quantity of retardation.

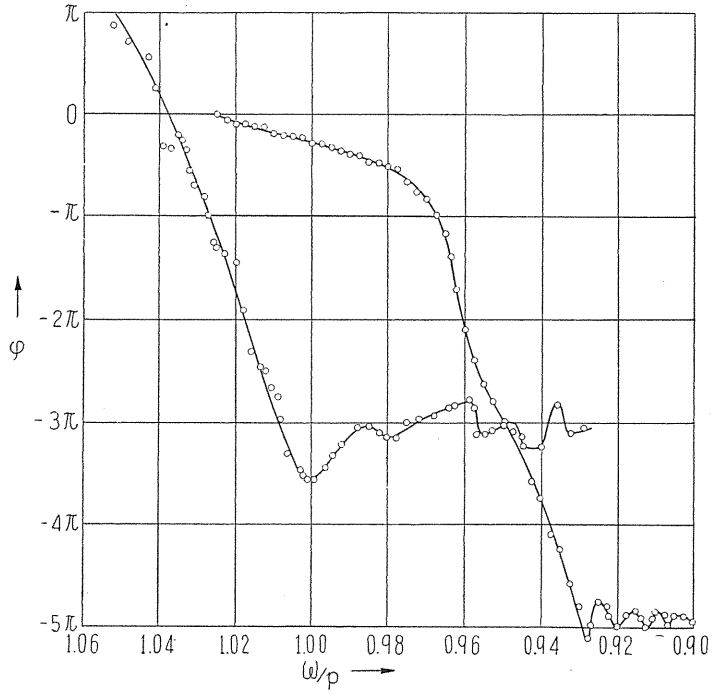

FIG. 72. $\varphi - \omega/p$ curves.

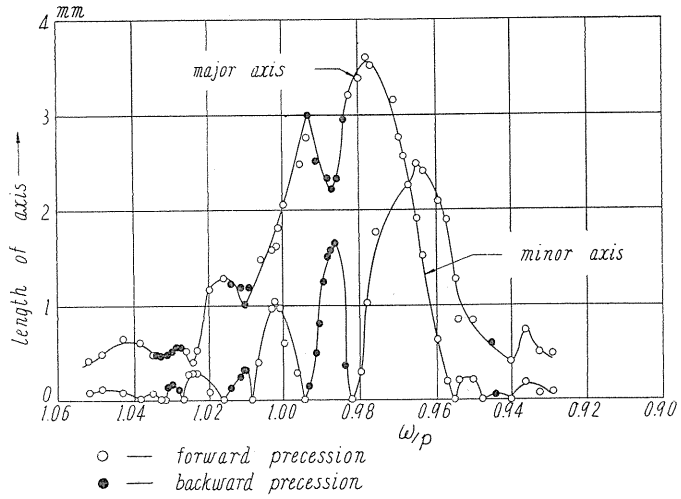

FIG. 73. Variation of magnitudes of major axis and minor axis.

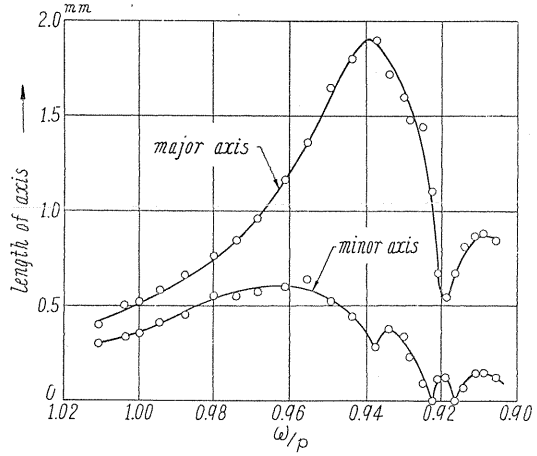

FIG. 74. Varitation of magnitudes of major axis and minor axis.

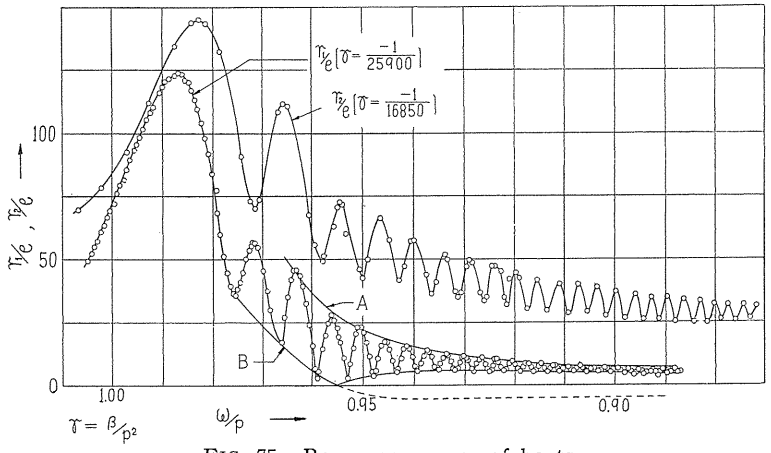

FIG. 75. Response curves of beats.

In Fig. 76, the relation $\omega_m/p - \gamma$ indicates that the difference $(p - \omega_m)$ increases with magnitude $|\gamma|$ or $|\beta|$.

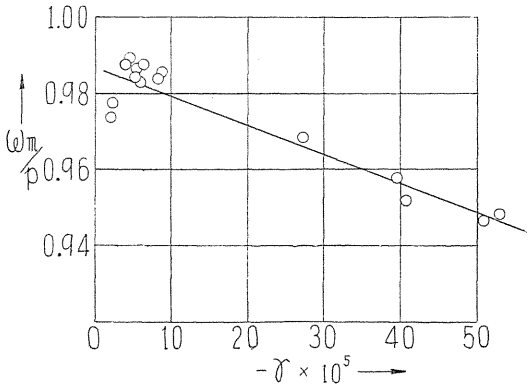

FIG. 76. ω_m/p diagram.

Two reasons for such a complicated whirling motion as explained above are the existance of retardation and the presence of directional non-uniformity of stiffness of shaft. When there is only directional non-uniformity of stiffness and no retardation, the motion is rather simple, as remarked in section 1, and when retardation exists and stiffness is equal in all directions, amplitude in OA direction is equal to that in OB direction and there is only a 90° difference of phase angle in vibrations between both directions. Consequently, although beating phenomena can appear after shaft passes through the critical speed, locus of path of shaft center S is always a circle and the whirling motion is rather simple.

5. Measurement of natural frequency

Since beating phenomena are the result of superposition of free and forced vibrations, by analyzing the beating pattern we can find the value of natural frequency p. In Fig. 77, let t_1 be the time interval between nodes I and II; let N_1 be number of revolutions of shaft during time t_1. When the shaft is retarded, beating always takes place in region of $\omega < p$. Accordingly, during t_1, free vibration oscillates $N_1 + 1$ times, and

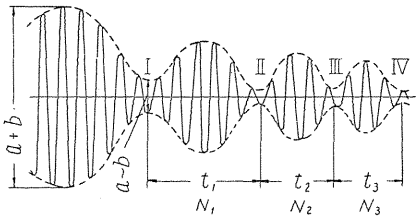

FIG. 77

$$p = \frac{N_1 + 1}{t_1} \text{ sec.}^{-1}, \quad \text{or} \quad p = \frac{N_2 + 1}{t_2} \text{ sec.}^{-1}, \ \ldots, \ p = \frac{N_n + 1}{t_n},$$

and for a general expression we have

$$p = \frac{\sum_1^n N_n + n}{\sum_1^n t_n};$$

therefore reading N_n, we can find the value of p. In the following two tables, we give the value p obtained by vibratory waves of beating.

The value p obtained by waves of beating coincides with that obtained by free vibration generated by a light tapping on shaft. This fact verifies that beating phenomena result from superposition of free and forced vibrations. In both Tables 9.1 and 9.2, p obtained from beating is slightly smaller than that furnished by free vibration because coefficient of friction in bearing during rotation of shaft is clearly

smaller than when it is at rest; then supporting condition of shaft when $\omega \neq 0$ is nearer to that of freely supported shaft when compared with resting state $\omega = 0$ in which free vibration by impulse is generated. Since stiffness in OA direction is larger than in OB direction, as explained in Chapter VI, then p in OA direction is larger than that in OB direction.

TABLE 9.1

	OA-direction			OB-direction		
n	t_n in sec.	N_n	p in r.p.m.	t_n in sec.	N_n	p in r.p.m.
1	1.444	32.274	1383.0	1.780	37.427	1348.6
2	1.299	28.802	1376.5	1.321	28.632	1346.4
3	0.958	21.072	1282.4	1.100	23.703	1347.4
4	0.943	20.583	1373.1	0.965	20.620	134.42
5	0.790	17.178	1380.6	0.870	18.565	1349.3
6	0.744	16.134	1382.7	0.805	17.082	1347.7
7	0.727	15.688	1377.3	0.703	14.807	1350.1
8	0.647	13.885	1380.4	0.702	14.798	1350.2
9	0.613	13.115	1381.6	0.686	14.313	1340.1
	Mean value $p=1377.8$			Mean value $p=1347.1$		
	Value obtained from free vibration induced by impulse $p_1=1384.9$			Value obtained from free vibration induced by impulse $p_1=1354.9$		

TABLE 9.2

	OA-direction			OB-direction		
n	t_n in sec.	N_n	p in r.p.m.	t_n in sec.	N_n	p in r.p.m.
1	0.611	12.988	1373.6	1.327	28.795	1347.2
2	0.590	12.501	1373.0	1.036	22.354	1353.2
3	0.530	11.153	1375.8	0.873	18.417	1343.2
4	0.513	10.707	1370.5	0.776	16.382	1344.0
5	0.482	10.024	1373.7	0.697	14.610	1344.8
6	0.474	9.829	1372.3	0.637	13.290	1346.0
7	0.454	9.403	1376.3	0.555	11.451	1347.3
8	0.434	8.934	1373.4	0.526	10.791	1346.3
9	0.419	8.556	1370.0	0.497	10.215	1353.9
	Mean value $p=1373.2$			Mean value $p=1346.9$		
	Value obtained from free vibration induced by impulse $p_1=1375.5$			Value obtained from free vibration induced by impulse $p_1=1354.1$		

6. Determination of direction and magnitude of eccentricity of disc

By analyzing vibratory waves of beating, we can separate free vibration from forced vibration. Since in (9.2) the part in root represents the magnitude of vibration which is shown by dotted lines in Figs. 77 and 78, we have

$$\left.\begin{aligned} \sqrt{\ } &= a+b \quad \text{for} \quad (p-\omega)t+(\varphi_b-\varphi_a)=0 \text{ or } 2\pi, \\ \sqrt{\ } &= a\sim b \quad \text{for} \quad (p-\omega)t+(\varphi_b-\varphi_a)=\pm\pi. \end{aligned}\right\} \tag{9.10}$$

Evidently amplitudes at beating loop and node are equal to $a+b$ and $a\sim b$ respectively (see Fig. 77). Although only absolute values of $a-b$ can be found

from the amplitude at node, by the following procedure we can determine that $a>b$ or $a<b$.

Putting

$$\frac{a}{b}=\lambda, \qquad (p-\omega)t+(\varphi_b-\varphi_a)=\zeta,$$

then from the first equation of (9.3) we have

$$\tan\psi_x=\frac{\sin\zeta}{\lambda+\cos\zeta}, \tag{9.11}$$

and mode of change of ψ_x during one beat can be represented by full and dotted lines in Fig. 78. When $a<b$ $(\lambda<1)$, there is $\pm 2\pi$ difference between $\omega t+\varphi_a$ and $\omega t+\varphi_a+\psi_x$ during one beat, and the number of vibratory waves in one beat is smaller or larger by just one than the number of revolutions of shaft; on the other hand, when $a>b(\lambda>1)$, these numbers agree with each other. Distinction between $\lambda<1$ and $\lambda>1$ can be brought out by comparing vibratory waves with rotating marks on recording oscillographic paper; thus we can determine $a>b$ or $a<b$. In Fig. 75, curve A passes through beating loops and curve B through nodes. Dotted line indicates the region of $b-a<0$. Since $a+b$ and $a-b$ are found from curves A and B, we can determine the magnitudes of a and b.

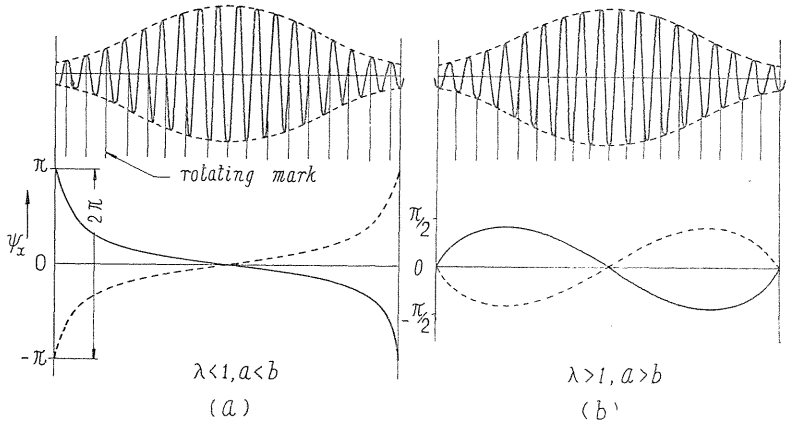

FIG. 78

In Fig. 79 vibratory waves in both $\lambda<1$ and $\lambda>1$ are indicated. By noting this record, we can readily distinguish one from the other.

Now we intend to obtain a differential equation of motion of disc having a constant acceleration. For brevity, we consider the vibratory system with no damping; then the differential equation is

$$m\ddot{x}+kx=ke\sin\theta, \tag{9.12}$$

where m is mass of disc, x is deflection of shaft center S, k is spring constant, e is eccentricity and θ is rotating angle of gravitational center of disc (see Fig. 70).

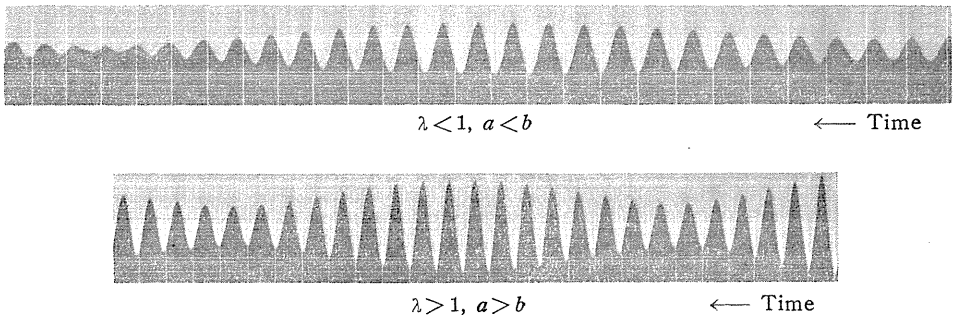

FIG. 79

As angular acceleration β is constant, then $\omega = \omega_0 + \beta t$ and

$$\theta = \int_0^t \omega dt = \theta_0 + \omega_0 t + \frac{1}{2}\beta t^2, \tag{9.13}$$

where θ_0 and ω_0 are values of θ and ω at $t = 0$, respectively. Putting $p^2 = k/m$, we have

$$\ddot{x} + p^2 x = p^2 e \sin\left(\theta_0 + \omega_0 t + \frac{1}{2}\beta t^2\right). \tag{9.14}$$

we now introduce dimensionless quantities as follows:

$$u_0 = \omega_0/p, \qquad \gamma = \beta/p^2, \qquad z = pt.$$

For rather small values of t, we can put

$$\sin\frac{1}{2}\beta t^2 \fallingdotseq \frac{1}{2}\beta t^2, \qquad \cos\frac{1}{2}\beta t^2 \fallingdotseq 1,$$

and then the general solution of (9.14) can be given by

$$\frac{x}{e} = E\cos z + F\sin z + \left\{\frac{\gamma z^2}{2(1-u_0^2)} - \frac{\gamma(1+3u_0^2)}{(1-u_0^2)^3}\right\}\cos(u_0 z + \theta_0) + \left\{\frac{1}{1-u_0^2} + \frac{2\gamma z u_0}{(1-u_0^2)^2}\right\}\sin(u_0 z + \theta_0), \tag{9.15}$$[24]

in which the first and second terms give free vibration and the third and fourth terms represent forced vibration, and E and F are constants determined by initial conditions. Putting sum of third and fourth terms as X/e, and considering γ^2 to be negligibly small, we obtain

$$\frac{X}{e} = \frac{1}{1-u_0^2}\left\{\frac{1}{2}\gamma z^2\cos(u_0 z + \theta_0) + \sin(u_0 z + \theta_0)\right\} + \frac{2\gamma u_0 z}{(1-u_0^2)^2}\sin(u_0 z + \theta_0) - \frac{\gamma(1+3u_0^2)}{(1-u_0^2)^3}\cos(u_0 z + \theta_0)$$

$$\fallingdotseq \left\{\frac{1}{1-u_0^2}+\frac{2\gamma u_0 z}{(1-u_0^2)^2}\right\}\sin\left(\theta_0+u_0z+\frac{1}{2}\gamma z^2\right)-\frac{\gamma(1+3u_0^2)}{(1-u_0^2)^3}\cos\left(\theta_0+u_0z+\frac{1}{2}\gamma z^2\right)$$

$$\fallingdotseq \frac{1}{1-(u_0+\gamma z)^2}\sin\left(\theta_0+u_0z+\frac{1}{2}\gamma z^2\right)-\frac{\gamma\{1+3(u_0+\gamma z)^2\}}{\{1-(u_0+\gamma z)^2\}^3}\cos\left(\theta_0+u_0z+\frac{1}{2}\gamma z^2\right).$$

Putting

$$\theta=\theta_0+u_0z+\frac{1}{2}\gamma z^2,\qquad u=u_0+\gamma z$$

hane

$$\frac{X}{e}=\frac{1}{1-u^2}\sin\theta+\frac{\gamma(1+3u^2)}{(1-u^2)^3}\cos\theta. \tag{9.16}$$

Eq. (9.16) gives amplitude a of forced vibration, thus

$$\frac{a}{e}=\sqrt{\left(\frac{1}{1-u^2}\right)^2+\left\{\frac{\gamma(1+3u^2)}{(1-u^2)^3}\right\}^2}\fallingdotseq\frac{1}{1-u^2},$$

then

$$e=a(1-u^2). \tag{9.17}$$

The difference between $\sqrt{\ }$ and $1/(1-u^2)$ becomes larger with increasing γ and decreasing $(1-u)$. If we assume $\gamma=10^{-4}$, this difference is 3.02% for $u=0.98$, 0.19% for $u=0.96$ and 0.04% for $u=0.94$. In our experiments, $\gamma=10^{-4}\sim4\times10^{-5}$, then (9.17) gives the exact value of e. Although damping force is present in actual experimental system, in our experiment the influence is negligible because damping coefficient is very small, being $0.5\sim0.1$ rad/sec. In as much as damping effect is not very large, the simple equation (9.17) can generally be used to determine the value of eccentricity. In Tables 9.3 and 9.4, the values of e are obtained as explained in the present section.

TABLE 9.3

OA-direction ($\gamma=-1/24680$)				*OB*-direction ($\gamma=-1/25900$)			
t in sec.	a in mm	u	e in mm	t in sec.	a in mm	u	e in mm
14	0.225	0.9566	0.0191	12	0.179	0.9454	0.0190
16	0.178	0.9455	0.0189	13	0.162	0.9396	0.0190
19	0.135	0.9291	0.0185	16	0.128	0.9229	0.0190
		Mean value $e=0.0188$				Mean value $e=0.0190$	

TABLE 9.4

OA-direction ($\gamma=-1/11560$)				*OB*-direction ($\gamma=-1/11980$)			
t in sec.	a in mm	u	e in mm	t in sec.	a in mm	u	e in mm
5.5	0.374	0.9721	0.0160	5.0	0.307	0.9607	0.0173
7.5	0.189	0.9500	0.0164	6.0	0.170	0.9443	0.0170
10.0	0.108	0.9235	0.0162	8.0	0.116	0.9282	0.0165
		Mean value $e=0.0162$				Mean value $e=0.0169$	

As we can see by Tables 9.3 and 9.4, although the motions between OA and OB directions are quite different, the values of eccentricity e obtained from records of motions in both directions coincide well. Direction in which eccentricity e is persent can be found by observing the vibratory waves at beating loop where both vector of free and forced vibrations coincide. At beating loop, free vibration, forced vibration, and the resultant vibration which appears actually on recording oscillographic paper and consists of free and forced vibrations, have the same phase angle, and as there is no difference in phase angle between forced vibration and angular position of eccentricity, we can thus find the direction of eccentricity.

TABLE 9.5

u	a in mm	e in mm
0.965	0.3735	0.0258
0.960	0.3300	0.0259
0.955	0.2885	0.0254
0.950	0.2565	0.0250
0.945	0.2295	0.0250
0.940	0.2070	0.0241
	Mean value = 0.0252	

One example of balancing test is shown in Table 9.5 where the values of eccentricity e obtained from procedure explained in the present section are given. Since weight of disc is 2.126 kg, we must put balancing weight 0.663 g at radius $r = 80.85$ mm. By soldering balancing weight at $r = 80.85$ mm, the maximum deflection is decreased to about one-fifteenth. To verify weight of solder balancing weight, we remove it from the disc and find that it weighs 0.683 g, not 0.663 g. If the solder balancing weight had the correct value 0.663 g, the maximum deflection would be decreased to one-thirtieth and the residual unbalanced moment in this experiment would be 0.1904 g-cm which is one two-hundredths of residual moment 40.21 g-cm given by Akimoff's empirical formula in a statical balancing test. Taking this into consideration, we can say that the exact balancing test of a rotating body can be carried out by our method.

Incidentally, we note that time mark is not needed to determine magnitude and direction of e. Let ω_1 be rotating speed of shaft at first node and ω_n at nth node; let N_1 be number of revolutions of shaft between first and second nodes and N_2 between second and third nodes. Then we have

$$\frac{1}{2}(\omega_1+\omega_2)t_1 = 2\pi N_1 \text{ rad.}, \qquad pt_1 = 2\pi(N_1+1) \text{ rad.}$$

provided that angular acceleration is constant. Putting $u_1 = \omega_1/p$ and $u_2 = \omega_2/p$, we obtain

$$\frac{1}{2}(u_1+u_2) = \frac{N_1}{N_1+1}, \tag{i}$$

$$\frac{1}{2}(u_2+u_3) = \frac{N_2}{N_2+1}, \tag{ii}$$

$$\frac{1}{2}(u_1+u_3) = \frac{N_1+N_2}{N_1+N_2+2}. \tag{iii}$$

From (i), (ii) and (iii), we can determine the values of u_1, u_2 and u_3. A comparison of values of u obtained by using time mark with values from (i), (ii) and (iii) is given in Table 9.6 where the difference between both values is seen to be so small as to be negligible. Consequently it is seen that balancing test can be carried out without

TABLE 9.6

u'	u''	Difference in %
0.9801	0.9788	0.13
0.9698	0.9702	0.05
0.9624	0.9628	0.04
0.9575	0.9566	0.09
0.9510	0.9513	0.02

time mark.

In Table 9.6, u' is the value of u obtained by using time mark and u'' is that determined without time mark.

7. Summary

In summarizing, the complicated whirling motion of shaft appears to be induced by angular acceleration and directional non-uniformity of stiffenss of shaft. Superposition of forced vibration caused by eccentricity e, on free vibration induced by angular acceleration results in such complicated motion. An analysis of this motion furnishes an excellent method for balancing test. Furthermore absence of a time mark is most convenient for designing a practical balancing machine.

Chapter X. On Stability Criteria for Forced Vibration in Non-linear Systems[9]

1. Introduction

In a previous paper by the author titled "On the Critical Speeds of a Shaft" (Chapter IV), our stability criteria for forced vibrations in non-linear shaft system with small radial clearance are presented without proof of establishment. In Chapter V of the present paper we use similar criteria for sub-harmonic oscillations. In this chapter we give proof underlining such stability criteria.

For stability criteria of forced vibrations in non-linear system, van der Pol,[29] Andronow and Witt,[10] and M. L. Cartwright[25] studied the so-called van der Pol's equation which was presented for a certain self-sustained vibratory system. Furthermore in order to obtain stability criteria for Duffing's equation, others studied variational differential equations[30] where they become Mathieu's equation with coefficients of periodic functions.[10]

Although there have been many studies on special dynamic systems made, as above mentioned, studies on stability criteria for forced vibrations in general systems are few. While in 1953, K. Klotter and E. Pinney[26] presented more generalized criteria for forced vibrations, these conditions still cannot be applied in every case.

In the present chapter, we give in a manner similar to that devised by Andronow and Witt,[28] stability[27] criteria for forced vibrations in generalized systems without any restriction and show that determination of response curves and separation of stable and unstable regions can be carried out rather simply. In addition, we discuss the physical meaning of stability criteria and compare our criteria with the criteria presented by K. Klotter and E. Pinney.

2. Stability criteria

Equation of motion of non-linear system can be represented by

$$\ddot{x} + p^2 x + \varepsilon f(x, \dot{x}) = F \sin \omega t, \qquad (F > 0) \tag{10.1}$$

where p is the natural frequency of linear system, $F \sin \omega t$ is an external force with period $2\pi/\omega$, $\varepsilon f(x, \dot{x})$ is a non-linear term and ε is a very small quantity as compared with unity. Furthermore, when linear term of $\dot{x}$ (viscous damping) exists, it is contained in this non-linear term. We must note that the vector of external force

$\overline{F}$ turns from negative to positive direction at the instant $t=0$ because $F>0$. Obviously (10.1) represents general vibratory system having non-linear damping and non-linear restoring force.

Putting the solution of (10.1)

$$x = b_1(t)\sin\omega t + b_2(t)\cos\omega t, \tag{10.2}$$

we consider that b_1 and b_2 are functions of time t. They are clearly constants in linear system. From (10.2) we have

$$\left.\begin{aligned}\dot{x} &= (\dot{b}_1 - \omega b_2)\sin\omega t + (\dot{b}_2 + \omega b_1)\cos\omega t,\\ \ddot{x} &= (\ddot{b}_1 - 2\omega\dot{b}_2 - \omega^2 b_1)\sin\omega t + (\ddot{b}_2 + 2\omega\dot{b}_1 - \omega^2 b_2)\cos\omega t.\end{aligned}\right\} \tag{10.3}$$

Since non-linear term $\varepsilon f(x, \dot{x})$ is small and deviation from linear system in solution of (10.1) is also small, then $\dot{b}_1$ and $\dot{b}_2$ are small quantities having same order of ε, and $\ddot{b}_1$ and $\ddot{b}_2$ have the same order of magnitude of ε^2. Inserting (10.2) into $\varepsilon f(x, \dot{x})$, we have

$$\begin{aligned}\varepsilon f(x, \dot{x}) &= \psi_1(b_1, b_2, \omega)\sin\omega t + \psi_2(b_1, b_2, \omega)\cos\omega t\\ &\quad + c_1(b_1, b_2, \dot{b}_1, \dot{b}_2, \omega)\sin\omega t + c_2(b_1, b_2, \dot{b}_1, \dot{b}_2, \omega)\cos\omega t + c_3,\end{aligned} \tag{10.4}$$

where

$$\left.\begin{aligned}\psi_1 + c_1 &= \frac{1}{\pi}\int_0^{2\pi} \varepsilon f[(b_1\sin\theta + b_2\cos\theta),\ \{(\dot{b}_1 - \omega b_2)\sin\theta + (\dot{b}_2 + \omega b_1)\cos\theta\}]\sin\theta \cdot d\theta,\\ \psi_2 + c_2 &= \frac{1}{\pi}\int_0^{2\pi} \varepsilon f[(b_1\sin\theta + b_2\cos\theta),\ \{(\dot{b}_1 - \omega b_2)\sin\theta + (\dot{b}_2 + \omega b_1)\cos\theta\}]\cos\theta \cdot d\theta.\end{aligned}\right\} \tag{10.5}$$

In (10.5) ψ_1 and φ_2 are as small as the same order of ε, c_1 and c_2 have the same order of ε^2 or smaller, c_3 is the term in which the period is not equal to $2\pi/\omega$. Clearly $\dot{b}_1$ and $\dot{b}_2$ are not contained in ψ_1 and ψ_2, since ψ_1 and ψ_2 are small quantities of the same order of ε.

Inserting (10.3) and (10.4) into (10.1) and assuming the higher powers of small quantities to be negligible, we have

$$\left.\begin{aligned}-2\omega\dot{b}_2 + (p^2 - \omega^2)b_1 + \psi_1 &= F,\\ 2\omega\dot{b}_1 + (p^2 - \omega^2)b_2 + \psi_2 &= 0.\end{aligned}\right\} \tag{10.6}$$

When motion is in a steady state, b_1 and b_2 become constants and $\dot{b}_1 = \dot{b}_2 = 0$, then

$$\left.\begin{aligned}(p^2 - \omega^2)b_1 + \psi_1 &= F,\\ (p^2 - \omega^2)b_2 + \psi_2 &= 0.\end{aligned}\right\} \tag{10.6a}$$

The relation between the magnitude of the external force F and the amplitudes b_1 and b_2 is readily obtained by squaring and adding (10.6a). The result is

$$(p^2 - \omega^2)^2(b_1^2 + b_2^2) + 2(p^2 - \omega^2)(b_1\psi_1 + b_2\psi_2) + (\psi_1^2 + \psi_2^2) = F^2, \tag{10.7}$$

and although (10.7) gives the response curve of forced vibration, we cannot obtain the direct relation between amplitude $a=\sqrt{b_1^2+b_2^2}$ and F until we know the phase of vibration and until b_1 and b_2 are determined separately. We will rewrite (10.7) in a more convenient form later.

From (10.6) we have

$$\frac{db_2/dt}{db_1/dt}=\frac{db_2}{db_1}=\frac{(p^2-\omega^2)b_1+\psi_1-F}{-(p^2-\omega^2)b_2-\psi_2}. \tag{10.8}$$

Since denominator and numerator in (10.8) vanish at the same time when $\dot{b}_1$ and $\dot{b}_2$ become equal to zero simultaneously, then the periodic solution of steady forced vibration corresponds to the singular point of the first order differential equation (10.8). For the purpose of establishing the stability criteria of forced vibration, it is sufficient to solve the stability problem for singular point.

Let b_1 and b_2 in a steady state ($\dot{b}_1=\dot{b}_2=0$) be b_{10} and b_{20} respectively, and let

$$b_1=b_{10}+\xi, \qquad b_2=b_{20}+\eta, \tag{10.9}$$

where ξ and η are small deviations from a steady state. Using (10.9), we have

$$\left.\begin{aligned}\psi_1(b_1,\ b_2,\ \omega)&=\psi_1(b_{10},\ b_{20},\ \omega)+\left(\xi\frac{\partial\psi_1}{\partial b_1}+\eta\frac{\partial\psi_1}{\partial b_2}\right)+\frac{1}{2!}\left(\xi\frac{\partial}{\partial b_1}+\eta\frac{\partial}{\partial b_2}\right)^2\psi_1+\cdots,\\ \psi_2(b_1,\ b_2,\ \omega)&=\psi_2(b_{10},\ b_{20},\ \omega)+\left(\xi\frac{\partial\psi_2}{\partial b_1}+\eta\frac{\partial\psi_2}{\partial b_2}\right)+\frac{1}{2!}\left(\xi\frac{\partial}{\partial b_1}+\eta\frac{\partial}{\partial b_2}\right)^2\psi_2+\cdots.\end{aligned}\right\} \tag{10.10}$$

Substituting (10.10) into (10.8), we have

$$\frac{d\eta}{d\xi}=\frac{\left(p^2-\omega^2+\dfrac{\partial\psi_1}{\partial b_1}\right)\xi+\dfrac{\partial\psi_1}{\partial b_2}\eta+P}{-\dfrac{\partial\psi_2}{\partial b_1}\xi-\left(p^2-\omega^2+\dfrac{\partial\psi_2}{\partial b_2}\right)\eta+Q}=\frac{A\xi+B\eta+P}{C\xi+D\eta+Q}, \tag{10.11}$$

where $\dfrac{\partial\psi_1}{\partial b_1}$, $\dfrac{\partial\psi_1}{\partial b_2}$, $\dfrac{\partial\psi_2}{\partial b_1}$ and $\dfrac{\partial\psi_2}{\partial b_2}$ take the values in a steady state ($\dot{b}_1=\dot{b}_2=0$), and

$$\left.\begin{aligned}A&=\left(p^2-\omega^2+\frac{\partial\psi_1}{\partial b_1}\right), \qquad B=\frac{\partial\psi_1}{\partial b_2},\\ C&=-\frac{\partial\psi_2}{\partial b_1}, \qquad D=-\left(p^2-\omega^2+\frac{\partial\psi_2}{\partial b_2}\right).\end{aligned}\right\} \tag{10.12}$$

In (10.11) P and Q are terms of higher powers of ξ and η.

According to the results obtained by Poincaré, we have

$$\left.\begin{aligned}&1)\ AD-BC<0, \quad \cdots\cdots\cdots\cdots\cdots\text{stable},\\ &\quad AD-BC>0, \quad \cdots\cdots\cdots\cdots\cdots\text{unstable},\end{aligned}\right\} \tag{10.13}$$

$$\left.\begin{aligned}&2)\ B+C<0, \quad \cdots\cdots\cdots\cdots\cdots\text{stable},\\ &\quad B+C>0, \quad \cdots\cdots\cdots\cdots\cdots\text{unstable}.\end{aligned}\right\} \tag{10.14}$$

Consequently, from (10.12) we obtain

$$AD-BC=-(p^2-\omega^2)^2-(p^2-\omega^2)\left(\frac{\partial\psi_1}{\partial b_1}+\frac{\partial\psi_1}{\partial b_2}\right)-\frac{\partial\psi_1}{\partial b_1}\frac{\partial\psi_2}{\partial b_2}+\frac{\partial\psi_1}{\partial b_2}\frac{\partial\psi_2}{\partial b_1}\gtreqless 0, \tag{10.15}$$

$$B+C=\frac{\partial\psi_1}{\partial b_2}-\frac{\partial\psi_2}{\partial b_1}\gtreqless 0. \tag{10.16}$$

Eqs. (10.15) and (10.16) furnish stability criteria of forced vibration for more general non-linear vibratory system.

3. General expression of stability criteria

In Fig. 80 (a), $\bar{F}$ is a vector of external force, and external force $F\sin\omega t$ in (10.1) can be represented by the projection of $\bar{F}$ in x-direction. In Fig. 80 (a), time $t=0$ is the instant when vector $\bar{F}$ coincides with $-y$ axis. Let time t be 0 when vector $\bar{a}$ of forced vibration agrees with $-y$ axis, as shown in Fig. 80 (b); then (10.1) is rewritten as follows:

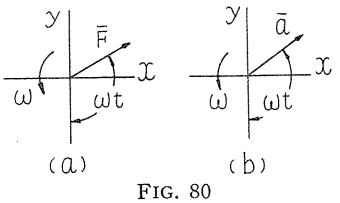

FIG. 80

$$\ddot{x}+p^2x+\varepsilon f(x,\dot{x})=F_1\sin\omega t+F_2\cos\omega t. \tag{10.17}$$

Consequently, instead of (10.2), we must put

$$x=a\sin\omega t, \qquad (a>0). \tag{10.18}$$

Obviously the relations

$$F^2=F_1^2+F_2^2, \qquad a^2=b_1^2+b_2^2, \tag{10.19}$$

can be held. Inserting (10.18) into $\varepsilon f(x,\dot{x})$, we have

$$\begin{aligned}\varepsilon f(x,\dot{x})&=\varphi_1(a,\omega)\sin\omega t+\varphi_2(a,\omega)\cos\omega t\\&\quad+c_4(a,\dot{a},\omega)\sin\omega t+c_5(a,\dot{a},\omega)\cos\omega t+c_6,\end{aligned} \tag{10.20}$$

where

$$\left.\begin{aligned}\varphi_1+c_4&=\frac{1}{\pi}\int_0^{2\pi}\varepsilon f\{a\sin\theta,\ (a\dot{\theta}\cos\theta+\dot{a}\sin\theta)\}\sin\theta\cdot d\theta,\\ \varphi_2+c_5&=\frac{1}{\pi}\int_0^{2\pi}\varepsilon f\{a\sin\theta,\ (a\dot{\theta}\cos\theta+\dot{a}\sin\theta)\}\cos\theta\cdot d\theta.\end{aligned}\right\} \tag{10.21}$$

In (10.21), c_4 and c_5 have the same order of ε^2 or smaller, and c_6 is the term in which the period is not equal to $2\pi/\omega$.

Inserting (10.18) and (10.20) into (10.17) and rejecting terms smaller than ε, we have

$$\left.\begin{aligned}(p^2-\omega^2)a+\varphi_1&=F_1,\\ 2\dot{a}\omega+\varphi_2&=F_2,\end{aligned}\right\} \tag{10.22}$$

where $2\dot{a}\omega$ represents Coriolis' force. Since we cannot deduce Poincare's criteria directly from (10.22), we introduce (10.6) and obtain criteria from (10.6) in section 2. In a steady state, $\dot{a}$ in (10.22) vanishes and we have

$$\left.\begin{aligned}(p^2-\omega^2)\,a+\varphi_1&=F_1,\\ \varphi_2&=F_2.\end{aligned}\right\} \tag{10.22a}$$

Squaring and adding (10.22a), we have response curve

$$\Phi=\{(p^2-\omega^2)\,a+\varphi_1\}^2+\varphi_2^2=F^2. \tag{10.23}$$

Now we rewrite (10.2) as follows:

$$x=b_1\sin\omega t+b_2\cos\omega t=a\sin(\omega t+\alpha), \tag{10.24}$$

in which α is a phase difference between vectors $\bar{F}$ and $\bar{a}$, and $\alpha=\tan^{-1}b_2/b_1$. Accordingly, we have

$$b_1=a\cos\alpha,\qquad b_2=a\sin\alpha. \tag{10.25}$$

Inserting (10.24) into $\varepsilon f(x,\dot{x})$, we have

$$\begin{aligned}\varepsilon f(x,\dot{x})&=\varphi_1\sin(\omega t+\alpha)+\varphi_2\cos(\omega t+\alpha)+c_4\sin(\omega t+\alpha)+c_5\cos(\omega t+\alpha)+c_6\\&=(\varphi_1\cos\alpha-\varphi_2\sin\alpha)\sin\omega t+(\varphi_1\sin\alpha+\varphi_2\cos\alpha)\cos\omega t+\ldots.\end{aligned} \tag{10.26}$$

Comparing (10.26) with (10.4), we can readily obtain the relations

$$\psi_1=\varphi_1\cos\alpha-\varphi_2\sin\alpha,\qquad \psi_2=\varphi_1\sin\alpha+\varphi_2\cos\alpha. \tag{10.27}$$

From (10.25), we have

$$\left.\begin{aligned}\frac{\partial\psi_{1,2}}{\partial b_1}&=\cos\alpha\frac{\partial\psi_{1,2}}{\partial a}-\frac{\sin\alpha}{a}\frac{\partial\psi_{1,2}}{\partial\alpha},\\ \frac{\partial\psi_{1,2}}{\partial b_2}&=\sin\alpha\frac{\partial\psi_{1,2}}{\partial a}+\frac{\cos\alpha}{a}\frac{\partial\psi_{1,2}}{\partial\alpha}.\end{aligned}\right\} \tag{10.28}$$

Substituting (10.27) into (10.28), then we have

$$\left.\begin{aligned}\frac{\partial\psi_1}{\partial b_1}&=\cos^2\alpha\frac{\partial\varphi_1}{\partial a}-\sin\alpha\cos\alpha\frac{\partial\varphi_2}{\partial a}+\frac{1}{a}(\sin^2\alpha\cdot\varphi_1+\sin\alpha\cos\alpha\cdot\varphi_2),\\ \frac{\partial\psi_1}{\partial b_2}&=\sin\alpha\cos\alpha\frac{\partial\varphi_1}{\partial a}-\sin^2\alpha\frac{\partial\varphi_2}{\partial a}-\frac{1}{a}(\sin\alpha\cos\alpha\cdot\varphi_1+\cos^2\alpha\cdot\varphi_2),\\ \frac{\partial\psi_2}{\partial b_1}&=\sin\alpha\cos\alpha\frac{\partial\varphi_1}{\partial a}+\cos^2\alpha\frac{\partial\varphi_2}{\partial a}+\frac{1}{a}(-\sin\alpha\cos\alpha\cdot\varphi_1+\sin^2\alpha\cdot\varphi_2),\\ \frac{\partial\psi_2}{\partial b_2}&=\sin^2\alpha\frac{\partial\varphi_1}{\partial a}+\sin\alpha\cos\alpha\frac{\partial\varphi_2}{\partial a}+\frac{1}{a}(\cos^2\alpha\cdot\varphi_1-\sin\alpha\cos\alpha\cdot\varphi_2).\end{aligned}\right\} \tag{10.29}$$

Using the relations of (10.29), Eqs. (10.15) and (10.16) become

$$AD-BC=-(p^2-\omega^2)^2-\left(\frac{\partial\varphi_1}{\partial a}+\frac{1}{a}\varphi_1\right)(p^2-\omega^2)-\frac{1}{2a}\frac{\partial a}{\partial}(\varphi_1^2+\varphi_2^2)\gtreqless 0, \tag{10.30}$$

$$B+C=-\frac{\partial(a\varphi_2)}{\partial a}=\frac{\partial}{\partial a}(-a\varphi_2)\gtreqless 0. \tag{10.31}$$

Furthermore, by using (10.29) we can prove that response curves of (10.23) coincide with those of (10.7).

Differentiating response curve (10.23) with respect to amplitude a, we have

$$\begin{aligned}\frac{\partial\Phi}{\partial a}&=-2a\left\{-(p^2-\omega^2)^2-\left(\frac{\partial\varphi_1}{\partial b}+\frac{1}{a}\varphi_1\right)(p^2-\omega^2)-\frac{1}{2a}\frac{\partial}{\partial a}(\varphi_1^2+\varphi_2^2)\right\}\\&=-2a(AD-BC).\end{aligned} \tag{10.32}$$

Observing (10.32), we find that in critical conditions of stable and unstable motions, the relation $\partial\Phi/\partial a=0$ can be held.

4. Physical meaning of stability criteria

Putting $d\omega/da=0$ and eliminating F from the following equations

$$\left.\begin{aligned}&\Phi-F^2=0, \qquad \text{(response curve)}\\&\frac{d(\Phi-F^2)}{da}=\frac{d\Phi}{da}=\frac{\partial\Phi}{\partial a}+\frac{\partial\Phi}{\partial\omega}\frac{d\omega}{da}=0,\end{aligned}\right\}$$

we obtain the equation of curves through the points on the response curves having vertical tangents. Clearly this equation itself is $\partial\Phi/\partial a=0$ and these curve furnish boundary lines separating the stable from the unstable region. Therefore the first criterion $AD-BC=0$ has the above physical and geometrical meaning.

Considering parameter F as variable, from (10.23), we have

$$\frac{\partial F^2}{\partial a}=2F\frac{\partial F}{\partial a}=\frac{\partial\Phi}{\partial a}. \tag{10.33}$$

As $F>0$, $a>0$, we can conclude that

$$\left.\begin{aligned}&AD-BC<0 \text{ corresponds to } \frac{\partial\Phi}{\partial a}>0,\ \frac{\partial F}{\partial a}>0 \text{ (stable)}\\&AD-BC>0 \text{ corresponds to } \frac{\partial\Phi}{\partial a}<0,\ \frac{\partial F}{\partial a}<0 \text{ (unstable)}\\&AD-BC=0 \text{ corresponds to } \frac{\partial\Phi}{\partial a}=0,\ \frac{\partial F}{\partial a}=0 \text{ (the critical case).}\end{aligned}\right\} \tag{10.34}$$

K. Klotter and E. Pinney proved that $\partial a/\partial\Phi>0$ represents stable condition and $\partial a/\partial\Phi<0$ unstable motion, which agrees with (10.34). But there is another criterion (10.16) or (10.31).

In order to prove that curves through points on response curves having vertical tangents become boundaries between stable and unstable regions, in Duffing's equation, for example, we usually introduce a linear variational differential equation which is Mathieu's equation, and determine stability of periodic solutions of that equation, and then prove that equations of boundary curves of stable region of Mathieu's equation correspond to curves through points on response curves with vertical tangents. Such a procedure is complicated, while that explained in this chapter is more simple and direct. Obviously, the geometrical meaning given above

is valid not only for Duffing's equation but also for all general non-linear systems, as we have already indicated.

Now we intend to consider the physical meaning of the second criterion (10.31). From (10.22a), for a steady forced vibration ($\dot{a}=0$), we obtain $\varphi_2=F_2$. Vector F_2 is the component of external force F and has 90° phase difference of $\bar{a}$, and when F_2 takes positive value it is 90° in advance of $\bar{a}$, and when $F_2<0$ it is behind by 90°. Since force $-\varphi_2$ is induced by motion, it vanishes when motion stops; then, in a rather wide sense, we can consider it to be a self-excited force which with F_2 is in equilibrium in a steady state. When $-\varphi_2$ is negative and F_2 is positive, $-\varphi_2$ is behind by 90° and the system becomes a damping system in which $-\varphi_2$ consumes energy of system and the system is given energy through F_2. The relation between forces is given in Fig. 81 (a). On the other hand, when $-\varphi_2$ takes a positive value and is in advance of $\bar{a}$ by 90°, the system becomes a self-excited system and $-\varphi_2$ gives energy to the system and F_2 becomes the resisting force. In such a case, the relation between forces becomes as shown in Fig. 81 (b).

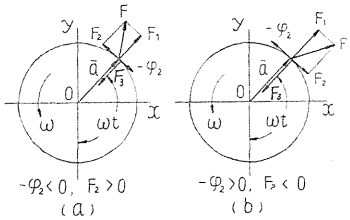

FIG. 81. $F_3=-F_1=-(p^2-\omega^2)a-\varphi_1$, (Force F_3 is the restoring force).

Sign $-\varphi_2$ governing the nature of the system is generally changed according to magnitude of amplitude. Energy given by $-\varphi_2$ during one cycle is

$$E_1=\int_0^{2\pi/\omega}-\varphi_2\cos\omega t\cdot dx=\int_0^{2\pi/\omega}-\varphi_2\cos\omega t\cdot\dot{x}dx=-\varphi_2 a\omega\int_0^{2\pi/\omega}\cos^2\omega t dt=-\pi a\varphi_2, \tag{10.35}$$

and energy induced by external force F_2 is

$$E_2=\pi aF_2. \tag{10.36}$$

When E_1 is positive, $-\varphi_2$ gives energy to the system, and when $E_1<0$, it becomes resistant. Comparing (10.35) with (10.31), we have

$$B+C=\frac{1}{\pi}\frac{\partial E_1}{\partial a}=\frac{-1}{\pi}\frac{\partial E_2}{\partial a}, \tag{10.37}$$

then

$$\left.\begin{aligned} &B+C<0\ \ldots\ldots\ \frac{\partial E_1}{\partial a}<0\ \text{(stable)},\\ &B+C>0\ \ldots\ldots\ \frac{\partial E_1}{\partial a}>0\ \text{(unstable)}. \end{aligned}\right\} \tag{10.38}$$

From (10.38), we can understand that when energy E_1 entering into the system through motion itself increases accordingly as amplitude a increases, then the motion is unstable, and when E_1 decreases with increasing a, the motion is stable, and then

$$\frac{\partial E_1}{\partial a} = 0, \tag{10.39}$$

gives boundary lines between stable and unstable regions and is equivalent to $B+C=0$. When curve E_1 to ω is given as shown in Fig. 82, hatched regions show unstable and unhatched stable regions. When φ_2 is not a function of ω, boundary lines of stable regions are given as horizontal straight lines in $a-\omega$ plane. But since φ_2 is usually a function of ω and a, boundary lines generally become curves.

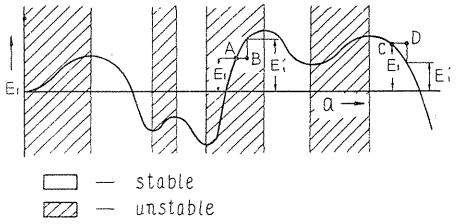

FIG. 82

In Fig. 82, when the motion given by point A is disturbed and deviates slightly from A to B, energy in the system becomes larger and amplitude a increases, and thus the motion deviates continuously from that represented by point A because energy E_1' at B is larger than E_1 at A; hence the motion is unstable. On the other hand, when the motion at point C deviates to D, energy decreases by this deviation and energy given by F_2 is smaller than that consumed because of $E_1 > E_1'$. Consequently, since amplitude decreases gradually and the motion returns to that of C, it is stable.

Incidentally, if we put

$$x = a\cos\omega t$$

we should rewrite (10.20) as follows:

$$\varepsilon f(x, \dot{x}) = \varphi_1 \sin\left(\omega t + \frac{\pi}{2}\right) + \varphi_2 \cos\left(\omega t + \frac{\pi}{2}\right) + \ldots = \varphi_1 \cos\omega t - \varphi_2 \sin\omega t + \ldots, \tag{10.40}$$

because of

$$a\sin\left(\omega t + \frac{\pi}{2}\right) = a\cos\omega t.$$

5. Examples

In the present section we show how much easier it is to obtain response curves and establish stability criteria as compared with procedures hitherto in use.

i) Duffing's equation

$$\ddot{x} + p^2 x + cx + \beta x^3 = F_1 \sin\omega t + F_2 \cos\omega t \tag{10.41}$$

Inserting $x = a\sin\omega t$ into $\varepsilon f(x, \dot{x}) = c\dot{x} + \beta x^3$, we can easily obtain

$$\varphi_1 = \frac{3}{4}\beta a^3, \qquad \varphi_2 = ca\omega. \tag{10.42}$$

Substituting (10.42) into (10.23), we have response curve

$$\Phi = \left[(p^2 - \omega^2)a + \frac{3}{4}\beta a^3\right]^2 + c^2 a^2 \omega^2 = F^2. \tag{10.43}$$

Condition $AD-BC=0$ or $\partial\Phi/\partial a=0$ is given by (10.43) as follows:

$$\left(p^2-\omega^2+\frac{3}{4}\beta a^2\right)\left(p^2-\omega^2+\frac{9}{4}\beta a^2\right)+c^2\omega^2=0. \tag{10.44}$$

For no damping ($c=0$), we have

$$\left(p^2-\omega^2+\frac{3}{4}\beta a^2\right)\left(p^2-\omega^2+\frac{9}{4}\beta a^2\right)=0. \tag{10.45}$$

Eqs. (10.43), (10.44) and (10.45) are well known equations and obviously curves represented by (10.45) have the physical and geometrical meaning as explained in section 4. From the second criterion, we have

$$B+C=-\frac{\partial(a\varphi_2)}{\partial a}=-2ca\omega. \tag{10.46}$$

For Duffing's equation, $B+C<0$ is always held and no unstable region is induced by $B+C>0$.

ii) van der Pol's equation

$$\frac{d^2y}{dt_1^2}+p_1^2y-\alpha\frac{dy}{dt_1}+\gamma\frac{d}{dt_1}(y^3)=F_1'\sin\omega_1t_1+F_2'\cos\omega_1t_1 \tag{10.47}$$

For the sake of brevity in calculation, it is convenient to introduce the dimensionless quantities as follows:

$$\left.\begin{aligned} &a_0^2=\frac{4\alpha}{3\gamma},\quad \frac{y}{a_0}=x,\quad t=\frac{t_1\alpha}{2},\quad p=\frac{2p_1}{\alpha},\\ &\omega=\frac{2\omega_1}{\alpha},\qquad F_1=\frac{4F_1'}{a_0\alpha^2},\qquad F_2=\frac{4F_2'}{a_0\alpha^2}. \end{aligned}\right\}$$

Substitution above equations into (10.47), we have

$$\ddot{x}+p^2x-2\dot{x}+8x^2\dot{x}=F_1\sin\omega t+F_2\cos\omega t, \tag{10.48}$$

where $\varepsilon f(x,\dot{x})=-2\dot{x}+8x^2\dot{x}$.

Inserting $x=a\sin\omega t$ into $\varepsilon f(x,\dot{x})$, we obtain

$$\varepsilon f(x,\dot{x})=2a\omega(a^2-1)\cos\omega t+\ldots,$$

and

$$\varphi_1=0,\qquad \varphi_2=2a\omega(a^2-1), \tag{10.49}$$

and thus from (10.23), response curve

$$\Phi=(p^2-\omega^2)a^2+4a^2\omega^2(a^2-1)^2=a^2\{(p^2-\omega^2)+4\omega^2(a^2-1)^2\}=F^2 \tag{10.50}$$

can be given. From (10.50) and (10.31), we have criteria

$$\frac{\partial\Phi}{\partial a}=(p^2-\omega^2)+4\omega^2(1-a^2)(1-3a^2)=0, \tag{10.51}$$

$$a^2 = \frac{1}{2}, \tag{10.52}$$

because of

$$B + C = \frac{\partial(-a\varphi_2)}{\partial a} = \frac{\partial}{\partial a}\{2a^2\omega(1-a^2)\} = 4a\omega(1-2a^2).$$

From (10.35), we have

$$E_1 = -\pi a\varphi_z = 2\pi\omega a^2(1-a^2), \tag{10.53}$$

which is shown in Fig. 83, and the region $a > \sqrt{1/2}$ is stable and region $0 < a < \sqrt{1/2}$ is unstable.

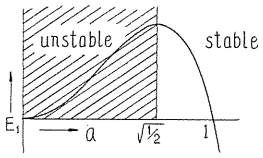

FIG. 83.

6. Conclusion

For general non-linear system, there are two stability criteria presented by (10.30) and (10.31).

The physical meaning of (10.30) and (10.31) is explained in section 4.

Through the procedure given in the present chapter, we can easily solve the problem of stability of motion in non-linear system. Actual application of results obtained in this chapter is described in Chapter IV of a previous paper titled "On the Critical Speeds of a Shaft" and in Chapter V of this paper.

Acknowledgement

The author expresses his appreciation to Professor Emeritus Dr. K. Shogenji for his encouragement, and acknowledges his debt to the late Dr. Y. Shimoyama for guidance and valuable advice, and especially for his instruction over a long period of time. Thanks go to Mr. A. Tsujii and Mr. H. Todoroki for their assistance in some of these experiments.

Notes and References

1) Yamamoto T., "On the Critical Speeds of a Shaft," Memoirs of The Faculty of Engineering, Nagoya University, Vol. **6**, No. 2, November, 1954.
2) "Critical speed" used in the present paper means the angular velocity of shaft in which amplitudes of vibration increase and peaks of amplitudes are formed.
3) Yamamoto T., "On the Critical Speed of a Shaft of Sub-hamonic Oscillation," Trans. of Japan Soc. of Mech. Engrs., Vol. **21**, No. 111, p. 853 (1955).
4) Nishino K. and Iwamoto M., "On the Vibratory Characteristics of the System with a small Clearance (II)," J. Japan Soc. of Applied Mechanics, Vol. **4**, No. 24, p. 81 (1951).
5) Yamamoto T., "On the Critical Speeds with Peculiar Modes of Vibration," Trans. of Japan Soc. of Mech. Engrs., Vol. **22**, No. 115, p. 172 (1956).
6) Yamamoto T., "On Sub-harmonic Oscillations and on Vibrations of Pecular Modes in Non-linear Systems Having Multiple Degrees of Freedom," Trans. of Japan Soc. of Mech. Engrs., Vol. **22**, No. 123, p. 868 (1956).
7) Yamanouch K., Ippan Rikigaku (1931).
8) For example, Nishino K., "Some Notes on the Sub-harmonic Resonance in the Non-linear Mechanical Vibratory System," J. Japan Soc. of Applied Mechanics, Vol. **3**, No. 18, p. 127 (1950).

9) Yamamoto T., "Contribution to the Stability Criterion for Forced Vibrations in Non-linear Systems," Trans. of Japan. Soc. of Mech. Engrs, Vol. **20**, No. 95, p. 501 (1959).
10) Stoker J. J., Nonlinear Vibrations (1950).
11) Yamamoto T., "On the Critical Speeds of Synchronous Backward Precession," Trans. of Japan Soc. of Mech. Engrs., Vol. **22**, No. 115, p. 167 (1956).
12) Shimoyama Y. and Yamamoto T., "On the Critical Speeds of a Shaft due to the Deflections of Bearing Pedestals," Trans. of Japan Soc. of Mech. Engrs., Vol. **20**, No. 91, p. 215 (1954).
13) Yamamoto T., "On the Vibrations of a Shaft Supported by Bearing having Radial Clearances," Trans. of Japan Soc. of Mech. Engrs., Vol. **21**, No. 103, p. 186 (1955).
14) Sawaragi Y., "On the 'Shaft Whipping' excited by Dry Friction of Bearings," Trans. of Japan Soc. of Mech. Engrs., Vol. **17**, No. 57, p. 61 (1951).
15) Yamamoto T., "On the Critical Speed of a Shaft at Lower Rotating Speeds," Trans. of Japan Soc. of Mech. Engrs., Vol. **22**, No. 123, p. 863 (1956).
16) Oki I., "The Lower Critical Sdeed of Horizontal Shaft," Jour. of Japan Soc. of Mech. Engrs., Vol. **21**, No. 52, p. 17 (1918).
17) Lorenz H., "Kritische Drehzahlen rasch umlaufender Welle," V.D.I., 63, s. 243 (1919).
18) Nakanishi F., "The Secondary Vibration of Revolving Shafts," Jour. of Japan Soc. of Mech. Engrs., Vol. **35**, No. 188, p. 1170 (1932).
19) Stodola A., Steam and Gas Turbines, Vol. **2**, p. 1122 (1927).
20) Yamamoto T., "On the Critical Speed of a Shaft supported in Ball Bearing (Part I)," Trans. of Japan Soc. of Mech. Engrs., Vol. **20**, No. 99, p. 750 (1954).
21) Yamamoto T., "On the Critical Speed of a Shaft supported in Ball Bearing (Part II)," Trans. of Japan Soc. of Mech. Engrs., Vol. **20**, No. 99, p. 755 (1954).
22) Shimoyama Y. and Yamamoto T., "Vibrations generated on a Rotating Shaft by Passing through its Critical Speed with Some Angular Acceleration," Trans. of Japan Soc. of Mech. Engrs. Vol. **15**, No. 50, p. 113 (1949).
23) Sasaki T., and others, "On the Planetary Motion of the Roller in the Roller Bearing," Trans. of Japan Soc. of Mech. Engrs., Vol. 8, No. 31, p. 64 (1932).
24) General solution of (9.14) is obtained by use of Fresnel's Integral. Pöschl T., Ingenieur-Archiv, Bd. IV, Heft 1 (1933).
25) Lefschetz S., Contributions to the Theory of Nonlinear Oscillations, p. 149 (1950).
26) Klotter K. and Pinney E., "Stability Criteria for Forced Vibrations in Non-linear Systems," Appl. Mech., J., Vol. **20** p. 9 (1953).
27) In the present chapter, "stability" means "Liapounoff's stability." See Minorsky N., Introduction to Non-linear Mechanics, p. 41 (1947).
28) Andronow, A. and Witt, A., "Zur Theori des Mitnehmens von van der Pol," Archiv fur Elektrotechnik, Vol. **24**, p. 90 (1930).
29) van der Pol, B., "Forced ascillations in a circuit with Non-linear Resistance," Philosophical Magazine, Vol. **3**, No. 8, p. 65 (1927).
30) "Studies in Nonlinear Vibration Theory," Institute for Mathematics and Mechanics, New York University, p. 104 (1946).